NTNU – Trondheim
Norwegian University of
Science and Technology

Mechanisms Governing the occurrence of Partial Discharges in Insulation Liquids

Torstein Grav

Master of Science in Physics and Mathematics
Submission date: June 2013
Supervisor: Steinar Raaen, IFY
Co-supervisor: Lars Lundgaard, Sintef Energi AS

Norwegian University of Science and Technology
Department of Physics

Problem description

Measurements of partial discharges is suggested as a method to evaluate the characteristics of insulation liquids. (IEC 61294)

The intention of this thesis is to evaluate the suitability of this test method and identify physical and chemical processes, which govern the occurrence of partial discharges in liquids. This includes describing the phenomena, test method, literature on discharges, liquids, measurements of partial discharges and experimental investigation of liquids. Different factors/methods to investigate will be space charges, voltage shape, electrode geometry, imaging of the process with optics, statistics of the occurrence, use of an automatic discharge acquisition system (Omicron) and an oscilloscope (Gage scope).

Sammendrag

Havari på elektriske komponenter på grunn av gjennomslag er svært uønsket og det er derfor viktig å velge metoder for isolasjon som har tilfredsstillnede pålitelighet. Væskeisolasjon er foretrukket i elektriske komponenter i undervannsinstallasjoner på grunn av utmerkede egenskaper med tanke på isolasjon, varmetransport, sikkerhet og inkompressibilitet. For å sikre at en isolasjonsvæske er egnet til bruken er det nødvendig å teste forskjellige væsker for å identifisere gode isolatorer. Det finnes forskjellige metoder for å teste disse egenskapene, slik som delutladningsmålinger. Denne oppgaven undersøker en eksperimentell innfallsmetode på testing av egenskaper til forskjellige væsker ved å benytte høyspent AC.

Ladninger i et elektrisk felt genererer en strøm. Dissosiativ ionisering under påtrykket spenning er den mekanismen som genererer flest ladninger i en væske, mens feltemmisjon på negativ polaritet og feltionisasjon på positiv polaritet også bidrar i noen væsker. Væsker i bevegelse resulterer i en målbar strøm på 10 - 80 nA ved en påtrykket AC spenning på 20 kV_{peak} og 20 mm punkt-plangap. Romladninger har vist seg å ha en effekt på delutladningsoppførselen i væsker. Forskjellige væsker har ulike kjemiske og fysiske egenskaper og delutladninger oppfører seg derfor forskjellig. Det er observert at delutladninger er stokastiske, og til en viss grad korrelert til tidligere påtrykket spenning. Delutladningshyppigheten økte eksponentielt som funksjon av påtrykket spenning, mens maksimum ladning per halvperiode så ut til å øke lineært i spenningen. Denne observasjonen er i overenstemmelse med tidligere rapporter.

Tilgjengeligheten på elektroner er viktig. En signifikant økning i delutladningsraten ved små amplituder i begge polariteter oppstod da testcellen ble utsatt for røntgenstråling. Delutladninger ser derfor ut til å starte ved sterkt felt eller elektronskred.

Det er essensielt å være i stand til å teste forskjellige væsker i laboratorieforhold, av økonomiske grunner, for å identifisere de mest passende isolasjonsmedia. Høy pålitelighet på kraftelektronikk forutsetter god og stabil kvalitet på isolasjonsmaterialer. Testoppsettet og metodene som har blitt benyttet kan enkelt bli overført til andre testobjekter enn det enkle punkt-plangapet, for eksempel byttes ut med kretser fra kraftelektronikk.

Forskjellige væsker har forskjellige delutladningsfasemønstre. Dette er et resultat av væskenes forskjellige egenskaper til å generere ladning og ulikheter i delutladningsinitieringsfeltverdiene. Delutladninger er hendelser som oppstår sjeldent (ved lave spenninger) og er sterkt avhengig av forhistorien til væska. Vi vet ikke om delutladninger i seg selv er skadelig eller ikke. Det er derfor ukjent om testmetoden IEC 61294, som bygger på delutladninger gir relevant informasjon om aldring eller ikke. Det er behov for mer forskning for å belyse og avklare dette.

Abstract

Breakdown of electrical equipment is unwanted and the use of reliable methods of insulation are therefore necessary. Liquid insulation is one preferred material for electrical devices used in subsea installations due to outstanding qualities related to insulation, heat transfer, safety and incompressibility properties. To ensure that the selected insulating liquid is suitable for the specific equipment it will be necessary to test its insulating quality. This is verified by stressing the liquid with voltages higher than the partial discharge inception voltage (PDIV). While there are existing tests for these properties, such as use of partial discharge measurements, this thesis examines an experimental approach to testing the properties of different liquids in a point-plane gap through the use of high AC voltage.

Charges, like ions, in an electrical field creates a current flow. In a liquid, dissociative ionization under applied voltage is the mechanism that generates the most charges. Field emission originating from the negative polarity contributes in some liquids. Moving charges in the liquids results in measurable currents of the order 10 - 80 nA under applied AC voltage of 20 kV_{peak} in a 20 mm point-plane gap in different liquids. Space charges are also found to affect the partial discharge (PD) behaviour in liquids. Different liquids have different chemical and physical properties and therefore different PD behaviour. It has been observed that PDs are stochastic, and in some sense correlated to earlier stress due to residual ions from previous half periods and permanently change of the chemical structure of some liquid molecules after a PD. The PD rate increases exponentially with increasing voltage, while the maximum charge per half period tends to increase linearly. This observed behaviour is in agreement with what is found in earlier reports.

The presence of free electrons is important. A significant increase in the rate of PD at low magnitudes in both polarities occurred when the test cell was exposed to X-rays. PDs start under the influence of a strong field or an electron avalanche.

It is essential to be able to test different liquids in laboratory conditions, for economical reasons, in order to identify the most suitable insulating media. Power electronics utilizing quality insulation is more reliable with a lower probability of downtime. The test setup and methods used in this thesis may easily be adapted for test of electrical components and equipment instead of the simple point-plane gap method.

Different liquids have different PD phase patterns. This thesis intends to describe the reasons to explain this difference. It is found to be the result of different properties in the liquids for charge creation and differences in their electrical field threshold for PD initiation. PDs of a certain size are rarely occurring events and are strongly dependent on the prehistory of the stressed liquid gap. We do not know whether PDs in itself is harmful to insulating properties or not. It is therefore uncertain whether the IEC 61294 test method, based on PDs, provides any useful information or not. More research is therefore needed in order to fully understand the PD phenomenon.

Notation

Vectors are represented by **bold** symbols, e.g. the electric field is written by $\mathbf{E}$ and not $\vec{E}$. Units are written normal - V means *volts*, while physical quantities are written in italic, V means the potential.

Important concepts

- *Active volume* - Electrical field region with $E > 0.9E_0$
- *Dissociative ionization* - ionization of neutral molecules caused by a strong electrical field
- *Field emission* - Injection of negative charge from an electrode to a liquid
- *Field ionization* - 'Injection' of positive charge from an electrode to a liquid
- *Heterocharge* - Charge with the opposite polarity as the electrode
- *Homocharge* - Charge with the same polarity as the electrode
- *Inception voltage* - A voltage at which the partial discharges start
- *Liquid bulk* - The volume of the liquid not in contact with the electrode
- *Partial discharge* - Local breakdown in insulating material
- *Space charge* - Charges in the bulk of a liquid
- *Tip radius* - A needle tip is approximated to a half sphere with a radius

Abbreviations

- AC - Alternating Current
- DC - Direct Current
- EHD - Electrohydrodynamics
- HV - High Voltage, i.e. voltages above 1000 V
- HVAC - High Voltage AC
- IEC - International Electrotechnical Commission
- PD - Partial Discharge
- PDIV - Partial Discharge Inception Voltage

Symbols

A list of commonly used physical quantities *A* with common units [unit]

- (η,ξ,ϕ) - prolate spheroid coordinates
- V - potential [V]
- $\mathbf{E}$ - Electrical field [kV/mm]
- $\mathbf{P}$ - polarization density [C/m^2]
- $\mathbf{D}$ - electric displacement field [C/m^2]
- d - gap distance [mm]
- r_p - tip radius [μm]
- σ - conductivity [m/Ω]
- C - capacitance [pF]
- Q and q - charge [pC]
- f - frequency [1/s]
- ω - angular frequency = $2\pi f$ [1/s]
- ϵ_0 - vacuum permittivity [F/m]
- ϵ_r - relative permittivity [1]
- τ - relaxation time [s]
- R - resistance [Ω]
- I and i - current [nA]
- k_D - dissociation rate [1/s]
- k_R - recombination rate [1/s]
- μ - mobility [m^2/Vs]
- c - concentration [mL/L]
- Φ - work function [eV]
- E_f - Fermi energy [eV]
- m - mass [kg]
- ρ - density [kg/m^3]
- v - speed [m/s]

Contents

Chapter 1

Introduction

Electrical devices need to be well insulated in order to operate reliably. The insulation might be any non-conducting material separating the electrical potential from other potentials; i.e. ground and other conductors. When insulation breakdown occur, the device will fail and the manufacturer and end-user will face financial consequences due to down-time or damages caused to the surroundings.

Subsea equipment needs to withstand a pressure of several hundred bar and dielectric liquids are one known reliable insulator suitable for this type of conditions. Liquids fill all voids and are incompressible. Since liquids have good compressibility properties, the surrounding walls can be made thinner and still withstand the outside pressure. On the other hand, gasses are compressed significantly during an increase in the pressure. Therefore, dielectric liquids are superior to gasses in pressurized electronic devices.

Local breakdown, called partial discharges (PDs), cause damage to materials, especially solids which are permanently damaged. On the other hand, fluids are self-healing materials. They will recover to a virgin state a short time after a local breakdown has happened. However, frequent occurrences of PDs gradually degrade and ages the insulation liquid and thus the dielectric and mechanical properties of the insulating material are weakened. This leads to a decrease in lifetime expectancy of the system and failure is more likely to occur.

Fluids have excellent heat transfer abilities, which is needed in order to cool the components and maintain a low operating temperature for the electronic device. These properties make pressurized fluid-insulated systems reliable, meaning that they can operate under pressure for longer periods of time without maintenance.

To maximize the lifetime of a system, it is necessary to have proper test methods in order to distinguish between the long lasting insulating material and the easily degraded insulation material. Methods exist for testing and classifying insulating liquids. The International Electrotechnical Commission, IEC, has developed several methods for liquid insulating testing. For example the IEC 61294 Technical report [1] specify a test method, which is based on the size and occurrence of PDs. However this technical report was released in 1993 and a revision is overdue as new technology and instrumentation is available. In addition, the relevance of this method is questioned for a various reasons. One example is the possibility of statistical fluctuations in the occurrence of PDs. This is

not considered in the test method when the fluctuations are large. It is not certain if PDs are relevant to the evaluation of the lifetime expectancy of an insulation liquid. In order to decide with credibility whether the test method is informative or not, it is necessary to understand more of the physical background for partial discharges in liquid insulation.

To find a correct physical understanding of PDs, one requires a good and representative test model to reveal the relevant parameters. Real electrical devices have a complicated structure and tests have difficulties distinguishing between the different parameters involved. The simplest model uses high voltage in a plane-plane gap. Because this model has difficulties obtaining strong electrical field values, the point-plane model is widely used, Lundgaard and Kyrkjeeide (1994) [2] and Denat (2011) [3]. The point-plane model might be the better representation of impurities in power electronics (sharp edges and needles enhance the field). It also obtains high field values at the point for relatively low applied voltages. The use of square edges, as Tho, Auge and Lesaint (2011) [4] demonstrated, are closer to reality but more difficult to describe. Donzel and Schuderer (2012) [5] studied impurities in power electronics caused in the manufacturing process. All these models might represent power electronic insulation in different ways.

Impurities in electrical devices, such as sharp points or welding residuals, enhance the electric field. A sufficiently strong electrical field that lasts for a certain period of time will ionize the liquid and produce space charges, e.g. low frequency AC or square pulse voltage. Space charges are affected by and contribute to the electric field and possibly also to the generation of PDs, as indicated by Lesaint and Top (2011) [6]. The presence of space charges is confirmed by measuring a conductive current in the gap, as Denat, Gosse and Gosse (1982) [7] have performed. Space charges, given their relationship to partial discharges, need to be studied in order to fully understand aging of insulating liquids.

This thesis is a study of the physics of partial discharges in a point plane gap under High Voltage AC (HVAC). Different insulating liquids will be investigated. The current through the point plane gap and the partial discharge phase-amplitude signature are the most important results to be obtained. Fluctuations in events are common and must be understood. This thesis will investigate whether space charges and PDs are appropriate test parameters for testing insulation liquids.

Chapter 2

Theory

Space charges in liquids are created by several processes when a strong electrical field is applied in the liquid. Charges in electrical fields are transported along the direction of the field. This means that for AC, space charges of alternating polarity, as illustrated in Figure 2.1, are transported into the liquid in a divergent field, e.g. in a point-plane geometry. These charges change the electrical field and thus affect the production of new space charges. In addition, liquids have a certain viscosity and therefore the charge transport is also producing a liquid flow.

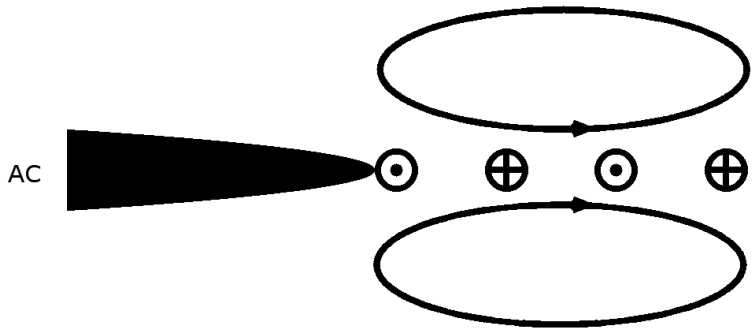

Figure 2.1: Schematics of the main idea behind this experiment under AC. Positive and negative space charges are produced alternately. This creates a liquid flow which makes the space charge distribution unpredictable and field enhancement and field reduction is probable to occur due to homo- and heterocharge.

Partial discharges are related to the electrical field and the presence of electrons. The initiation rate increases for increasing field values above a certain threshold value. Space charges change the electrical field and must be considered when they are present. DC is not tested, due to transportation of space charges from the tip. AC conditions make the space charges stay close to the tip and field change occur.

This chapter is meant to explain the physics behind this idea.

2.1 Point-plane geometry

Point-plane geometry is useful when there is a need for obtaining a localized, divergent, strong electrical field which provides streamers without breakdown. The wire-point might be approximated to a rotational hyperboloid. The Laplace equation in this approximation is separable in prolate spherical coordinates, and is easily solved, Moon and Spencer [8]. The potential over the gap is given by

$$V(\eta) = B \ln \tan(\eta/2) \tag{2.1}$$

and the electric field

$$\mathbf{E} = \frac{1}{a\sqrt{\sinh^2 \xi + \sin^2 \eta}} \frac{B}{\sin \eta} \hat{\eta}, \tag{2.2}$$

where η and ξ are prolate spheroid coordinates, explained in Appendix A. B and a are constants, given by

$$B = \frac{V}{\ln(\tan(\pi/2 - \sqrt{(1 - d/a)/2}))} \tag{2.3}$$

$$a = d + r_p/2 \tag{2.4}$$

where r_p is the point tip approximated radius and d is the point-plane distance. The field along the axis in Cartesian coordinates are given by

$$E_{axis} = \frac{aB}{a^2 - x^2} \tag{2.5}$$

and at the point

$$E_{tip} = \frac{2V}{r_p \ln \frac{4d}{r_p}}, \tag{2.6}$$

where V is the applied voltage across the gap. The field in a point-plane gap is given in Figure 2.2. A visualization of equation (2.5) and (2.6) are given in Figure 2.3 with voltage level V = 20 kV and d = 20 mm. Note the strong field in the area close to the tip.

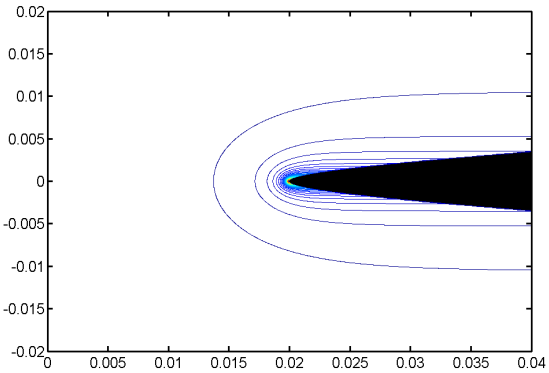

Figure 2.2: Equi-field-lines for the magnitude of the electrical field, note the strong field at the tip.

The sensitivity of the electrical field at the tip is given by

$$\frac{\Delta E_{tip}}{E} = \frac{\Delta V}{V} + \frac{\Delta r_p}{r_p}\left(1 + \frac{1}{\ln\frac{4d}{r_p}}\right) + \frac{\Delta d}{d}\left(\frac{1}{\ln\frac{4d}{r_p}}\right), \tag{2.7}$$

which yields that a small change of 1% in the voltage will change the field with the same magnitude. A change of 5 ± 1 μm of the tip gives 22% change in E and a change of d = 20 ± 1 mm gives 0.5% change in E. This indicates that the field is highly sensitive to changes in the tip radius and not that sensitive to voltage or distance changes. Changes in the tip radius of about 1 μm is most likely to occur due to etching under strong field stress. The other parameters involved have less uncertainty, which means that it is important to check the tip radius frequently in order to have the right tip radius.

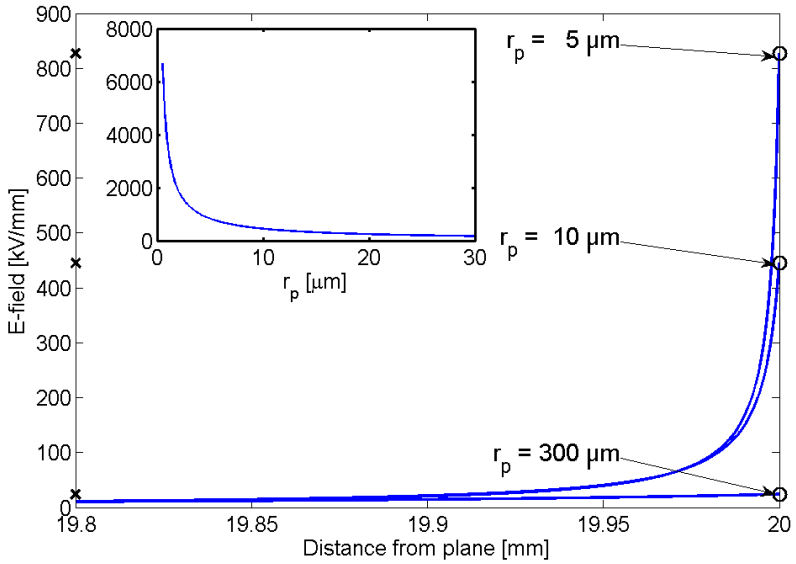

Figure 2.3: The calculated electrical field at the tip of a needle (small picture) and at the axis (large picture), at gap distance 20 mm and voltage peak value 20kV.

An active volume might be defined as the volume with field value above $0.9E_0$. Figure 2.4 illustrates how the active volume change with changing tip radius.

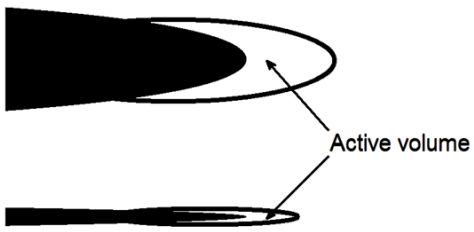

Figure 2.4: How the active volume increases for increasing r_p

2.1.1 Field change

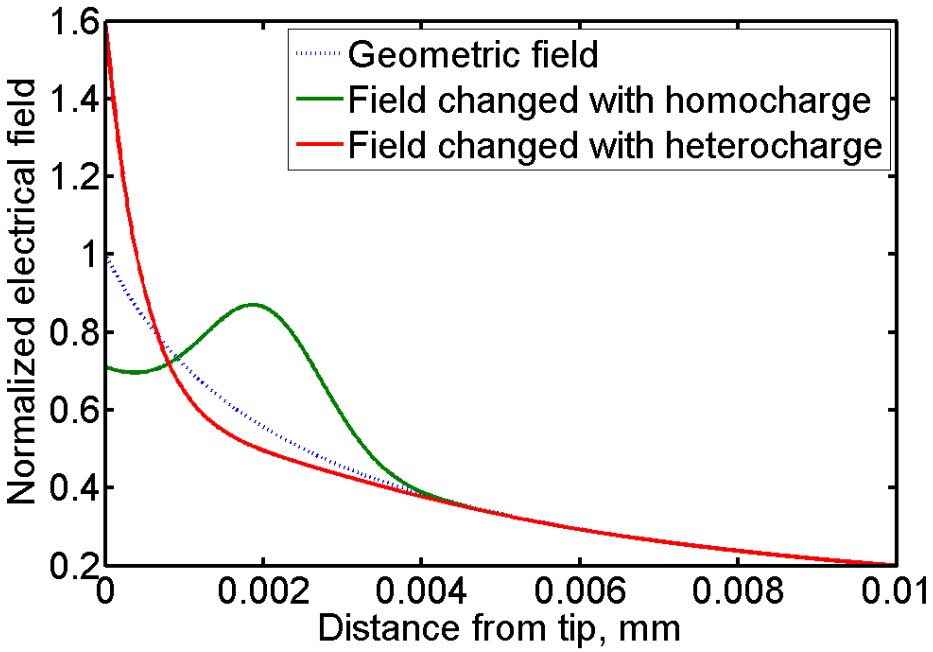

Figure 2.5: Field change with homocharge and heterocharge

Figure 2.5 describes qualitatively how space charges affect the electric field. The maximum electrical field is enhanced with heterocharges, opposite polarity as the electrode, present, e.g. from last half period, and slightly reduced for homocharges, same polarity as the electrode, at the tip, mostly generated in the same half period.

Blocking effects, i.e. covering the electrode by a thin insulating layer, have been studied by Hjortstam et al. [9], both simulations and measurements. Some important results were that blocking of the ionic flow on metal-oil interfaces strongly affects the current by increasing it. This means that charges do shield the electrode, but exactly how is difficult to state.

A field modification in a point-plane gap at the point by space charges have been suggested by Atten et al. [10] in the following formula:

$$E_{th} = \frac{2V}{r_0 \ln(4d/r_0)} - \left[\frac{\eta I}{8\pi\epsilon^2}\right]^{1/2} \int_0^d \frac{g(x)}{[E(x)]^{1/2}} dx \tag{2.8}$$

where g(x) expresses the influence of the charge Q(x) and η the dynamic viscosity. The factor g(x) is difficult to determine and the formula is not useful in practical considerations.

2.2 Space charges and currents in point-plane gap

An electrical current is a measure of the magnitude of the flow of charged particles. Charged particles in the bulk of a liquid (space charges) affect the electrical field and probably the creation of partial discharges. Therefore, it is important to know something about the liquid's ability to create charges, e.g. dissolve and dissociate ions. This leads to an importance of the understanding of the molecular structure and electronic configuration of the liquid, as mentioned by Zaky and Hawley [11].

It has been discovered that carefully purified non-polar liquids have no intrinsic conductivity that might be measured. However, all dielectrics show measurable conductivity [3]. This means that the conductive current should always be possible to measure, but small for purified liquids.

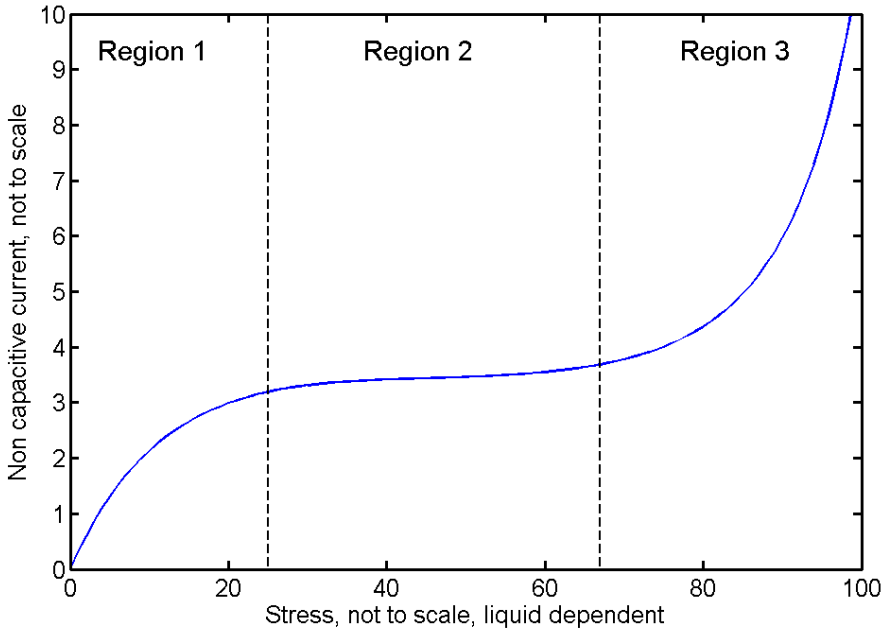

Figure 2.6: General relationship between current and field strength for liquid dielectrics. Region 1: Low stress 'Ohmic region', Region 2: Intermediate stress, Region 3: High stress. Boarder values is different for different liquids

Zaky and Hawley [11] collected data from Nikauradse (1934), Green (1955), Zaky et al. (1963), Kao and Calderwood (1965) for uniform fields, resulting in Figure 2.6. The figure gives relevant information for divergent fields as well, but then only on small scales where the field is approximately constant. The figure is divided into three regions. Region 1 has an ohmic nature and the current increase almost linearly with stress. Region 2 has a saturation current depending on the ion production rate. Region 3 has an approximately exponential shape and indicates new sources of charge carriers. The border between 2 and 3 is unpredictable, depending on several factors such as geometry. Field emission and field ionization might explain the increase in this part of the curve. Table 2.1 summarizes the most important mechanisms.

Table 2.1: Important mechanisms for charge production in liquids, the actual numbers vary for different liquids. Numbers for Cyclohexane presented (from [12])

	E kV/mm	Translated to maximum r_p (20 mm 20 kV)
Dissociative ionization	low	high
Field ionization (positive)	1500	2.5 μm
Field emission (negative)	2000	1.9 μm

2.2.1 Conductive current

All materials have a certain conductivity. A pure conductive current follow Ohm's law (Region 1 in Figure 2.6), combined with Pouillet's law for resistors gives

$$I = \frac{V}{R} = \frac{V}{l/(A\sigma)} = V\sigma\frac{A}{l}, \tag{2.9}$$

where σ is the conductivity, V the voltage, A the area of conduction and l the length of the conductor. Some typical numbers for insulating liquids: $\sigma \approx 3\cdot10^{-11}\frac{m}{\Omega}$, V = 20 kV, l = 20 mm and $A \approx 0.05$ cm^2. To use a plane-plane model as an description of a point-plane geometry is a bad approximation, but it is done to get some numbers to get an idea of a probable upper limit of the size of the current.

$$\begin{aligned} I &< V\sigma\frac{A}{l} \\ &< 20kV \cdot 3\cdot10^{-11}\frac{1}{\Omega m}\frac{0.05\cdot10^{-4}m^2}{0.02m} \\ &< 1.5\cdot10^{-10}\frac{V}{\Omega} \\ &< 0.15nA \end{aligned}$$

The ions mobility μ relates to the viscosity η by Stokes' law (after G. Berg's PhD [13])

$$\mu = \frac{e}{6\pi\eta r} \tag{2.10}$$

$$i = \mu E \tag{2.11}$$

where r is the ion radius, i the current and E the electrical field.

2.2.2 Capacitive current

A capacitor has a capacitance given by

$$C = \frac{Q}{V}, \tag{2.12}$$

with the charge Q and voltage V, which leads to a current

$$I = \frac{dQ}{dt} = C\frac{dV}{dt} = C\omega jV, \tag{2.13}$$

which states that the capacitive current will increase linearly with increasing frequency and with a phase difference of 90°. The expression for the capacitance is *geometrically* determined. This geometrical factor in the capacitance for a point-plane gap is not easily determined analytically.

$$C_{point-plane-gap} = \epsilon_r \epsilon_0 f(r_p, d) \tag{2.14}$$

where $f(r_p, d)$ is a geometric factor and $\epsilon_r \epsilon_0$ is the permittivity of the liquid. A point-plane configuration with d = 20 mm, r_p = 6 μm has approximately a capacitance[1] of 0.1 pF ± 0.01 pF, and it changes slightly with different tip radii and distances.

The capacitive current will therefore be increasing with increasing frequency, and larger for larger relative permittivities. For 50 Hz and V = 20 kV the capacitive current will be of the order

$$I = const \cdot \epsilon_r \omega V = 0.1\text{pF} \cdot 2 \cdot 2\pi \cdot 50\text{Hz} \cdot 20\text{kV} \qquad \approx 628\text{nA}$$

and 0.1 Hz

$$I = const \cdot \epsilon_r \omega V = 0.1\text{pF} \cdot 2 \cdot 2\pi \cdot 0.1\text{Hz} \cdot 20\text{kV} \qquad \approx 1.26\text{nA}$$

The conducting current following Ohm's law is therefore small compared to the capacitive current and can therefore be neglected.

2.2.3 Liquid relaxation and polarization

Polarization in liquids do not happen instantly. It takes some time for the molecules to align with the electric field. Experiments show that the conductive current decreases with time from an initial maximum value to a final equilibrium value. This might take from seconds to hours, [11]. The charge relaxation time $\tau = \epsilon/2\sigma$ (permittivity/low field conductivity) in non polar liquids [3] is a measure on how fast this process is.

There are mainly four different polarization mechanisms, electronic, ionic, molecular orientation and interfacial. The two first mechanisms might be considered as instantaneous and the latter two need some time to become fully polarized.

Electronic polarization is caused by the fact that the electrons orbiting atomic nuclei tend to concentrate on one side of the atom. The electric field momentary make this dipole effect of the atom.

Ionic polarization is when polar materials is affected by an electrical field, they tend to align in the same direction as the field. Negative and positive parts are affected opposite by the electrical field.

Molecules with non-symmetrical arrangement of charge [e.g. dipole] will normally have a randomly distributed orientation in the liquid. An applied electrical field will tend to line up these molecules. Dipoles in liquids will normally quickly align with the electrical

[1] Obtained in this work by manually fitting the derivative of the voltage times the capacitance to the measured current by changing the capacitance

field. Thermal movement will try to maintain disorder and thereby reduce the resulting dipole moment.

Interfacial polarization is mainly due to polarization of impurities and cavities or at interfaces between different insulating materials.

In a parallel plate capacitance, the polarization might be written as

$$P(t) = P_e + P_i + P_d(t), \tag{2.15}$$

where P_e and P_i are momentary electronic and ionic polarization and $P_d(t)$ is the active dipole relaxation mechanism. Debye assumed that the dipole polarization varies in a rate proportional to the deviation from equilibrium $P_d(\infty)$.

$$\frac{dP_d(t)}{dt} = \frac{1}{\tau}\left[P_d(\infty) - P_d(t)\right] \tag{2.16}$$

$$P_d(t) = P_d(\infty)\left[1 - e^{-\frac{t}{\tau}}\right] \tag{2.17}$$

where $\tau = RC = \frac{G}{\sigma} \cdot \frac{\epsilon}{G} = \frac{\epsilon}{\sigma}$ and G is a geometric factor, $G = l/A$ for parallel plane capacitance. The current then becomes

$$i(t) = \frac{dQ}{dt} + \sigma E A \tag{2.18}$$

$$= \left(\frac{dD}{dt} + \sigma E\right) A \tag{2.19}$$

$$= \left(\frac{d(\epsilon_0 E + P)}{dt} + \sigma E\right) A \tag{2.20}$$

$$= \left(\frac{d(\epsilon_0 E + P_m)}{dt} + \frac{dP_d}{dt} + \sigma E\right) A \tag{2.21}$$

$$= \left(J_\delta(t) + \frac{P_d(\infty)}{\tau} e^{-t/\tau} + \sigma E\right) A \tag{2.22}$$

where $J_\delta A = \epsilon_m E \delta(t)$ is the amount of charge momentarily supplied to the capacitance. Figure 2.7 describes this polarization current with a decay time τ.

The connection between electric field and displacement field might be written as

$$D^* = De^{-j\delta} = \epsilon_r^* \epsilon_0 E \tag{2.23}$$

This makes the complex relative permittivity ϵ_r^* to be

$$\epsilon_r^* = \frac{D\cos\delta}{\epsilon_0 E} - j \cdot \frac{D\sin\delta}{\epsilon_0 E} = \epsilon_r{}' - j\epsilon_r{}'' \tag{2.24}$$

where it is common to write

$$\frac{\epsilon_r{}''}{\epsilon_r{}'} = \frac{\sin\delta}{\cos\delta} = \tan\delta \tag{2.25}$$

and $\tan\delta$ is widely known as the loss factor. Due to different phase between the AC-caused $\mathbf{E}$ and the displacement $\mathbf{D}$.

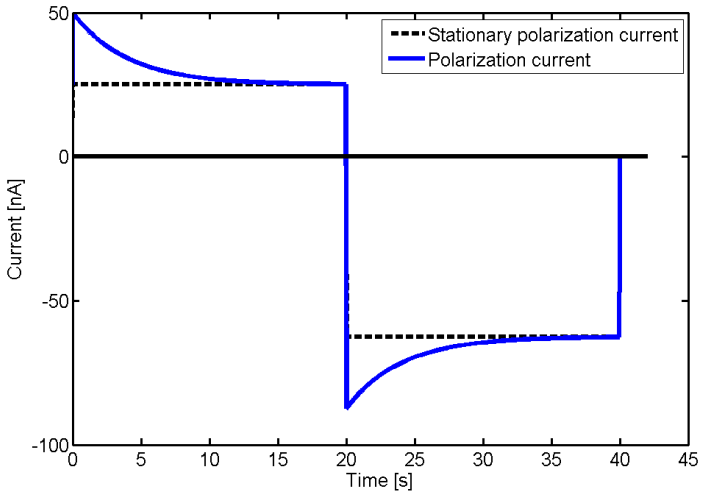

Figure 2.7: Polarization current with a certain relaxation time, based on equation (2.22) .

The effect of frequency

The dipoles have to switch back and fourth when AC is applied. With a certain inertia in the ionic movement, the AC might vary faster than the polarization speed. This implicate that the polarization will decrease for higher frequency.

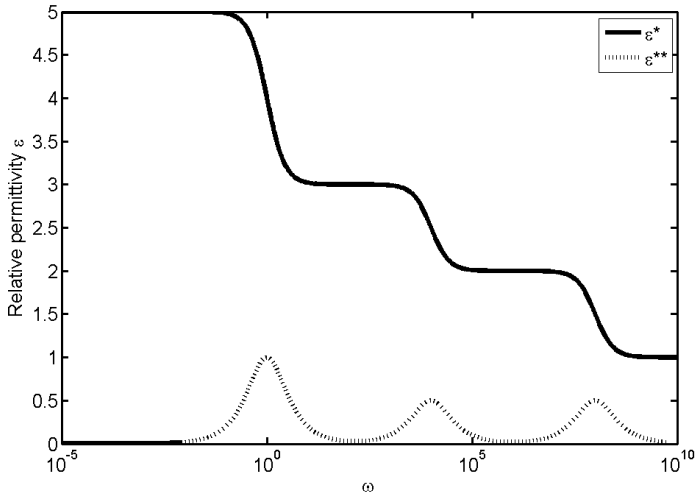

Figure 2.8: Real ϵ^* and imaginary ϵ^{**} part of the relative permittivity as function of frequency with three different polarization mechanisms. Arbitrary units to illustrate the polarization phenomenon.

At low frequencies, all dipoles follow the applied field perfectly, without loss. When the frequency is increased, there will be loss when each polarization mechanism falls behind. In addition, for higher temperatures the polarization process will be slower.

2.2.4 Dissociative ionization

Dissociation and recombination are two important processes acting in liquids in an electrical field. It is relevant for all electrical field ranges, until the liquid is fully ionized and no more ion pairs can be produced. Impurities and additives highly affect these values. As a general rule, solubility of electrolytic impurities increase with liquid permittivity, [3]. In the same way, the concentration of free ions is decreasing with ϵ_r.

Atten [14] has a description of the process. Liquids will always tend to be in equilibrium between molecules and their dissolved ions

$$AB \underset{k_R}{\overset{k_D}{\rightleftharpoons}} A^+ + B^-. \tag{2.26}$$

where the recombination k_R and dissociation k_D rate are given by the conductivity and electrical field

The Langevin approach gives

$$k_R = q(\mu_p + \mu_n)/\epsilon_0\epsilon_r \tag{2.27}$$

where q is the charge, μ is the mobility of positive and negative ions and ϵ the permittivity. The Onsager relation [15] for the dissociation is

$$k_D = k_D^0 \cdot \frac{I_1(4b)}{2b}, \tag{2.28}$$

where I_1 is the modified Bessel function of first kind and $b = \sqrt{q^3E/16\pi\epsilon_0\epsilon_r k^2T^2}$. For weak fields is $k_D = k_D^0$. q is the charge, E the electric field, k Boltzmann's constant, $\epsilon_0\epsilon_r$ the permittivity and T the absolute temperature. This might be asymptotically simplified to

$$k_D(E) \propto k_D(0)e^{\sqrt{\frac{E}{E_c}}} \tag{2.29}$$

where E_c is about 0.24 kV/mm for non-polar liquids at room temperature which implies a strong dependence on k_D for $E > 10$ kV/mm [14]. Translated to tip radius in a point plane gap, this is $r_p < 500$ μm and the electrical field is above 10 kV/mm in a region inside 0.2 mm for all radii below 500 μm. This implies that the dissociative rate k_D will typically be much greater than the recombination rate k_R when an electric field is applied in the point-plane geometry.

From the mass-action law

$$\frac{d[A^+]}{dt} = \frac{d[B^-]}{dt} = k_D[AB] - k_R[A^+][B^-] \tag{2.30}$$

$$\frac{dc_p}{dt} = \frac{dc_n}{dt} = k_D c - k_R c_p c_n, \tag{2.31}$$

where c, c_p and c_n are the concentrations of the dissociable molecules, the concentration of the positive ions and the concentration of the negative ions. This equation describes the dynamics of the concentrations, and under AC this will most likely not be in equilibrium.

The the concentration of ions are given by Denat [3]

$$n_{ions} = \frac{0.5}{k_r \tau} \tag{2.32}$$

$$n_{ions} = \frac{0.5}{k_r} \frac{\sigma}{\epsilon} \tag{2.33}$$

$$n_{ions} = \frac{\sigma}{\epsilon k_r / 0.5} \tag{2.34}$$

$$n_{ions} = \frac{\sigma}{q_e \mu_{ion}} \tag{2.35}$$

$$n_{ion^{\pm}} = \frac{0.5\sigma}{q_e \mu_{ion^{\pm}}} \tag{2.36}$$

which is about $n_{ion} \approx 10^{15}$ for typical values.

When the electric field is strong enough, the liquid is ionized in a small region around the tip. The charges will then form a current and is described by Corona current that follows the empirical formula, found by Townsend [16]

$$I = A(\mu) \frac{V(V - V_0)}{d} \tag{2.37}$$

where V_0 is the corona onset voltage, μ the dominant ion mobility, d is the gap width and $A(\mu)$ is a geometrical factor which cannot be easily calculated.

2.2.5 Electrode effects: Field emission and field ionization

Electrode effects happen at sufficient strong electrical fields. Electrons might pass from the metal to the liquid in *field emission* at the cathode, or tunnel from molecules in the liquid to the anode in *field ionization* at the anode. Figure 2.9 describes both field emission and field ionization at the border between liquid and metal.

Lewis, [17], assumes that electrons are transported from the liquid to the anode neutralizing a 'hole' in the metal and creating a hole in the liquid.

There is an energy barrier at the interface between a fluid and a metal. This energy barrier is lowered by an electric field,see Figure 2.9. The field emission effect is given by the Fowler Nordheim model

$$I = \frac{e^3 E^2}{8\pi h \phi} \cdot \exp\left(-\frac{4}{3} \sqrt{\frac{2m}{h^2}} \frac{\phi^{3/2}}{eE} \right) \propto E^2 \exp(-\alpha E^{-1}) \tag{2.38}$$

where e is the electron charge, h Plank's constant, $\phi = \Phi - E_f$ the difference between the work function and the Fermi energy of metal and m the electron mass. This mechanism is important for strong fields (> 1500 kV/mm), [12]. The constant α is different for field emission and field ionization.

Field emission is usually regarded as more probable to happen than field ionization. This might be easily deduced from the fact that there is an abundance of electrons available in the cathode and bound electrons in the liquid. Even if one electron has a larger probability for tunnel to the anode than from the cathode, the great difference in number of electrons available makes the total expected value for electron movement largest at the cathode.

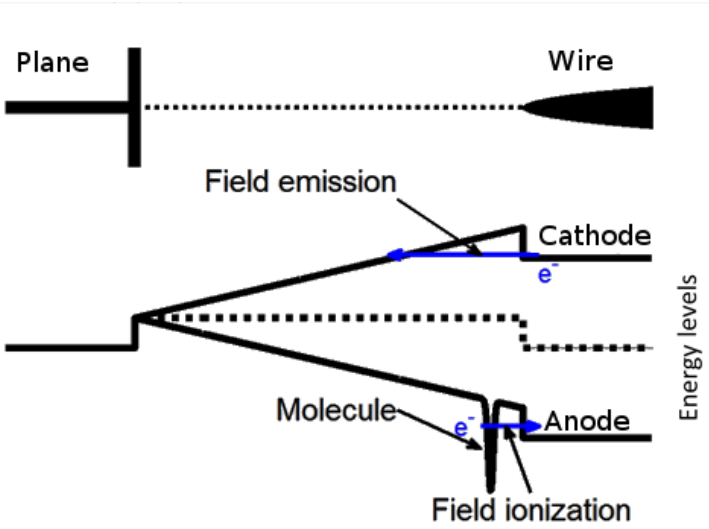

Figure 2.9: Schematics of the conducting level of energy barriers with applied field along the axis of the point plane. Field emission and field ionization happen when an electron manage to tunnel through the energy barrier.

2.2.6 Space charge limited current

Ion mobility is low in dielectric liquids. This leads to a limited current compared to what is expected in gasses. Space charges in a *plane-plane* gap contributes to the total current by the *Space charge limited current formula* [13]

$$j = \frac{9}{8}\epsilon\mu\frac{V^2}{d^3}, \tag{2.39}$$

where j is the current density, $\epsilon = \epsilon_r\epsilon_0$ the permittivity, μ the mobility, V the applied voltage and d the gap distance. This leads to $I \propto V^2$. A charge density ρ_0 of residual ion pairs lead to a current density of

$$j_0 = \rho_0\mu\frac{V}{d}, \tag{2.40}$$

where the symbols are as before. If equation (2.39) and equation (2.40) are compared, the residual ions dominate if

$$\frac{d^2}{\mu V} > \frac{\epsilon}{2\rho_0\mu} = \frac{\epsilon}{\sigma}, \tag{2.41}$$

$$\frac{d^2}{V} > \frac{\epsilon\mu}{\sigma} \tag{2.42}$$

where σ is the conductivity of the dielectric. This means that space charges dominates if the inequality in (2.42) has opposite direction, with typical numbers that vary slightly between liquids

$$\frac{0.02^2}{20\cdot 10^3} \leftrightarrow \frac{2.2\cdot 8.85\cdot 10^{-12}\cdot 10^{-7}}{3\cdot 10^{-11}}$$
$$2\cdot 10^{-8} \leftrightarrow 6.49\cdot 10^{-8}$$

which states that both space charges and residual ions will contribute in the area of interest. The space charges dominate if the liquid has less conductivity than this upper limit.

These formulae are derived for plane-plane gaps. They do not give the accurate solution for point-plane gaps, but can be used as an indicator for which processes might be important.

2.2.7 Shockley-Ramo theorem

Charges with a velocity $\mathbf{v}$ induce a current in wires between electrodes. Or the other way around, a current might be used to deduce the movement of charged particles. The Shockley-Ramo theorem gives the relation between induced current and the velocity of the moving particles, after Sigmonds explanation in [18] of Ramo [19] and Shockley [20].

$$I(t) = -\sum_k q_k \mathbf{v}_k(t) \cdot \mathbf{E}_k(\mathbf{r}_k(t)) \tag{2.43}$$

where q_k[C] is the charge of particle k, $\mathbf{v}_k(t)$[m/s] the velocity of particle k and $\mathbf{E}(r_k)$ [(V/m) /V] the electric field obtained when raising the voltage by one volt.

The theorem assumes that only charge k is moving when summing, that means that all the other charges are assumed to be stationary causing a stationary electrical field. Because the electrical field is additive, there is possible to add all contributions to the current from each 'source' of potential.

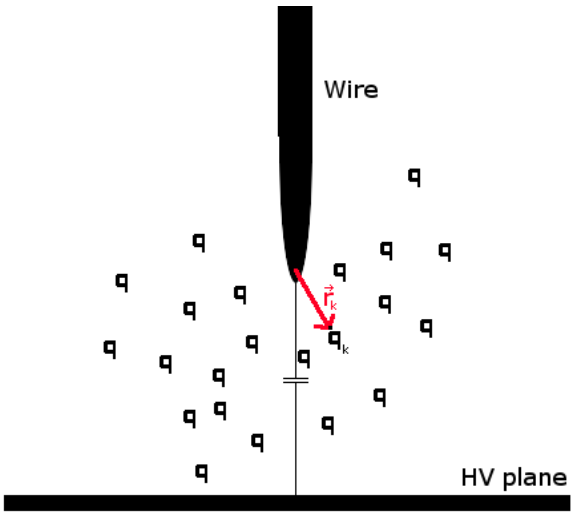

Figure 2.10: Illustration of the Shockley-Ramo theorem

From the Shockley-Ramo theorem, equation (2.43), it can be deduced that only the charges in the region near the tip, which affect the current. The current is proportional to the product of velocity and the local electrical field. The electrical field is rapidly decreasing for increased distance from the tip, and if the speed is considered constant (or larger in a region near the tip), the result from the Shockley-Ramo theorem is that the current from charges are proportional to the electrical field. This means that only charges in the region near the tip contribute to the current.

2.2.8 Electrohydrodynamics (EHD)

Molecules in a viscous liquid stick together and couple in a liquid flow, opposite to in a gas where the molecules travel almost unaffected by each other. Ions follow the flow like the other molecules, rather than the theoretical movement created by the electrical field. This let the tip make a liquid jet. It might be turbulence or laminar flow. This will strongly affect the conductive current.

EHD mobility with typical values, density as for water and permittivity approximately as for insulating liquids

$$\begin{aligned}\mu &= \sqrt{\epsilon/\rho}[\mathrm{m}^2/\mathrm{Vs}] \\ &\approx \sqrt{2 \cdot 8.85 \cdot 10^{-12}/1000} \\ &\approx 1.33 \cdot 10^{-7}\end{aligned}$$

Coelho and Debeau [21] solved the transit time in a point plane gap with DC. This yields

$$T = \frac{a^2}{\mu B}(\cosh^2 \xi - 1/3) \tag{2.44}$$

$$T_0 = \frac{2a^2}{3\mu B}, \tag{2.45}$$

where μ is the mobility, $a = d + r_p/2$ and B is given as earlier described in Point plane geometry, $B = \frac{V_0}{\ln \tan\left(\frac{\pi}{2} - \sqrt{\frac{(1-d/a)}{2}}\right)}$. T_0 is along the axis, i.e. the shortest way. With typical numbers for a configuration, d = 20 mm, r_p = 5 μm, V_0 = 20 kV and $\mu = 10^{-7}$ m^2/Vs the transit time is 0.6455 s, which corresponds to a frequency of

$$f_0 = \frac{1}{2 \cdot 0.6455} = 0.78\mathrm{Hz} \tag{2.46}$$

which means that charges in a field with frequency below this have the possibility of reaching the other electrode and neutralize. The speed of the liquid v is given by

$$v = \mu_H E, \tag{2.47}$$

where μ_H is the electro hydrodynamic mobility and E the electric field.

If the liquid has $\mu_H > 1\frac{m^2}{Vs}$ then the ion drift velocity is than the liquid velocity and the ions are transported along the flow they induce. This happens for weak fields, and similarly for strong fields when the drift velocity of the ions is higher than the viscous velocity.

Electrohydrodynamic plumes, see Figure 2.11 are thin and have a high velocity gradient and unsteady character [10]. This will make the space charges move most unpredictable and the space charge distribution will be impossible to determine. Since space charges affect the total field, the field in the liquid bulk is unknown on a detailed level.

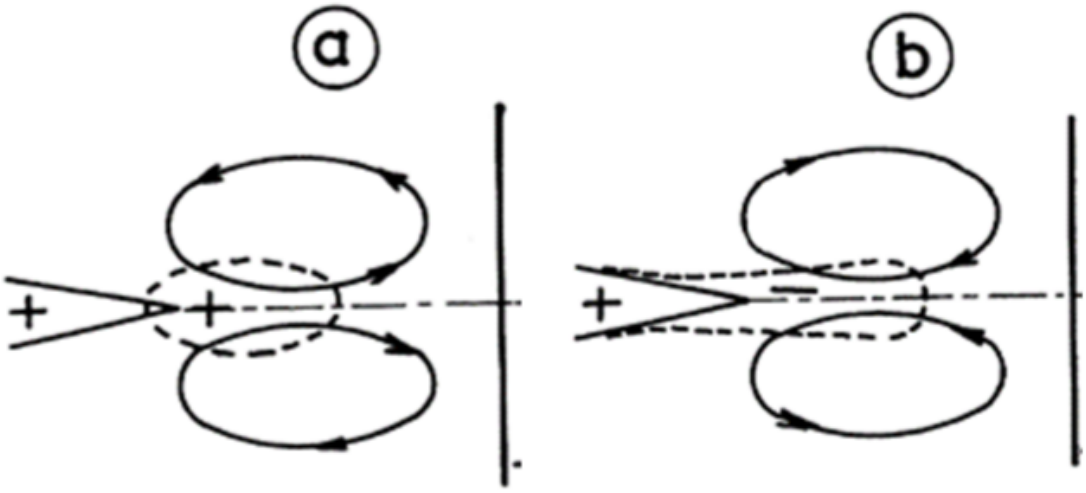

Figure 2.11: EHD in liquids, [22]: Schematic representation of (a) injection by the wire and (b) constant rate dissociation with no injection

2.3 Partial discharges

Discharges cause degradation of the insulation and might cause breakdown over time. When a discharge does not create an arc between two conductors, it is called a partial discharge (PD). The increased concentration of charges heat the insulation slightly and may form micro-bubbles, [23], or electron avalanches. PDs are likely to occur in the micro-bubble due to weaker insulating properties in gas or a created avalanche. This decrease the insulating effect and may therefore degrade the liquid

Liquids are self-healing, which means that the micro-bubbles, in which the PD occur, collapse right after the PD has vanished. The liquid reach virgin state right after PDs have disappeared.

PDs in liquids are random phenomena. A typical PD pattern under AC, see Figure 4.20a, might be considered as a probability distribution of PDs. It is a typical phase-amplitude PD pattern showing PD occurrence rate in an amplitude vs phase plot, colours denote occurrence rate. The figure is included to qualitatively show how the pattern looks like. It is noteworthy that there are many small negative PDs and a few large positive PDs. The figure describes that the PD phenomenon is asymmetric.

Multiple PDs might be observed in succession. They create 'bushes'. Based on the measurement of light emission, Lundgaard and Kyrkjeeide [2] made a hypothesis that the liquid is gradually charged by multiple small negative discharges until the field has exceeded the inception field for positive PD. The exact processes causing PDs in liquids are still undiscovered.

2.3.1 Stochastic phenomena in partial discharges

Partial discharges in gasses need start electrons to ignite. These start electrons occur stochastically and might be affected by (from [24]) injected electrons depending on an electric field, dynamics of surface charging, growth rate of cavities in liquids, discharge

generated space charges of metastable molecules, fluctuation in gas density, presence of ionizing radiation and memory propagation from previous PD pulses. All these factors have a stochastic nature. van Brunt and Kulkarni (1990) [25] have demonstrated a non-Marcovian behaviour of PD occurrence in gasses. In liquids it is yet to be investigated.

The two most important electron providing mechanisms, field emission and field ionization, are only properly described by quantum mechanics. Fowler and Nordheim [26] used quantum mechanics to derive the relations for field emission. Quantum mechanics is totally stochastic and therefore phenomena directly affected by it must be stochastic.

A general connection between the generation of electrons, collisions and PDs in gasses was found by Laue [27] who discovered that the statistical time lag of a PD sequence follow a Poisson distribution.

$$\frac{n(t)}{n(\infty)} = e^{-R_e(\Delta V)P(\Delta V)t},$$

where $\frac{n(t)}{n(\infty)}$ is the fraction of PDs with delay time greater than t, R_e the rate at which the electrons are released into the strong field regions and $P(\Delta V)$ the probability for one electron to create a PD. $\Delta V = V - V_s$ where V_s is the onset voltage. This formula only works for non-memory negative PDs. It is common to describe PDs to happen inside small gaseous bubbles in the liquid and thereby the gas theory for initiation might be used.

PDs might be correlated to each other over a long time. van Brunt et al. [28] found that memory effects play an important role for PDs in gasses. The occurrence of PD pulses in a positive half cycle influences the initiation and development of PD pulses in the subsequent negative half cycle. There can also be significant memory propagation from one event to the next within a given half cycle. Metastable molecular species generated by a PD might remain a long time. PDs might create space charges and direct release of electrons.

Geometric distribution

The PD phenomenon is discretized when it is divided into half periods. A geometric distribution can be used to describe the process. For continuous cases, it is common to use the exponential distribution. The geometric distribution yields

$$P(X = k) = (1 - p)^k \cdot p \tag{2.48}$$

where p is the inverse expectation value and k is the period number. The expectation value is known to be $E(X) = \frac{1}{p}$ and the variance $Var(X) = \frac{1-p}{p^2}$. The probability p might be found, using the estimator $\hat{p}$

$$\hat{p} = \frac{n}{\sum_{i=1}^{n} k_i} \tag{2.49}$$

where n is the total number of events and k number of periods to next event.

The geometric distribution is the discrete version of the exponential distribution. The exponential distribution describes the time between events in Poisson distributions. Known processes which follow a Poisson distribution are radioactive decay, telephone calls etc.

Low level counting Poisson statistics

Nuclear Physics - Principles and Applications, [29], has a chapter on low level counting. Uncorrelated radioactive decay and uncorrelated PD rate both follow Poisson statistics and are both dependent on random events.

Rarely occurring events are hard to describe. Even if tests give a null result, there is a probability of events. In Poisson statistics, the probability of detecting n events are given by

$$P(n) = \frac{\mu^n e^{-\mu}}{n!} \tag{2.50}$$

$$P_0(T, \lambda) = e^{-\lambda T} \tag{2.51}$$

where μ is the mean value, λ is a mean occurrence rate and T is the recording time. The mean number of events in the interval is then $\mu = \lambda T$. The probability for the rate λ to be less than a certain chosen value λ_0 is then

$$\begin{aligned} P_0(T, \lambda \leq \lambda_0) &= \frac{\int_0^{\lambda_0} P_0(T, \lambda) d\lambda}{\int_0^{\infty} P_0(T, \lambda) d\lambda} \\ &= 1 - e^{-\lambda_0 T} \end{aligned}$$

Rearranging

$$\lambda_0 = -\frac{1}{T} \ln(1 - P_0(T, \lambda \leq \lambda_0)) \tag{2.52}$$

And with a certainty of 90% of a rate below λ_0

$$\lambda_0 = -\frac{1}{T} \ln(1 - 0.9) = \frac{2.3}{T}$$

or 99%

$$\lambda_0 = -\frac{1}{T} \ln(1 - 0.99) = \frac{4.6}{T}$$

For $5 \cdot 120$ s = 600 s one can be 90% sure the rate is below 0.0038s^{-1} and 99% sure the rate is below 0.0076s^{-1}.

2.3.2 Effects of geometry

A plane-plane gap has a uniform electrical field and the field values are therefore relatively low. There is no field enhancement except from impurities detaching at the surface. The point-plane geometry has a divergent field distribution and thereby the ability to reach high electrical field values in the bulk of the liquid for the same voltages as in plane-plane. Sharp points and edges cause field enhancement and strong field phenomena happen in these regions. The geometry is therefore of great importance due to a direct connection between the geometry and the field distribution.

Sharp edges and sharp points creates strong electrical fields. This makes the PD pattern sensitive to the tip radius in a point-plane gap. With small electrode separations, the

large positive discharges result in breakdown, [2]. When the liquid has low speed and AC voltage is applied, the charges will stay close to the tip. Thus, the tip might be shielded and strongly affected by space charges. If the electrons are easily detached, the conditions are favourable for electron avalanches. This may explain the occurrence of the large positive PDs.

Streamer inception frequency increases with decreasing tip radius, [6]. For all radii, the inception frequency increase exponential as a function of the voltage applied. A single field value for inception frequency does not exist; it is dependent on the tip radii. This means e.g. different *active* volumes at the tip.

Dielectric strength of a liquid gap E_{BD} has been found by Ziodla et al. to be a power function of the equivalent volume [30].

2.3.3 Effects of voltage form steepness

The formula for the electrical field is linear to the voltage, equation (2.6). It is found that streamer inception increases exponentially versus the field [6] [and thereby the voltage].

In [6] Lesaint and Top list a number of factors which contribute to streamer inception, among them is injected space charges which reduce the electrical field by homocharge and increases the field with heterocharge. A steep voltage rise will therefore not manage to transport space charges away from the tip before the maximum value is reached. A slowly rising voltage has time to transport space charges and affect the PD inception with different dynamics.

When the voltage is increased, the field is also increased. This means that the liquid is stressed to a higher level and ionization and formation of small bubbles are more likely to occur.

2.3.4 Effects of chemical additives

Ingebrigtsen et al. [31] reported that different electronically active chemical additives affect streamers in a different way. E.g. some additives will only affect the positive polarity, some only affect the negative polarity, some both and others have no effect. This is due to the different properties of the additives and possibility for ionization. Avalanches propagate faster and further in the presence of electron scavenger additives as compared to dried and degassed cyclohexane.

Figure 2.12 clearly shows that an increase in the concentration of N,N-dimethylaniline changes the streamer shape, and thereby the current and degradation of the liquid. This experiment were performed with impulse and no space charges were present.

Not all additives affect the streamer process. Those with properties close to the liquid itself will not change the electrical properties notably, [32]. Conductive currents to a point anode in cyclohexane increase with the low ionization potential additives 1-methylnapthalene and N,N-dimethylaniline, [32].

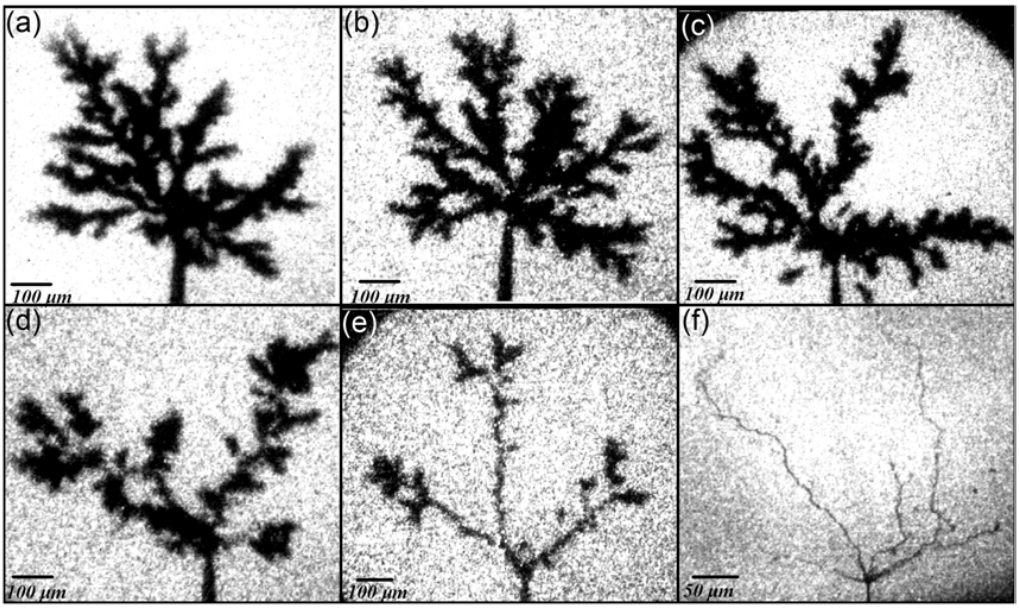

Figure 2.12: Figure from [32]. Shadowgraphic images of point anode streamers in cyclohexane with additive N,N-dimethylaniline for an applied voltage V = 16 kV, (a) from bottle, (b) dried/degassed, (c) 0.1 mg g^{-1}, (d) 1.0 mg g^{-1}, (e) 10 mg g^{-1}, (f) 50 mg g^{-1}.

Lesaint and Top discovered that additive effects are dependent on geometry as well as the additive itself, [6]. The high concentration of additives affected the larger tip radius of 8 mm more than the smaller radius of 10 μm.

2.3.5 Effects of moisture

Figure 2.13 indicates that the different ability of moisture absorption is important. Midel 7131 has a very high moisture absorption, and large amounts of water will not reduce the breakdown voltage. The graph changes if relative moisture is used instead of absolute moisture. Then all liquids align in almost the same way.

Dielectric strength decrease as relative humidity increase. Bubble formation appear at lower temperature in a moist area. Free water particles might form when cooling the moist liquid. Water has much lower breakdown strength than insulating liquids. Free water must therefore be avoided. The relative humidity is therefore important.

2.3.6 Streamer initiation

Jones and Kunhardt [33] have suggested a series of events to explain the pulsed breakdown of liquids: It first starts with field emission. This leads to liquid heating and nucleation process, which again leads to a phase change and evaporation of the liquid. Avalanche discharge happen in the vaporized liquid and an ionizing front develops (streamer), which might lead to breakdown.

Streamer inception is a statistical process because it depends on several random processes, e.g. ion collision and cosmic radiation. The streamer inception voltage is therefore never

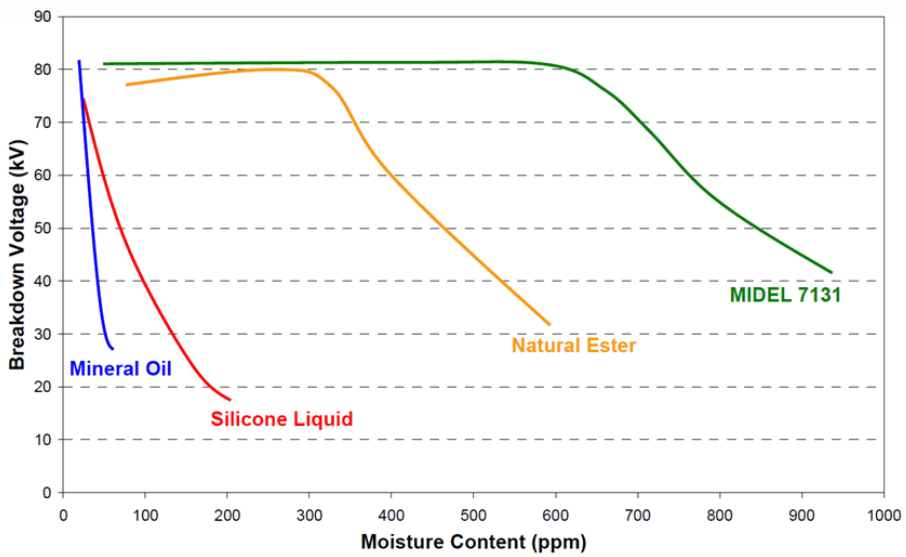

Figure 2.13: Breakdown voltage vs moisture content at 20°C. Figure from Midel7131 data sheet

the same in different experiments.

If sufficient energy is developed locally to vaporize the liquid, discharges may occur in the vapor cavity and streamers develops, [34]. On the tip of the point electrode one usually defines a critical volume where the electric field strength will be adequately high over a distance large enough to develop an avalanche above a critical size, [35].

Lesaint and Top conclude in their study [6] that the maximum field strength is a good parameter to describe streamer inception in point plane geometry. This is concluded on the fact that their results for different tip radii and distances group together to form a unique plot. The exponential inception increase with voltage seen in all radii might prove the initiation process to be the same in all cases. A single field value do not exist to describe streamer initiation, due to geometry dependence.

2.3.7 Propagation of streamers

After a streamer is initiated, it propagates. Cavities form at the electrode, induced by a fast electronic avalanche in the liquid phase [36]. The streamers are known to have several modes, with different speed: For instance a slow mode < 200 m/s and a second mode > 1 km/s

Streamers in moderately divergent fields will lead to breakdown because the field is almost uniform, and the streamer is maintained. On the other hand, in divergent fields, the streamers appear, but do not need to propagate to breakdown due to relative low field strength in the propagation area.

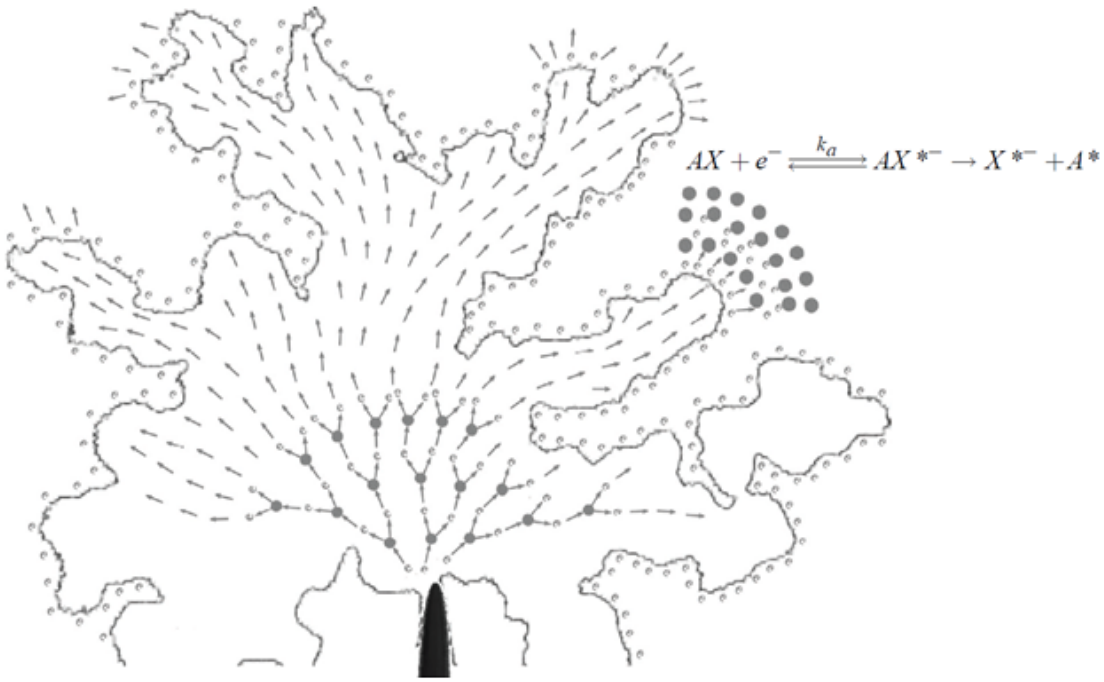

Figure 2.14: An illustration of streamer propagation, Ingebrigtsen PhD [37]: The propagation of slow negative streamers occurs via repetitive partial discharges in a gaseous void (contour-line). Electrons produced by the electron-avalanches in the gas bombard the liquid in front of the cavity, thereby inducing local vaporization by inelastic collisions, as well as electrohydrodynamic instabilities. The accumulation of charge at the gas-liquid interface also influences the field distribution in the void.

2.3.8 Stopping of streamers

The electrical field in a point-plane geometry is highly divergent. This allows the field fall below the propagation magnitude of the streamer and thus it is quenches.

A larger discharge and streamer will last longer than a smaller discharge. Typical numbers are 1 pC last for less than 1 μs and >1μC last longer than 100 μs. During the propagation of large streamers, a large number of fast current pulses are detected. This might lead to a considerably overestimate of the number of events, [6].

2.4 Test method according to IEC 61294

IEC 61294 Technical report test method [1] describes a PDIV-test on liquids. The IEC 61294 requires a test cell containing a point-sphere electrode gap about 50 mm ± 1 mm with a volume of about 300 ml. The sphere diameter should be between 12.5 mm and 13 mm and the tip radius of the point electrode should be 3 μm. The liquid should rest for 15 min after filling and before applying voltage.

The test circuit should provide AC voltage with a frequency between 48 Hz and 62 Hz. A constant increase of 1 kV/s in the voltage from 0 to 70 kV should be applied on the liquid to record the voltage at which a PD occurs of apperent charge equals to or greater

than 100 pC. Ten PD inception voltage (PDIV) measurements are made on each of two different fillings of the cell. The average of the two results is taken as PDIV of the liquid tested.

Some improvements for IEC 61294 are suggested in [38].

Chapter 3

Method

The tests performed have been chosen in order to be able to investigate the mechanisms governing PDs in liquid insulation and thus be able to explain why or why not the test methods described in IEC 61294 are suitable to use for classification and approval of liquid insulation.

PDs and conductive currents have been investigated in a point-plane gap using high voltage AC. An automatic data recording system for PD, Omicron MPD 600, and a high resolution four channel digitizer, Gage-oscilloscope, are used to measure the PDs and the current, respectively.

The point-plane gap was chosen in order to model impurities or sharp edges in electrical devices, which enhance the electrical field. IEC 61294 requires a point-*sphere* gap, but the point-plane has an electrical field distribution that is known and therefore preferred when studying the PD mechanisms. In addition, with a localized strong electrical field it is possible to localize the PDs. The measuring equipment were sensitive to electrical interference caused by the light switch in the room due to induction into signal cables. The test cell, Figure 3.1 was therefore placed in a Faraday cage in order to shield it properly from the surroundings. A voltage up to 22 kV was applied to the top and bottom electrode and controlled by the test setup.

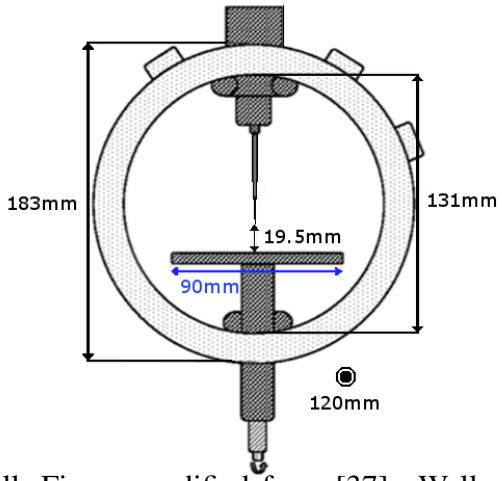

Figure 3.1: The test cell, Figure modified from [37]. Walls of Teflon covered with a conducting layer. Conducting parts of stainless steel. Glass at front and back and a round plane.

3.1 Setup

A tungsten point/wire electrode was used in the point plane gap, tip radius ≈ 5 μm and diameter 100 μm. When etched, it might be approximated to a rotational hyperboloid at the tip, see Figure 3.2. The tip radius was measured frequently, due to the crucial importance of knowing the tip radius and thereby know the electrical field. The radius was measured with a microscope connected to a computer. Carl Zeiss MicroImaging GmbH equipment with AxioVision softqare and AxioCam MRc5 camera connected to a Discovery V12 SteREO microscope 12-150x zoom.

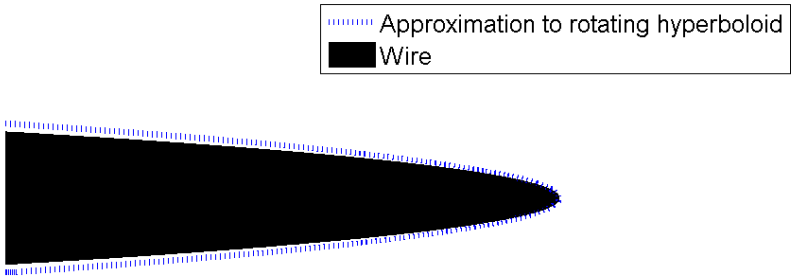

Figure 3.2: The tip approximated to a rotational hyperboloid

The tungsten wire was placed in a configuration shown in Figure 3.3 which gives the ability of shielding the wire from the surrounding ground and reduce noise.

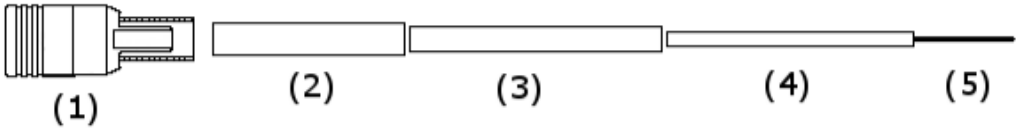

Figure 3.3: Design: L.Lundgaard, G.Berg (2002). Configuration of the needle used: (1) Huber Suhner 11 SMB-50-2-41/111NE (2) threaded steel tube, (3) insulating plastic tube, (4) Teknolab chromatograph needle, (5) electrochemically etched tungsten wire Ø100μm.

Figure 3.4 describes the experimental setup. A signal generator, Wavetek 187 pulse/function generator, is used to produce different AC signals, such as sine, triangle and different forms for square wave. The signal generator is able to generate frequencies from 0.06 Hz to 40 000 kHz. The signal generator gives a signal of ± 10 V. (with rise times of 0.01 ms)

The signal is amplified 2000 times by a Trek 20/20C-HS high voltage amplifier with good amplification specifications (slew rate 800 V/μs [specification] and observed 400 V/μs yields 100μs rise time on 40 kV peak-peak)

The high voltage signal is connected to the plane in a point-plane configuration. The gap in the test cell is filled with insulation liquid for testing. The point is obtained by a wire with approximately parabolic shape with a tip radius of about 4 μm to 9μm depending on the use. When used, the tip radius increase due to electrochemical etching of the wire in strong field areas.

List of elements:

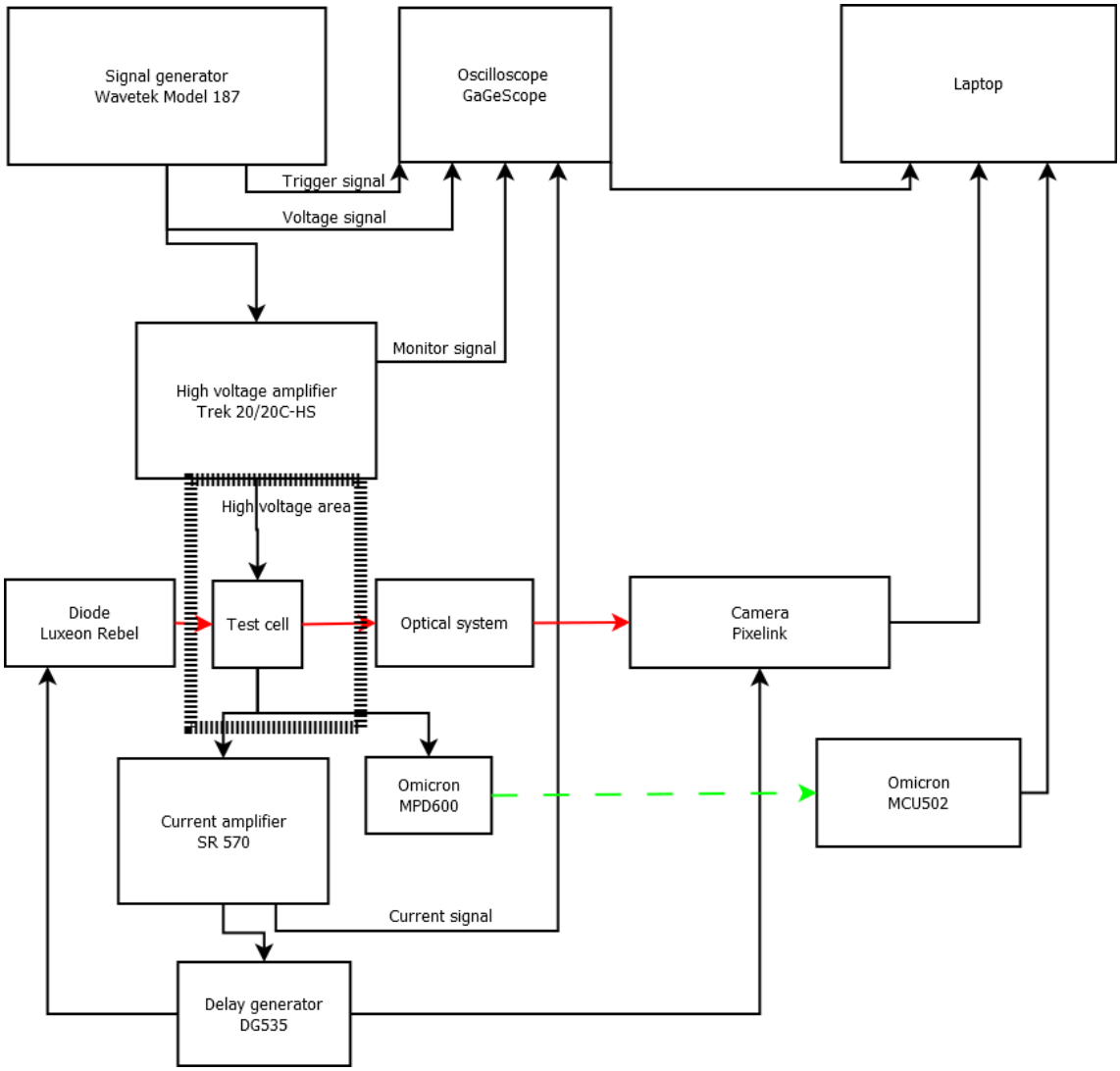

Figure 3.4: The test setup; black arrows are coaxial cables, red arrows are light and green dotted arrow is optical cable.

- Signal generator, Wavetek Model 187
- Oscilloscope, Gagescope
- Laptop
- High voltage amplifier, Trek 20/20C-HS
- Current amplifier, Standford Research Model SR 570
- Delay generator, Standford Research Model DG 535
- Automatic discharge acquisition system, Omicron MPD600 and MCU502
- Camera, Pixelink
- Diode, Luxeon Rebel
- Test cell
- Optical system, lenses from Edmund Optics

The current from the grounded wire goes either to the automatic discharge acquisition system Omicron MPD 600 and MCU 502 *or* Standford Research SR570 current amplifier and then finally to a Gage oscilloscope. A delay generator, Standford Research DG 535, was connected to the current amplifier and was triggered by the PD pulse. The delay generator provided delayed signals for the diode and the camera. The diode, mounted on a LDP-V pulsed laser diode driver module from Schulz Electronic, and the camera was delayed long enough so that the streamer had reached its maximum value in such a way that a picture of the full size streamer was obtained.

A phase-amplitude plot or time sequence was obtained from Omicron. The oscilloscope is able to produce data to find the conductive current.

The signal generator does not produce a pure sine wave. There is a discontinuity in the derivative at the top of the sine wave. This is handled by simulating the capacitive current as the derivative of the voltage times the capacitance.

3.1.1 Oscilloscope

A 14 bit oscilloscope, GageScope, provides excellent resolution both in time and amplitude. This makes it possible to derive the signal and get the capacitive current from the voltage. With less resolution, the derivative would be inaccurate and the signal processing would be impossible. The conductive current is less than 10% of the total current for high frequencies which leads to the signal being masked by the noise level.

3.1.2 Discharge acquisition system

The discharge acquisition system Omicron, Model MPD600 and MCU502, has the possibility for measuring over longer time periods than the oscilloscope. It makes it possible to increase the time scales and do statistics. Omicron mtronix is a commercially available measuring equipment to measure PDs out in the field. It measures current and derives charge via numerical integration. It is optimized to get the accurate number and size of the partial discharges, although, it has some known weaknesses. The frequency integration function do not choose the right polarity of the PDs in liquids. But the error might be as low as 0.5 pC which is not reached in the time domain. In the time domain, the integration must be performed for several microseconds in order to record the whole sequence of partial discharges. They often occur in ascending order or trains over several μs. One drawback with this long integration time is that the capacitive current is measured as PDs at a level of 10 pC for 100 Hz.

3.1.3 Shadow graphic imaging

The blitz and camera are triggered by the start of the PD current signals. The signals are delayed with a delay generator, Standford Research Model DG535, which has adjustable delay time. The delay time was adjusted to hit the maximum length of streamers. The shadow graphic imaging is just a projection of streamers, not possibly representative for the length. It is a projection in the plane perpendicular to the optical axis.

Streamers have a lower refractive index than the liquid due to differences in the conducting volume. This leads to deflection of any light passing. A background light-source will therefore provide light to make a shadow of the streamer.

A Pixelink CMOS camera (1392 × 1040 pixels) is used with pixel size of 4.65 μm × 4.65 μm. The sensor area is then 7.60 mm × 6.20 mm. With the lenses described in Figure 3.5 and a magnification of 8, each pixel captures an area of 0.5813 μm × 0.5813 μm.

Figure 3.5 illustrates how the different optical components were placed in order to obtain a proper magnification of the tip and streamer. Several rays are drawn to clarify the idea.

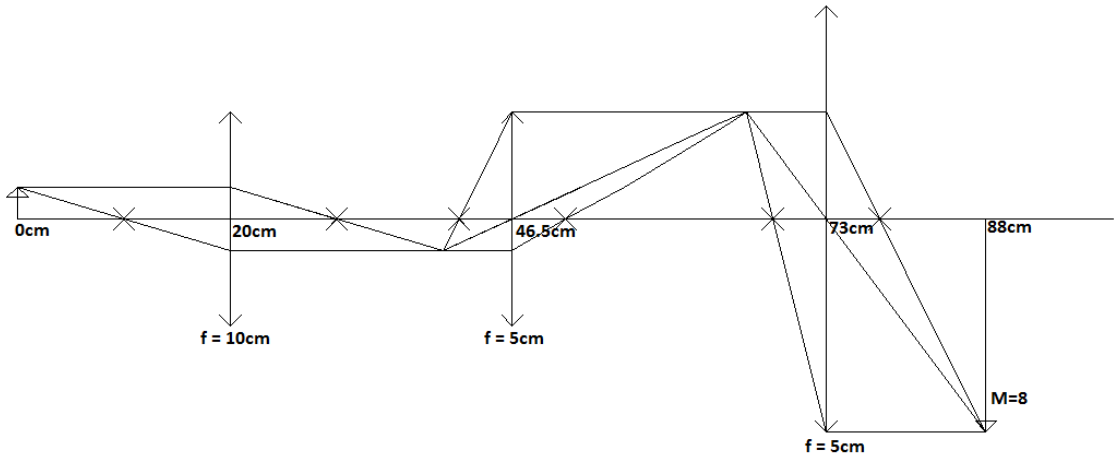

Figure 3.5: The optics used for shadow graphics, consists of three lenses of focal lengths 10 cm, 5 cm and 5 cm. This system magnifies 8 times.

3.2 Choice of liquids

Cyclohexane is a simple naphtenic liquid with a saturated ring shaped hydrocarbon molecule which is well known and used a lot as a model liquid. The liquid was chosen in order to have a reference for the methods. Its simple chemical structure has made it well documented.

One well-used unknown transformer oil has been tested in order to have a comparison liquid with insufficient properties.

Nytro 10XN, Marcol 52 and Shell Diala DX are widely used insulating liquids and are known to work well. Another insulating liquids as Galden, which is a fluorinated liquid, has different properties from the others and is therefore interesting to investigate.

Midel7131 is a new synthetic ester based liquid and its popularity increases due to good environmental properties. In order to know how it will work as insulating liquid we need to test it.

Biotemp is a new renewable and biodegradable vegetable oil with good environmental properties as well as insulating properties.

3.3 Measurement of water content, permittivity and density

The water content of the liquid samples were measured with the Karl Fisher method using a *737KF Coulometer* from ΩMetrohm. The solution used was Hydranal. Several samples of approximately 2 mL liquid were added successively into the measure solution by a syringe and the water content were given by the equipment in μg. The ppm-water content was obtained with some simple calculation.

The permittivity was measured with IRLAB model LDTRP-2.The permittivity and conductivity of the liquid might be found by adding approximately 20 mL liquid to the test cell with electrodes. IRLAB has two settings, either capacitance or conductivity. The permittivity is easily obtained by comparing the capacitance C to the capacitance of air C_0, $\epsilon_r = \frac{C}{C_0}$. IRLAB also has settings for measuring the conductivity by switching a button.

The density was easily determined by a Densito 30PX hand-held measuring device. One only needs to press the on-button and pump some liquid into the system and the density and temperature is given on the screen. However it is very important that the equipment is clean before use.

3.4 Test procedure

The test procedure developed in order to investigate different liquids and to find the differences is described as follows.

1. Fill the test cell with some liquid (100 mL) and close the cell
2. Shake the test cell to 'clean' it.
3. Empty the test cell and assume 'homoeopathic quantities' of the 'old' liquid compared to the 'new'
4. Refill with new liquid, avoid air bubbles inside the test cell
5. Center the test cell in the test rack. Line up with the optics.
6. Start the measurements for different waveforms with

   First, current measurement

   Second, PD measurement, ignition voltage and long-time effect

   (Third, Shadowgraphic imaging if time)
7. Analyse and compare the results

3.5 X-ray of the test cell

The test cell was exposed to X-ray in periods of approximately 6 seconds several times during one day with some hours of rest between. Acceleration voltage was 275 kV and

gave 99 pulses with equal on/off time and 50 % duty cycle. The X-ray gun XRS-3 was operated by personnel from Axess, which is a professional company in handling X-ray equipment. Both PD patterns and current measurements were performed as usual during the measurements.

3.6 Signal analysis

Raw data from the oscilloscope are voltage, trigger and current signal. The current signal is represented as a voltage with a certain magnitude. A Matlab script, see Appendix B, has been developed in order to analyse the measured current signals. It mainly loads the signals and low pass filter and smoothens them in order to remove noise. The measured current both contain a capacitive and conductive current. The capacitive current is the derivative of the voltage multiplied by the capacitance. The conductive current is then obtained by subtracting the capacitive current from the total current. The conductive current is then plotted as a function of time and the square of the voltage and saved to .png file. The frequency of the signal is also found by comparing time to the zero crossings of the voltage.

Another script was made, to be found in Appendix C, to analyse the obtained PD data. The raw data consists of several files where one contains the voltage vs time and the other the PD size vs phase and vs time. This makes it easy to plot the PD events in the time domain and to obtain the PD-phase-pattern. The long time data makes it possible to analyse longer time series and find correlations between the different partial discharge events. The script starts by counting the number of half periods until the next PD happen and gather the results in a histogram-like graph. The PDs are also grouped in order to get the time to next PD. This is done in order to get the time dependence of the PDs. Both grouped with number of PDs per half period and maximum charge per half period.

3.7 Simulation of space charge movement

A simple simulation of space charges has been done in Matlab in order to obtain the current in the gap. The point plane geometry and skeleton of the script was originally developed and implemented by Stian Ingebrigtsen at Sintef Energy Research. The author of this thesis has modified the script and implemented the Shockley-Ramo theorem and a 'correct' distribution of space charges in order to get an idea of the conductive current.

The Shockley-Ramo theorem explains that only charges in the volume near the tip contribute to the current. Therefore charges are implemented only in this volume. The charges are randomly distributed in ion pairs within this volume with concentration n_c as found in equation (2.36), well aware of the mistake of not considering dissociative ionization or other charge creation processes in order to get a dynamic charge concentration. It is easier to model a constant number of charges rather than changing the number of ions all the time. The intent of this simulation is only to give qualitative information. A detailed and accurate simulation result is not the scope of this thesis.

Due to limitations in computer power, only 1/1000 of the ions were modelled. The total current was multiplied by the factor 1000 to get the correct magnitude. The simplest model is to let the ions only interact with the geometrical field and not each other.

A time vector of voltage values in high voltage AC is made and iterated over. For each iteration the ions find a new place due to the geometrical field. The ion-ion interactions are not considered in this model. The contributions to the current are obtained by the Shockley-Ramo theorem, equation (2.43). The geometrical field is given in prolate spherical coordinates and the charges follow the field lines in the simplest approximation. This should give acceptable results as long as long as the number of ions present is correct. For long relaxation times, the number of ions will be about constant over time.

The model has limitations and assumes only interactions between the charges and the *geometrical* field. This will result in an incomplete physical description, but on the other hand give a qualitative idea of current from space charges in a point-plane gap.

Chapter 4

Results

The voltages presented in the result part of the thesis are referring to the potential between the point and the plane. The tungsten wire has a positive charge when the high voltage plane is negative. The relative voltage on the wire is shown in the graphs. This means that a positive period is referring to a positive wire. This is however not the case for the Omicron phase pictures, where it is the opposite due to the way the pictures are produced in Omicron.

The point plane gap was measured to be 19.5 ± 0.5 mm during the experiment. The tip radii were measured with an uncertainty of 0.5 μm by using a microscope connected to a computer and a correctly scaled ruler.

The results presented in this chapter are provided to give an understanding of space charges in an insulating liquid and the corresponding PD phase pattern. The currents measured were approximately stationary for most liquids, with only a few nA of variations between the periods. The only exception was Cyclohexane where sudden jumps in the current were observed. Therefore, stationary currents are a sufficiently precise approximation for all the liquids except Cyclohexane. The PD-phase patterns are stochastical. There will be some variations in the measurements, but the patterns included are representative for a typical two minutes PD recording.

First the current dependence on tip radii r_p, frequency f and voltage shape was investigated for two liquids. Then the behaviour of eight different liquids was compared using $r_p \approx 6$ μm tip and $V \approx 14.3$ kV_{peak} . A non-stationary behaviour of current in Cylohexane is documented. Then PD-patterns were recorded for different parameters. Two liquids was investigated with different tip radii r_p and frequencies f. Statistics of longer time series with PDs was performed in three liquids. Eight different liquid PD patterns were obtained and statistics on each liquid using $r_p \approx 7$ μm tip. Lastly, one liquid was exposed for X-rays several periods during one day. Optics for imaging was also established, but not performed to a large extent in this work.

Some relevant liquid properties are listed in Table 4.1.

Table 4.1: Important liquid factors from literature

		Cyclohexane	Marcol 52	Trafo oil	Shell Diala DX	Midel 7131	Galden HT 135	Biotemp	Nytro 10XN
Heath capacity @20°C	[J/kgK]	1842[g]		-	1911[c]	1880[d]	974400[e]		
Thermal conductivity @20°C	[W/m]	0.12[h]		-		0.144[d]	0.065[e]		
Heat of vaporization	[J/kg]	393300[i]		-			67200[e]		
Density	[kg/m^3]	778.5[a]	830[b]	-	878[c]	970[d]	1720[e]		
Kinematic viscosity	[mm^2/s]	1.26[a]@20°C	7.4[b] @40 °C	-	8.0[c] @40°C	28[d] @40°C	1.0[e] @25°C		
Boiling point	[°C]	81[a]		-		> 300[d]	135[e]		
Literature permittivity ϵ_r	[F/m]	2.03[a]	2.13[b]	-	2.20[c]	3.20[d]	1.92[e]		
Measured permittivity[f] ϵ_r	[F/m]	2.01	2.11	2.23	2.18	3.17	1.96	3.07	2.17
Conductivity[f] σ	[S/m]	$1.043 \cdot 10^{-12}$	$2.048 \cdot 10^{-14}$	$2.203 \cdot 10^{-11}$	$1.585 \cdot 10^{-13}$	$2.361 \cdot 10^{-11}$	$1.654 \cdot 10^{-13}$	$1.26 \cdot 10^{-10}$	$6.0 \cdot 10^{-13}$
Measured water content[j]	[ppm]	16.35	10.22	11.88	11.85	200.63	5.6	60	10
Relaxation time $\tau = \epsilon/\sigma$	[s]	17.1	911	0.90	122	1.19	105	2156	32
Measured density[k]	[kg/m^3]	777	830	870	870	970	1710	912	872

[a] Data from manufacturer Merck Millipore
[b] Data from manufacturer Exxon Mobile
[c] Data from manufacturer Shell
[d] Data from manufacturer Midel
[e] Data from manufacturer Solvay
[f] Measured with IRLAB equipment
[g] Dortmund Data Bank [39]
[h] Dortmund Data Bank [40]
[i] Dortmund Data Bank [41]
[j] Measured with 737 KF Coulometer Karl Fisher method
[k] Measured with Densito 30PX equipment

4.1 Current measurement

The current was amplified and filtered through a low pass filter using a current amplifier, Standford Research Model SR570. This is necessary in order to measure currents in the size of nano ampere. The current amplifier has a built-in low pass filter, shown in Figure 4.1. In addition, the data from the conductive current are filtered by a matlab program that sets all frequencies above $100 f_0$ to 0, where f_0 is the voltage frequency. Without this filtering, the signal would be hidden within the noise generated in the measure equipment.

Due to small changes in the gap distance and tip radii, the capacitance of the gap vary between 0.9 pF and 1.1 pF. This results in slightly different capacitive currents from day to day when changing the tip. $I \propto C\dot{V}$

Statistical fluctuations are only significant in Cyclohexane, as shown in Figure 4.11.

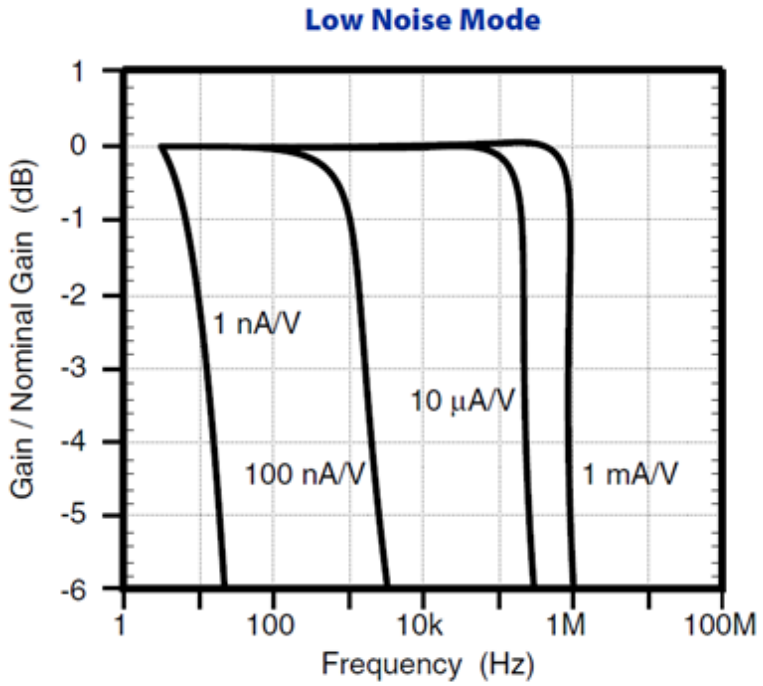

Figure 4.1: Standford Research SR570 bandwidth for different magnifications. The lowest magnification has the highest bandwidth.

4.1.1 Influence of different tip radii and frequency

Different tip radii and different frequencies were tested for different frequencies. Figure 4.2 and 4.3 are both results from these measurements. Due to inaccurate adjustment of the distance d between the tip and the plane after changing to a different wire with a different radius, the capacitive current changes slightly from what is expected. The noise level also make these current values uncertain. Figure 4.4 is a summary of Figure 4.3 with the current peaks extracted.

The different frequency currents are measured right after each other, which implies that the charges have no time to relax and the current may thereby be affected.

Figure 4.5 shows the differences between starting at a high frequency and then lowering it and vice versa in Cyclohexane.

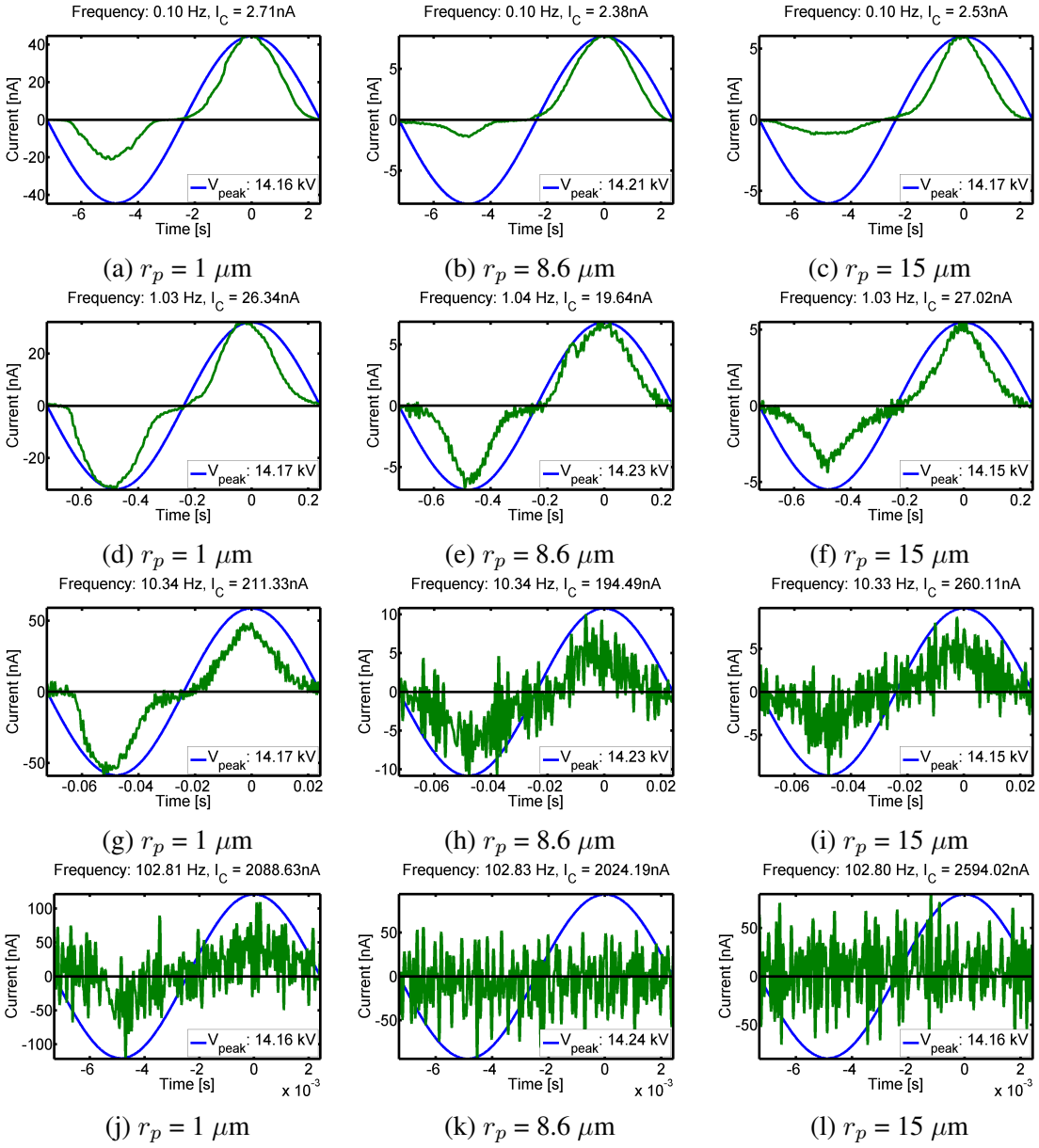

Figure 4.2: One period of the conductive current (green) measured in Galden 135 for different tip radii and frequency of AC voltage. Data low pass filtered; frequencies above $100 f_0$ are set to 0 through a Fourier transform. Note the small asymmetry in the polarities, especially at low frequencies.

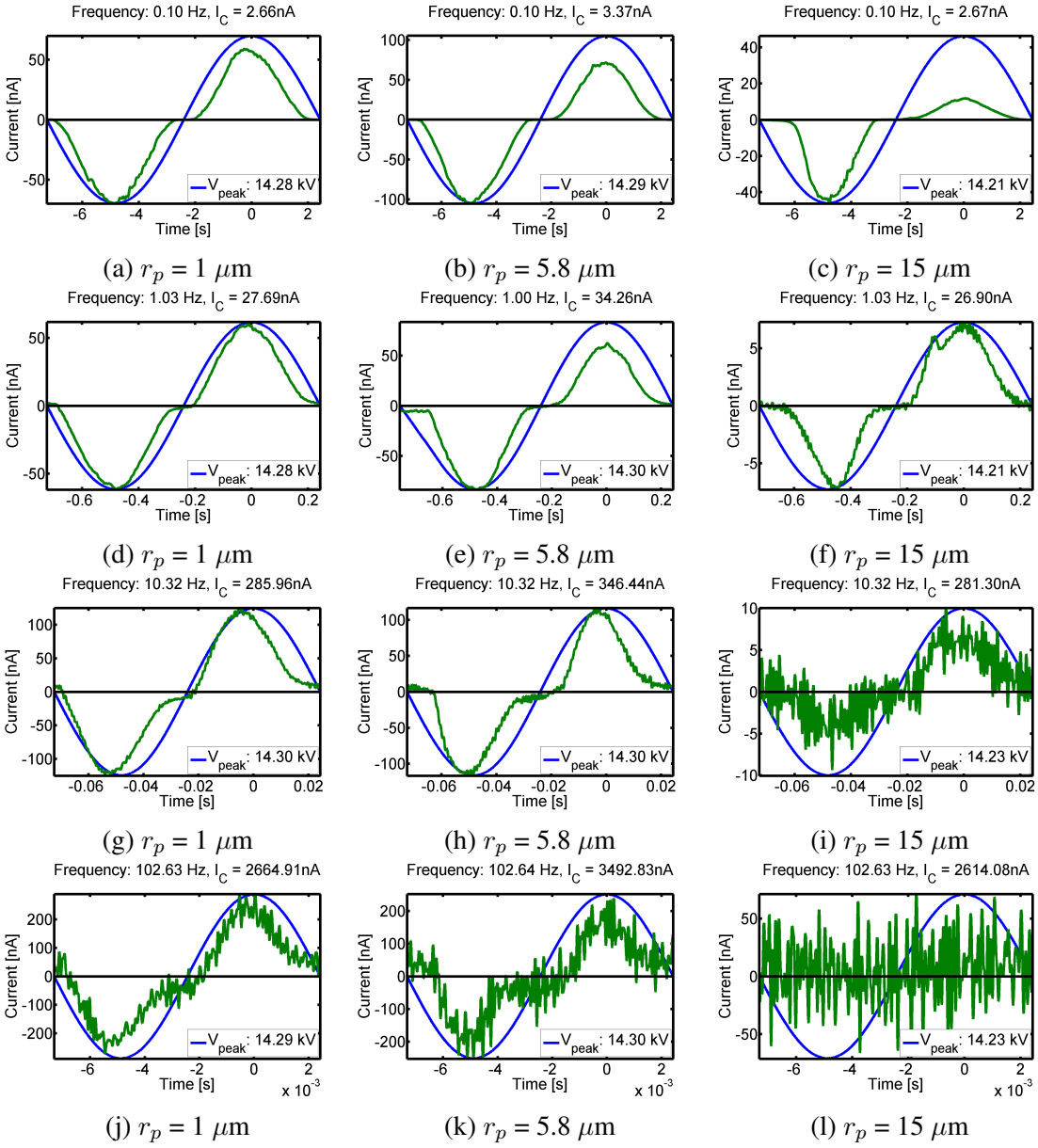

(a) $r_p = 1\ \mu$m (b) $r_p = 5.8\ \mu$m (c) $r_p = 15\ \mu$m

(d) $r_p = 1\ \mu$m (e) $r_p = 5.8\ \mu$m (f) $r_p = 15\ \mu$m

(g) $r_p = 1\ \mu$m (h) $r_p = 5.8\ \mu$m (i) $r_p = 15\ \mu$m

(j) $r_p = 1\ \mu$m (k) $r_p = 5.8\ \mu$m (l) $r_p = 15\ \mu$m

Figure 4.3: One period of the conductive current measured in Marcol 52 for different tip radii and frequency of AC voltage. Data low pass filtered, frequencies above $100 f_0$ are set to 0 through a Fourier transform. Note the symmetry in the current and the phase shift of the current on rising edge.

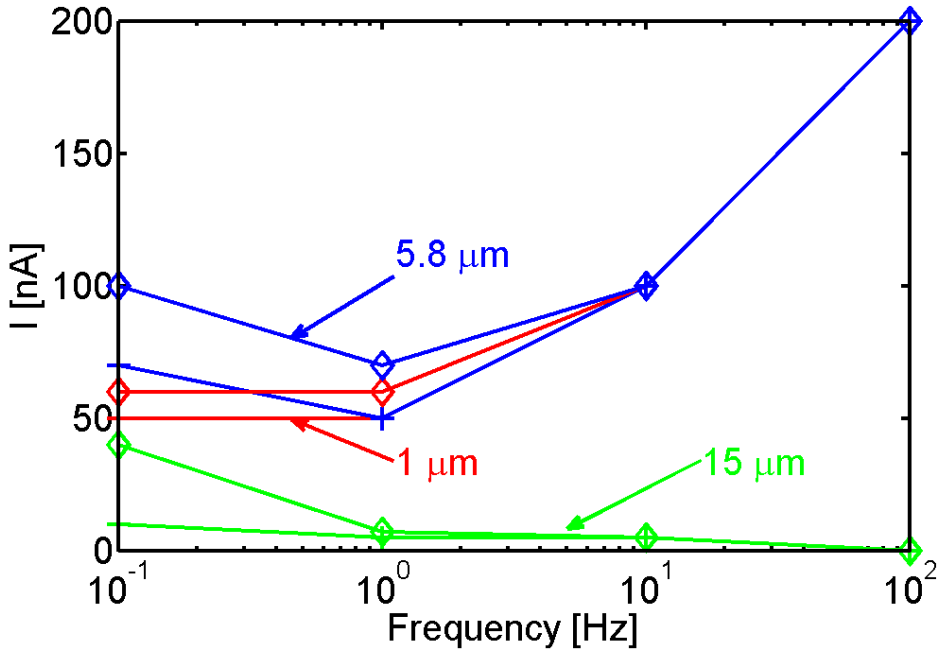

Figure 4.4: The conductive current vs frequency in Marcol 52 for different tip radii. '+' indicates a peak of positive half period of the current and '$\diamond$' a peak of negative half period. Note the significant difference between tip radius of 15 μm and 5.8 μm and 1 μm. Relaxation time τ = 911 s

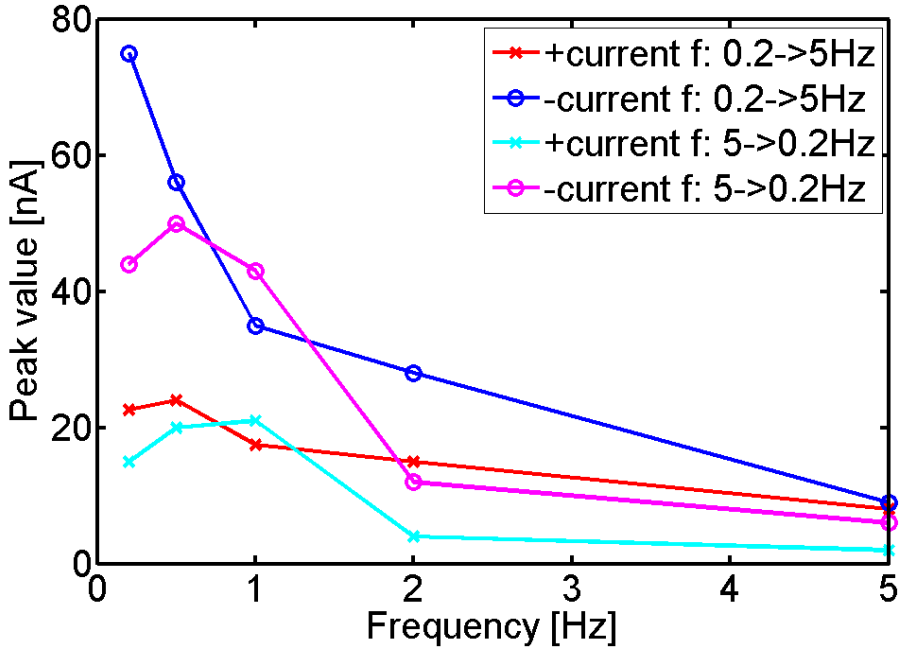

Figure 4.5: The Conductive current in Cyclohexane vs frequency. $r_p \approx 8$ μm. Compare with Figure 4.4 where the current also decreases for large tip radius. Relaxation time τ = 17.1 s

4.1.2 Voltage dependence of current

Figure 4.6 shows the current for different voltages. At the left column in the figure the measured signal is shown. In the middle column instantaneous current is plotted vs voltage and in the right column current is plotted vs the square of the voltage. The Fourier filtering, which removes all frequencies above $100f_0$, results in the small oscillations for the smallest voltage, due to the fact that the signal amplitude is close to the noise level.

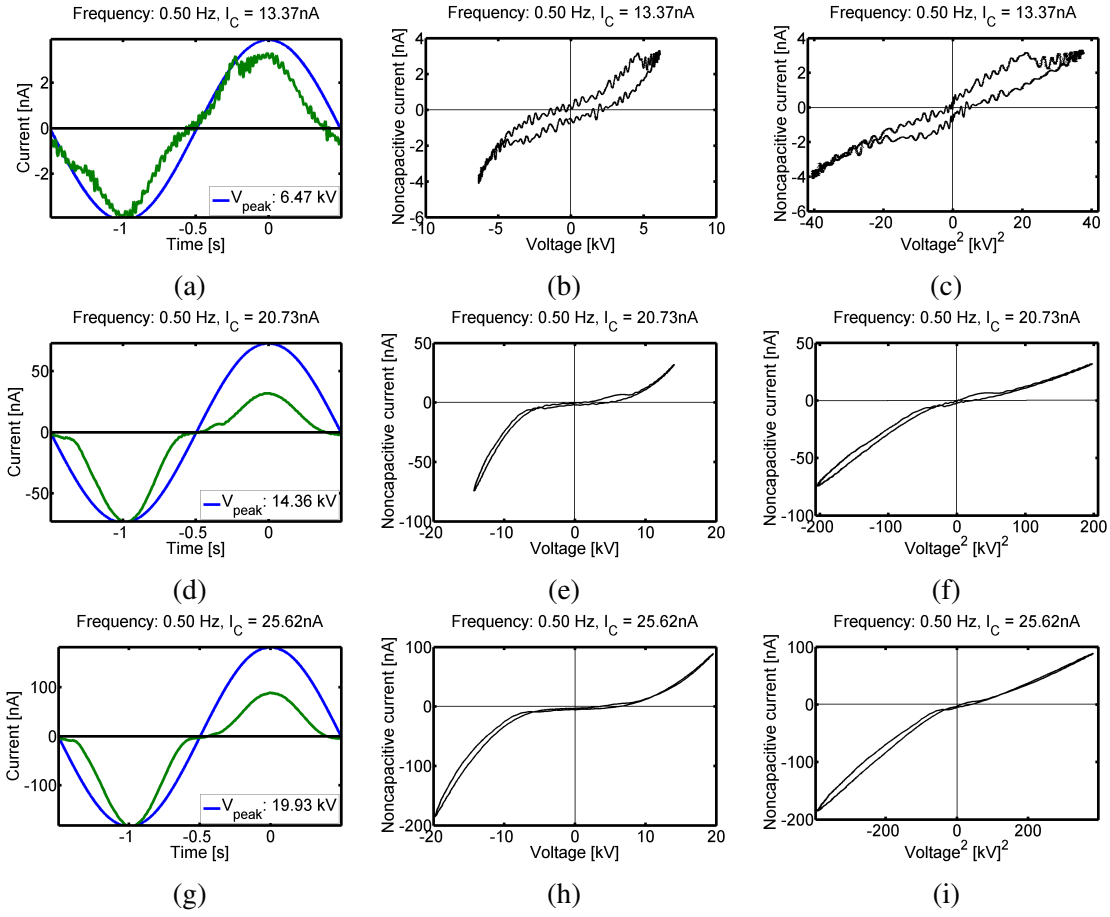

Figure 4.6: Conductive currents for different voltages. (a),(d),(g): I vs t, (b),(e),(h): I vs V, (c),(f),(i): I vs V^2. Data low pass filtered, frequencies above $100f_0$ are set to 0 through a Fourier transform. Note the straight lines for I vs V^2. This is a typical space charge dependent current. Also note the asymmetry in the polarities for higher voltages, indicating new injection processes present at negative polarity.

4.1.3 Current under sine, step and triangular voltage

Current measured under some different waveforms in Marcol 52 are given in Figure 4.7.

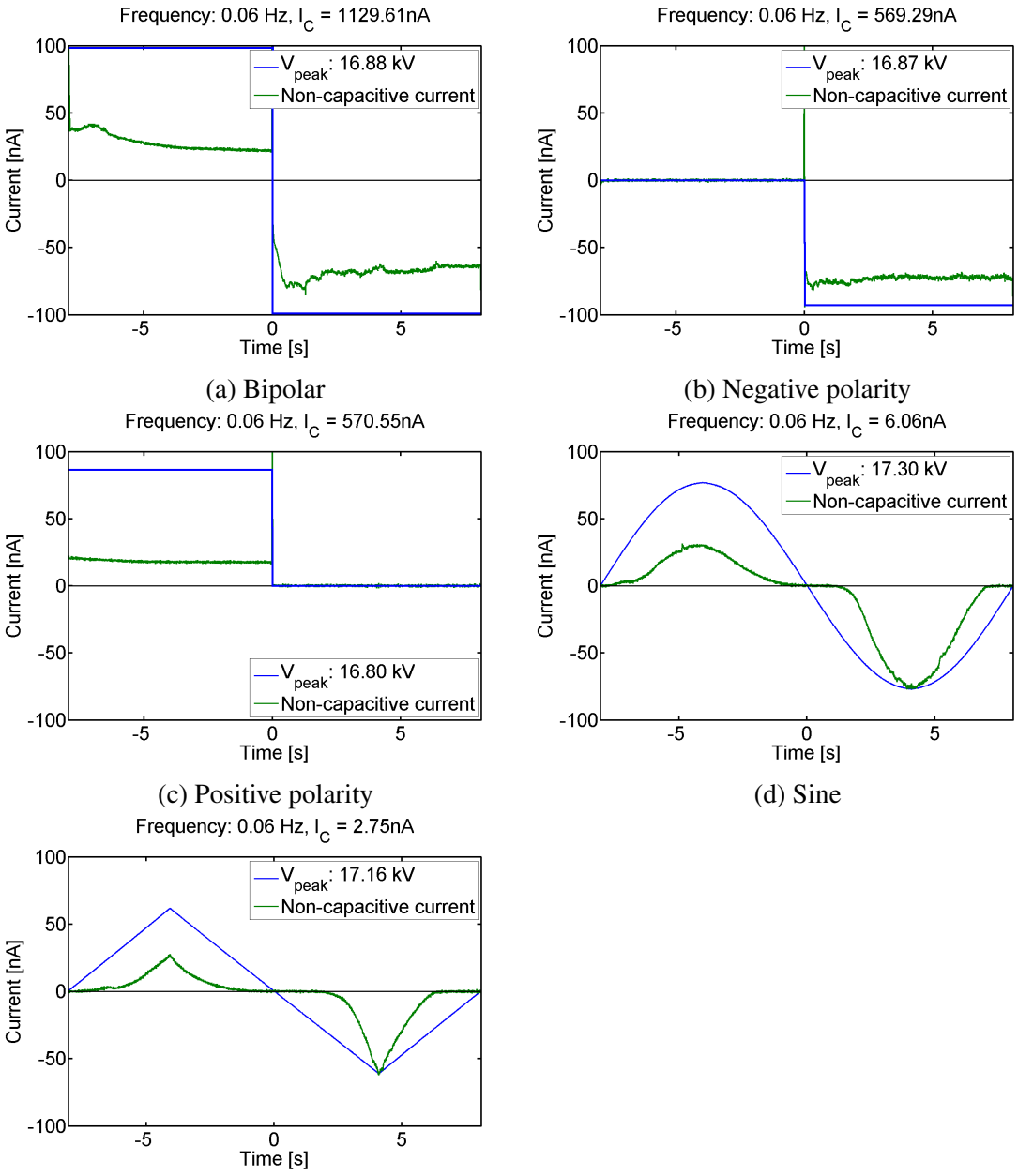

(a) Bipolar

(b) Negative polarity

(c) Positive polarity

(d) Sine

(e) Triangular

Figure 4.7: Different waveforms in Marcol 52. Note the difference between unipolar and bipolar square wave.

4.1.4 Different liquids

Several different liquids were tested, all done for similar $r_p \approx 6$ μm and frequency of 0.1 Hz. Figures 4.8 and 4.9 compares the different liquids in such a way that it is easy to see the differences. The overall shape seems to be the same, but there are some differences due to different threshold values for the different charge generating processes in the different liquids.

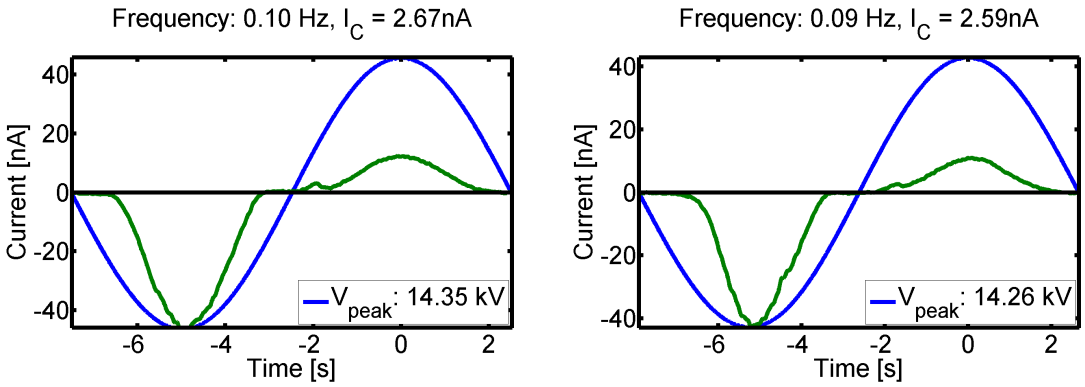

(a) Cyclohexane

(b) Marcol 52

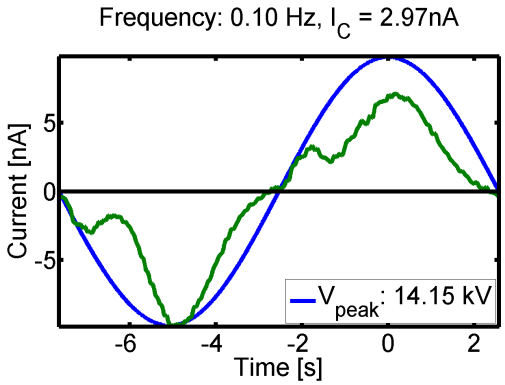

(c) Used Transformer Oil

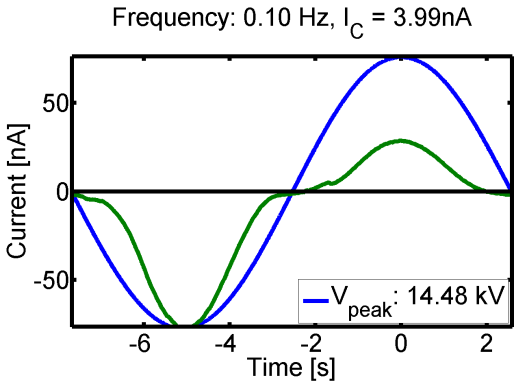

(d) Midel 7131

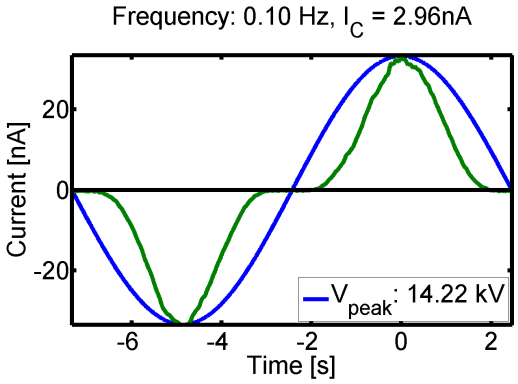

(e) Shell Diala DX

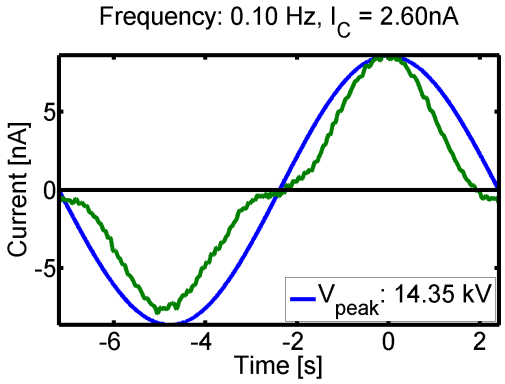

(f) Galden 135

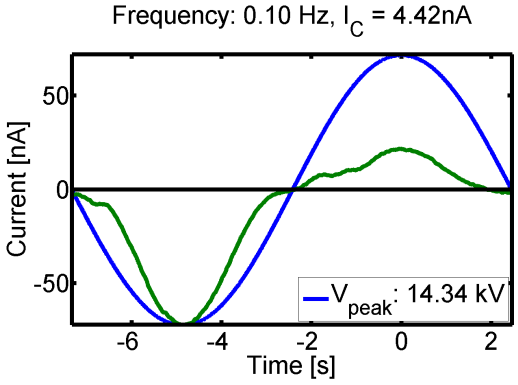

(g) Biotemp

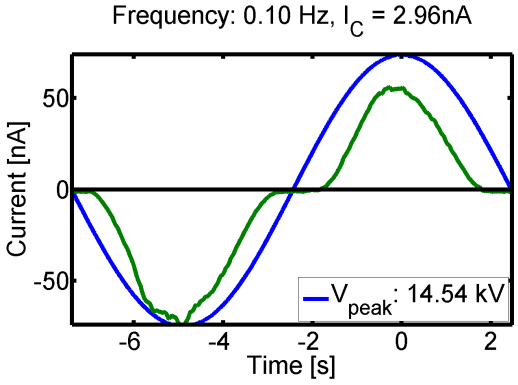

(h) Nytro 10XN

Figure 4.8: Conductive currents (green) vs time in different insulation liquids. Important to note the difference in symmetry in polarities and magnitudes for the different liquids. Tip radius r_p about 6 μm.

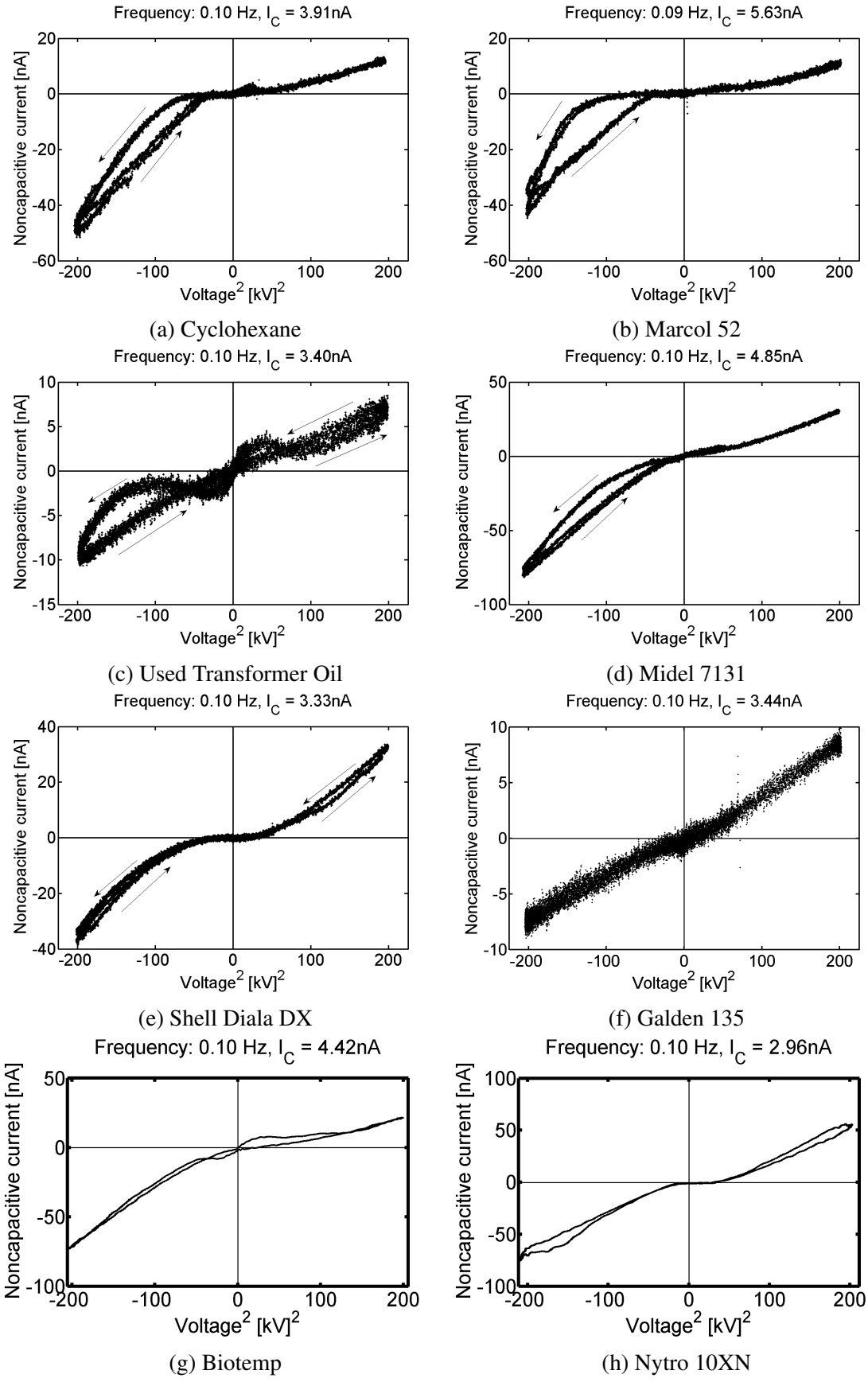

Figure 4.9: Instantaneous current vs V^2 illustrating the typical behaviour of space charge limited current. The same signals as in Figure 4.8. Important to note the linearity in I vs V^2.

4.1.5 Simulation

A simulation with parameter data values for Cyclohexane was performed, the result is presented in Figure 4.10. This gives an upper bound for the space charge limited current without any interactions between the ions.

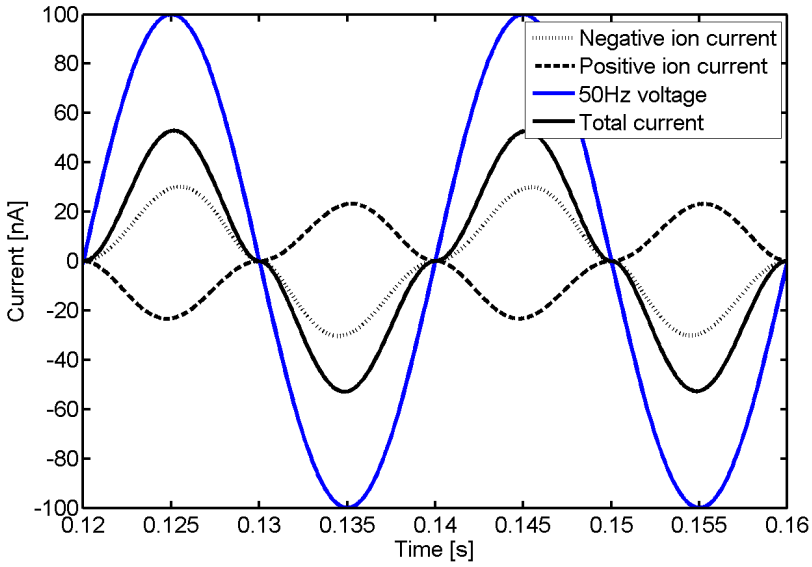

(a) Simulated current from positive and negative charges and the voltage applied.

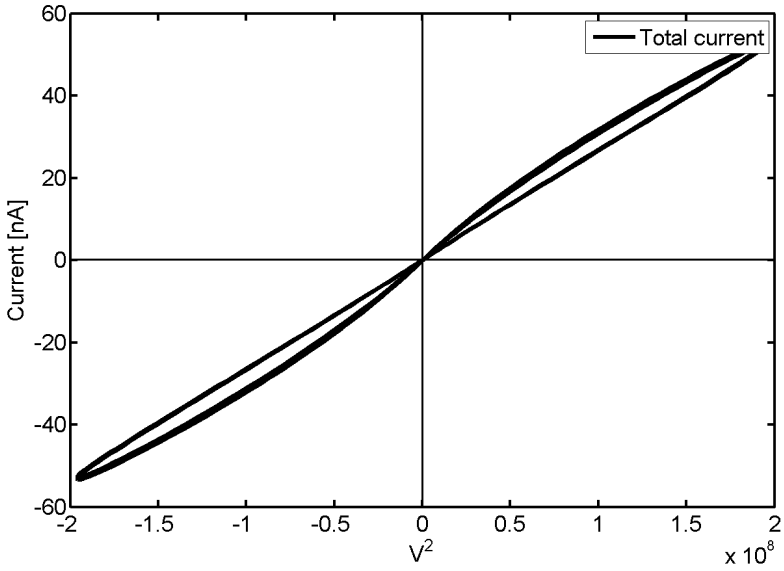

(b) I vs V^2. Almost a perfect straigth line.

Figure 4.10: Simulated current with values for Cyclohexane

4.1.6 Statistical fluctuations in Cyclohexane

During the experiment, several statistical fluctuations occurred. There were some minor fluctuations in the current for all liquids (approximately 1 nA). In addition the sample of Cyclohexane had sudden current pulses and a non-stationary current, illustrated in Figure 4.11. Cyclohexane had several larger particles within the bulk liquid, probably paper parts from the cleaning process or other large molecules added.

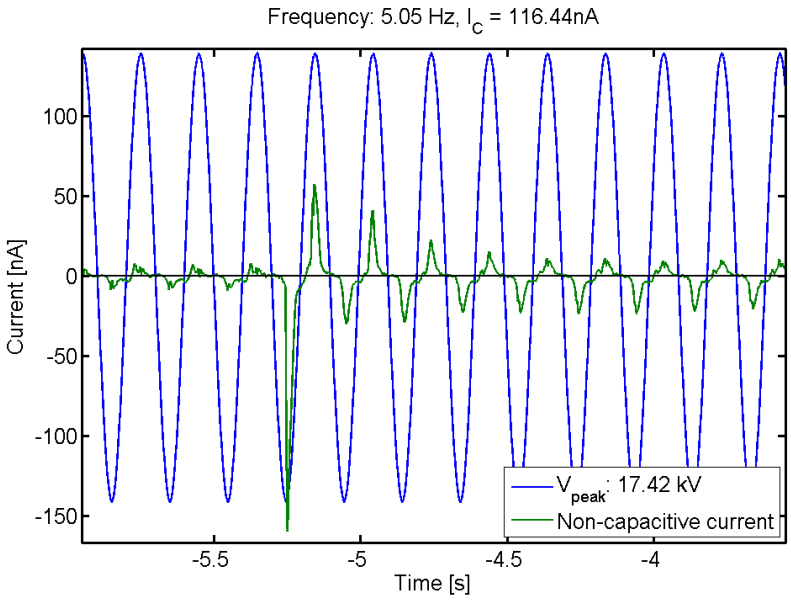

Figure 4.11: conductive current measured in Cyclohexane. This event rarely happens and is only observed in Cyclohexane.

4.2 Partial discharges

Partial discharges were recorded with an automatic discharge acquisition system, Omicron. Due to the measurement setup, the voltage and discharges are inverted and refer to the voltage at the plane instead of the tip. To obtain the right discharges and voltages, one simply needs to 'multiply' by -1. The figures from Omicron are PD-phase-amplitude-plots. Each point in the figures is a PD, and different color describes how many PDs at each spot in the phase-amplitude-diagram.

PD pulses are observed at low frequencies at square wave polarity change. They disappear at higher frequencies. Observations give no PDs at 500 Hz, but large PDs at 50 Hz.

4.2.1 Different tip radii

Different tip radii will change the active volume and the electrical field. The partial discharge activity for this change are shown in Figure 4.12. Note the sudden increase in PD rate in Marcol 52 at r_p = 6 μm and the general decrease in PD rate Galden 135 due to changed active volume and increased electrical field.

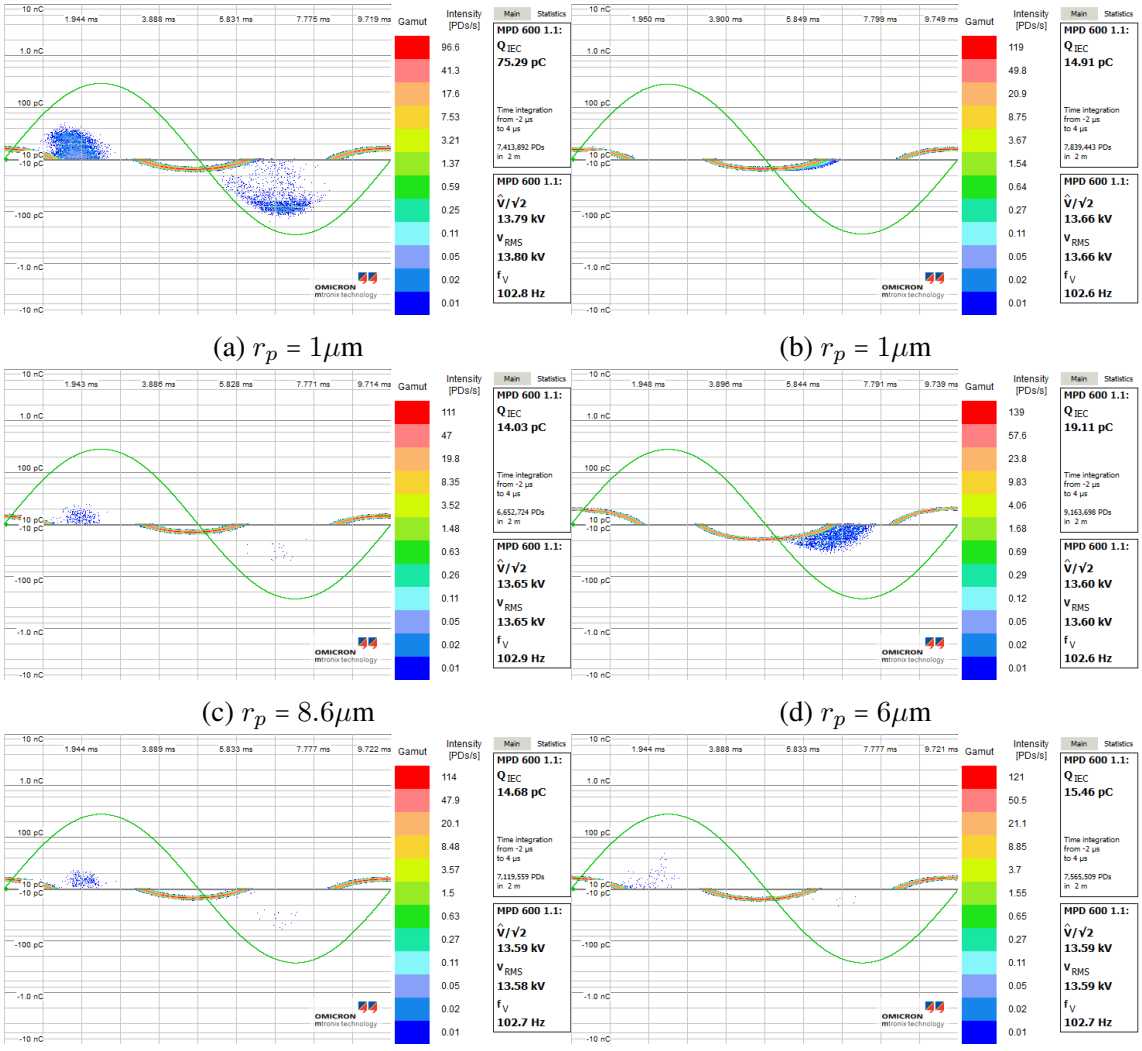

(a) r_p = 1μm (b) r_p = 1μm

(c) r_p = 8.6μm (d) r_p = 6μm

(e) r_p = 15μm (f) r_p = 15μm

Figure 4.12: Distribution of PD amplitude vs phase angle measured in Galden (left) and Marcol (right). The wave shaped 'PDs' centred at the zero crossing of voltage are due to the current. The measurement need a long integration time and therefore the current is also recorded as several PDs. $V \approx 19.5\ \mathrm{kV}_{peak}$ and $f \approx 102.7$ Hz.

4.2.2 Frequency dependence

Partial discharges seems to be highly frequency dependent, Figure 4.14 is measured in a sequence right after each other, implying more space charges present in 4.14d than in 4.14a due to the relaxation time of the liquid. Due to asymmetric current injection, there will be a larger number of negative than positive charges present. There generally is an increase in the number and amplitude of the discharges with frequency, Figure 4.13 in Nytro 10XN is a typical example.

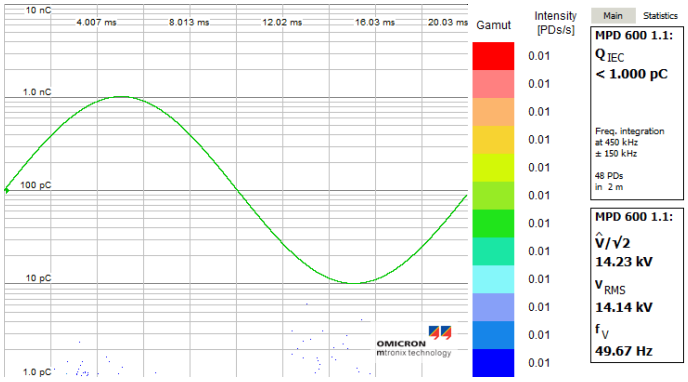

(a) 50Hz, r_p = 6μm

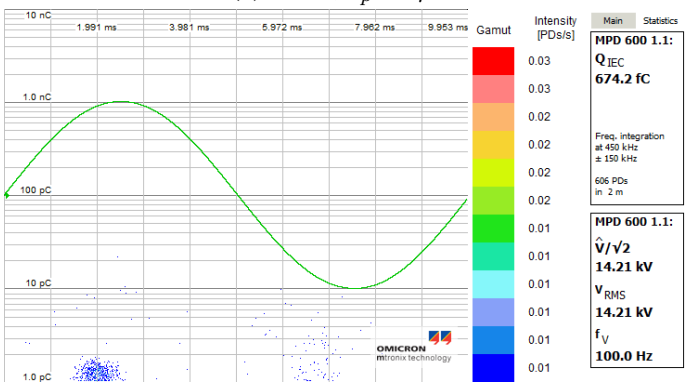

(b) 100Hz, r_p = 6μm

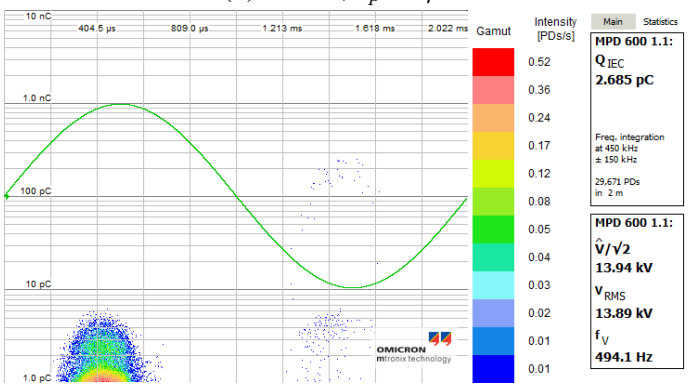

(c) 500Hz, r_p = 6μm

Figure 4.13: Distribution of PD amplitude vs phase angle measured in Nytro 10XN for different frequencies at $V \approx 20$ kV$_{peak}$. Frequency integration option in Omicron chosen due to high frequency AC voltage. The rate increases linearly by frequency

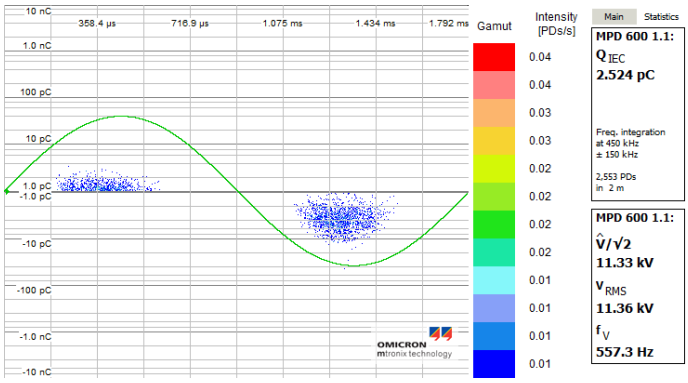

(a) 580Hz, r_p = 6μm

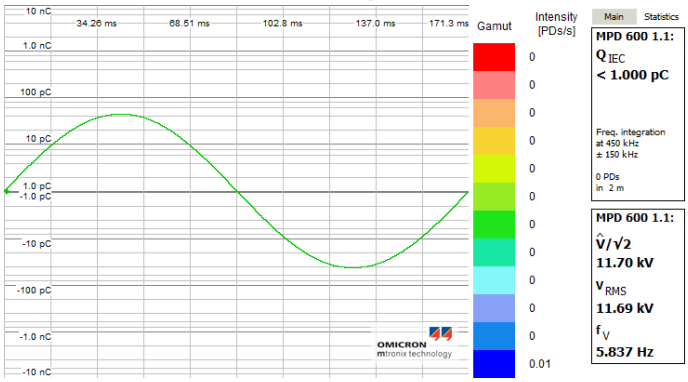

(b) 5.8Hz, r_p = 6μm

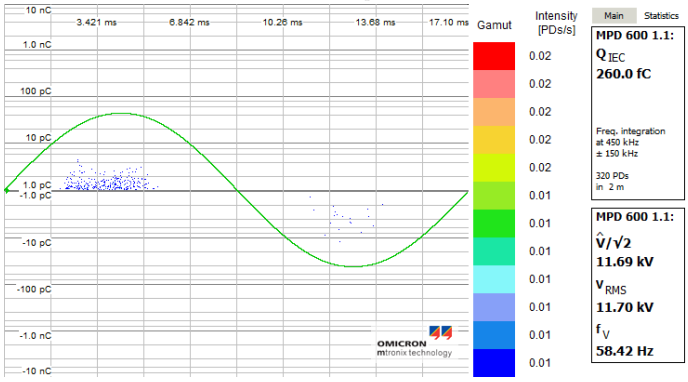

(c) 58Hz, r_p = 6μm

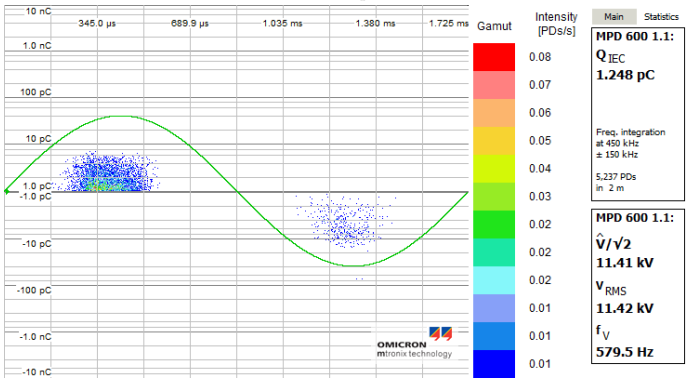

(d) 580Hz, r_p = 6μm

Figure 4.14: Distribution of PD amplitude vs phase angle measured in Marcol 52 for different frequencies at $V \approx 16$ kV$_{peak}$. Frequency integration option in Omicron chosen due to high frequency AC voltage. The activity increases linearly by frequency

4.2.3 Different waveforms

Different waveforms affect the creation of space charges and thereby the partial discharge rate, due to field change originating in space charges. The strong electrical field area is achieved at different places in the phase for different voltage shapes, and therefore the PD phase patterns are different.

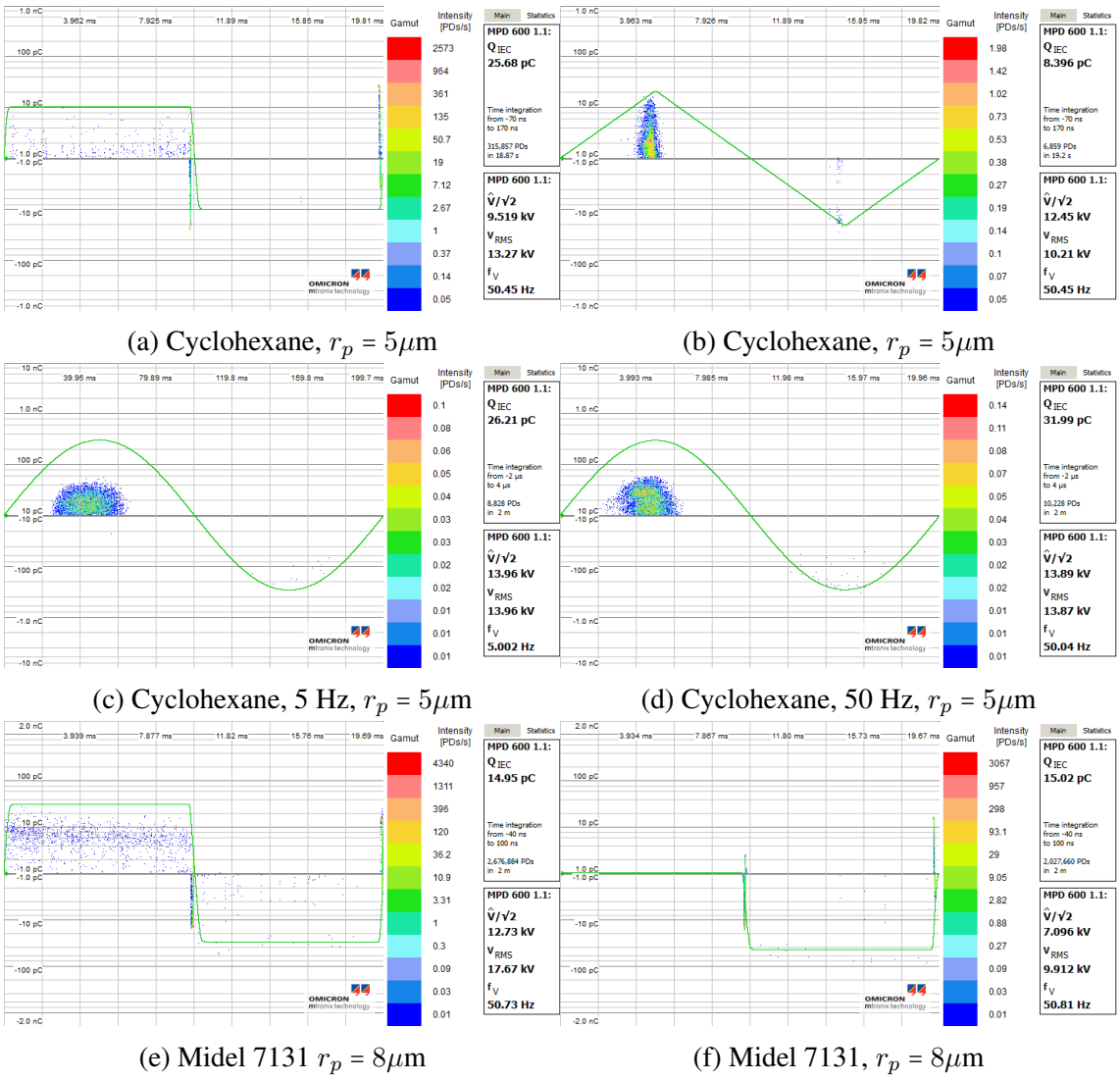

(a) Cyclohexane, r_p = 5μm

(b) Cyclohexane, r_p = 5μm

(c) Cyclohexane, 5 Hz, r_p = 5μm

(d) Cyclohexane, 50 Hz, r_p = 5μm

(e) Midel 7131 r_p = 8μm

(f) Midel 7131, r_p = 8μm

Figure 4.15: Distribution of PD amplitude vs phase angle measured in Cyclohexane and Midel 7131 for different waveforms

4.2.4 Statistics

Midel 7131 has a PD rate which fits quite well to a geometric distribution. Cyclohexane has a larger probability for PD occurrence next half period after a PD has happened. In Galden 135 PDs came in bursts, which means there may be no PDs for several hundred periods, and then there may occur several PDs within a few periods. Figures 4.17 and 4.16 show the number of half periods before the next PD and since the last PD, distributed for the size of the PD at the given half period. The same data is displayed in Figures 4.18 and 4.19 and sorted by how many events there are at each point (Q,# half periods) vs charge in Figures 4.17 and 4.16.

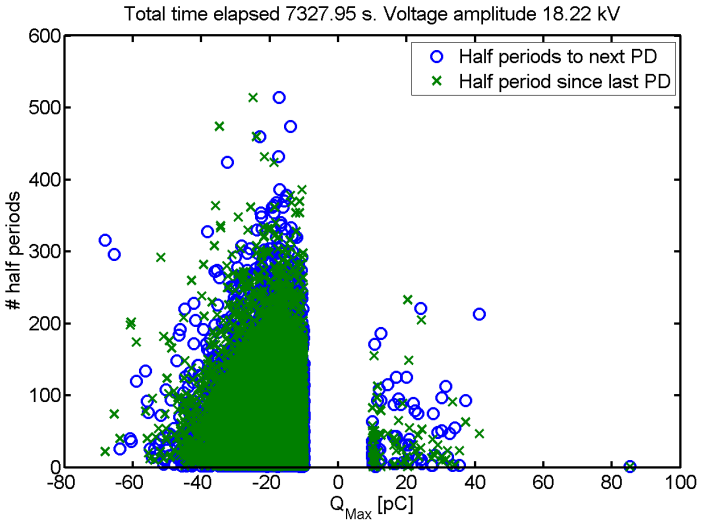

Figure 4.16: The time between two PDs in Midel 7131. There is no apparent relation between positive and negative PDs.

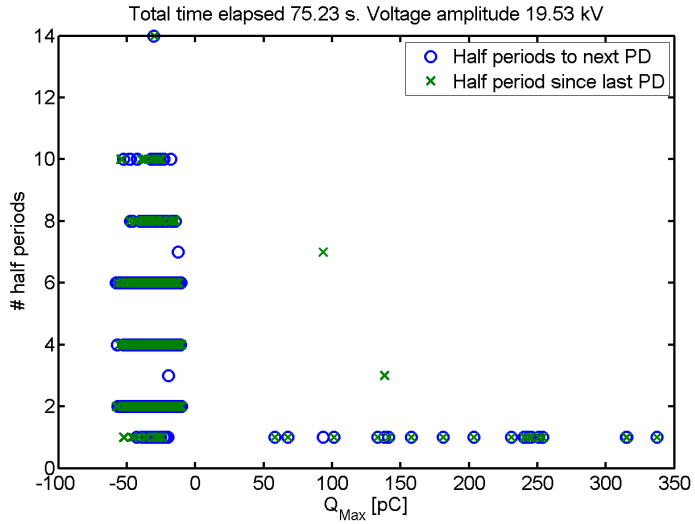

Figure 4.17: The time between two PDs in Cyclohexane. Note that almost every positive discharge follows and is followed by a negative discharge. The negative PDs seem to be random, but the positive PDs are correlated to the negative by following in the next half period after a negative PD.

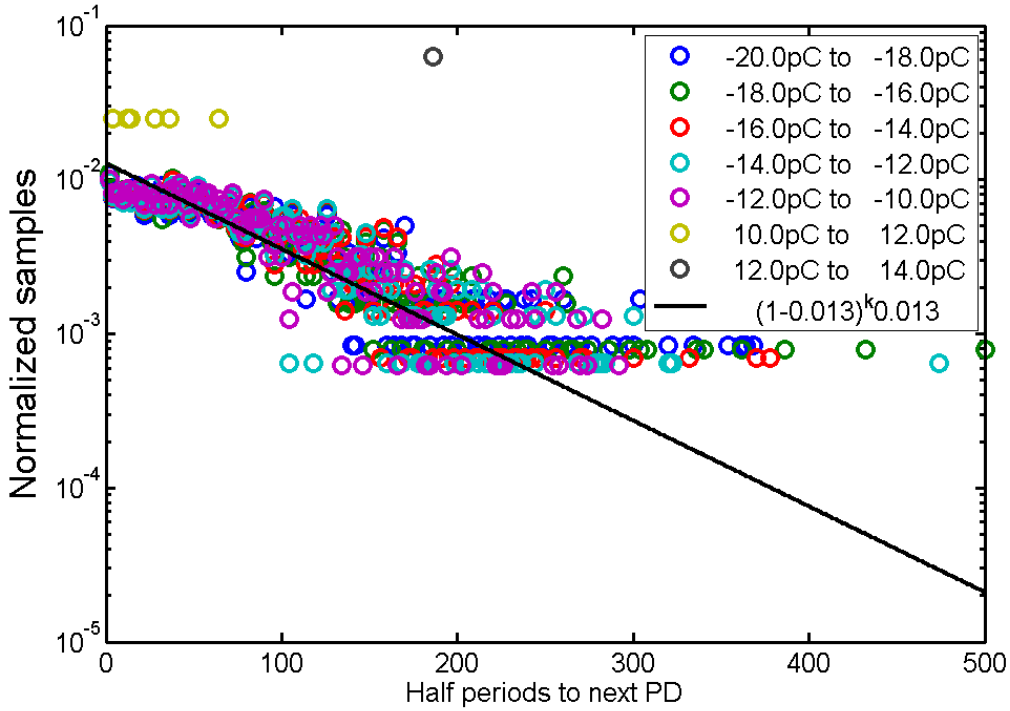

(a) Normalized number of samples with a given number of half periods to next negative PD, sorted by maximum charge per period

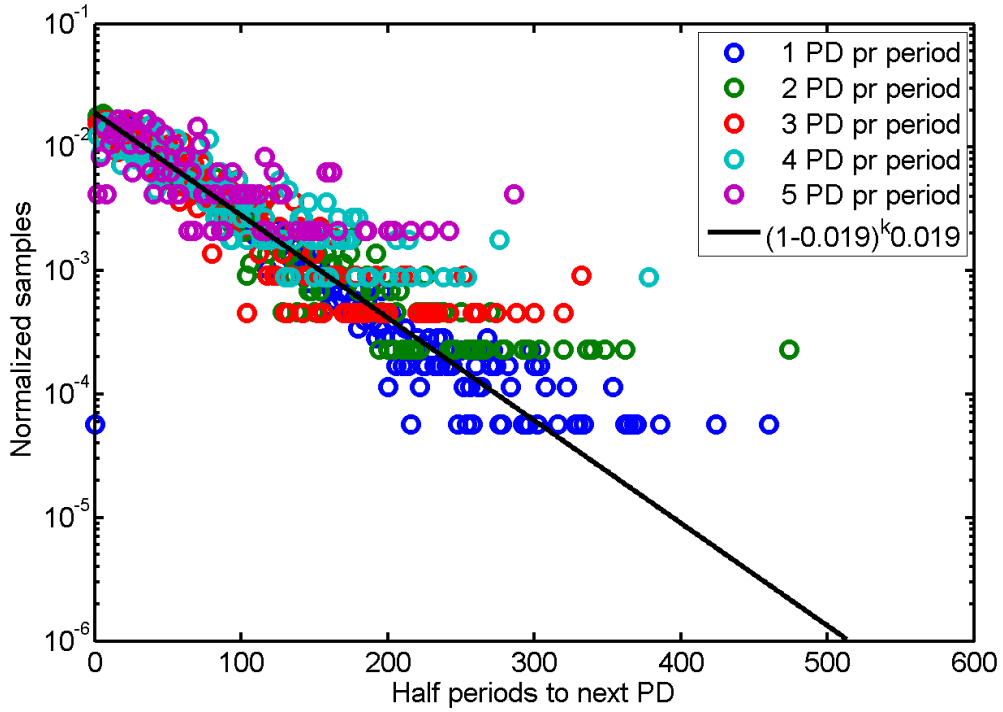

(b) Normalized number of samples with a given number of half periods to next negative PD, sorted by number of PDs per period. The positive PDs are too few to get any useful information in this graph

Figure 4.18: Time, in half periods, to next negative PD event in Midel 7131 for different numbers of PDs or maximum charge size pr period.

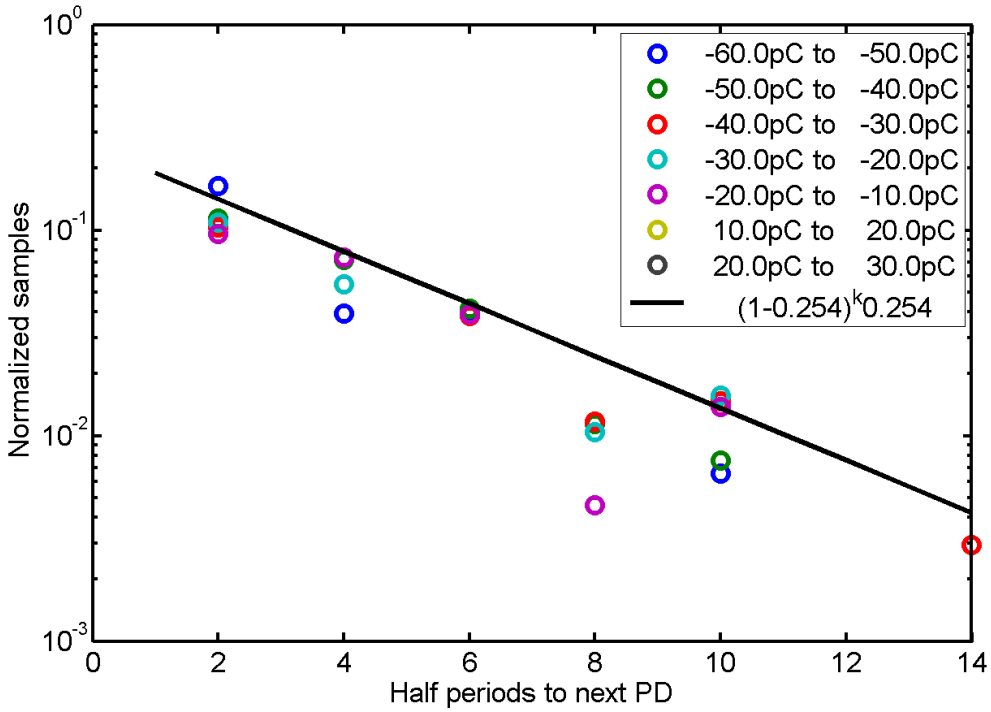

(a) Normalized number of samples with a given number of half periods to next negative PDs, sorted by maximum charge pr period

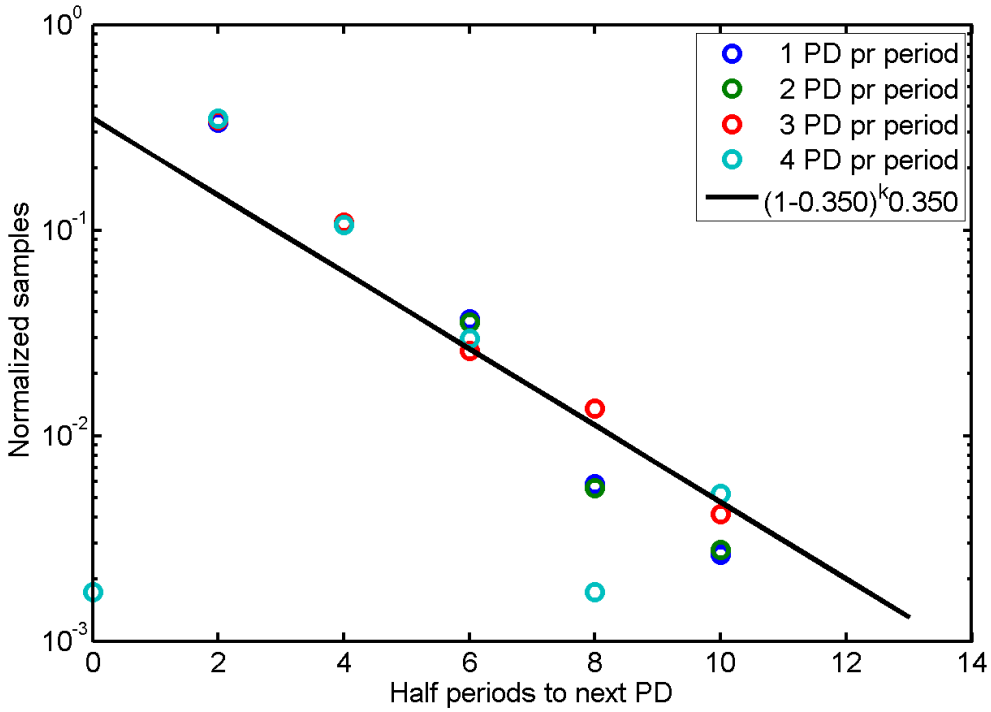

(b) Normalized number of samples with a given number of half periods to next negative PDs, sorted by number of PDs pr period. Note the more probable of PD event in a shorter time than in Midel 7131.

Figure 4.19: Time, in half periods, to next negative PD event in Cyclohexane for different numbers of PDs or maximum charge size pr period.

4.2.5 Liquid dependence in PD patterns

Different liquids have different composition, and they therefore have different PD rates. Figure 4.20 is to be considered as a representative pattern for the relevant liquids, although this pattern will never be exactly the same when repeating the experiment. Therefore, some statistics on PDs are presented in Figure 4.21 and 4.22.

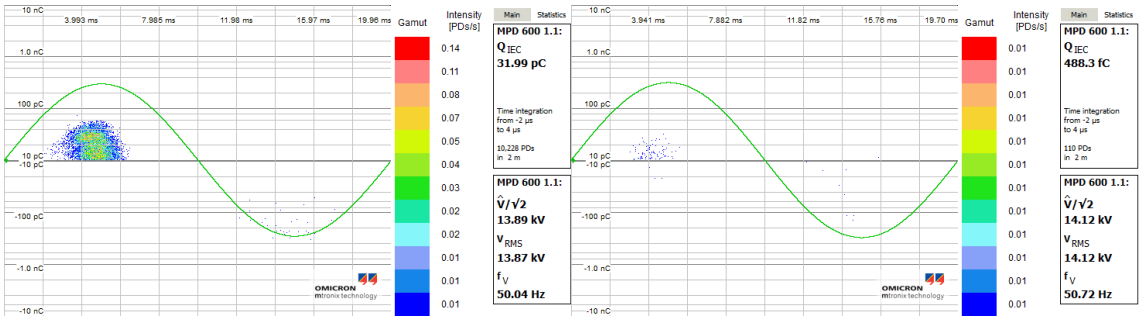

(a) Cyclohexane (b) Marcol 52

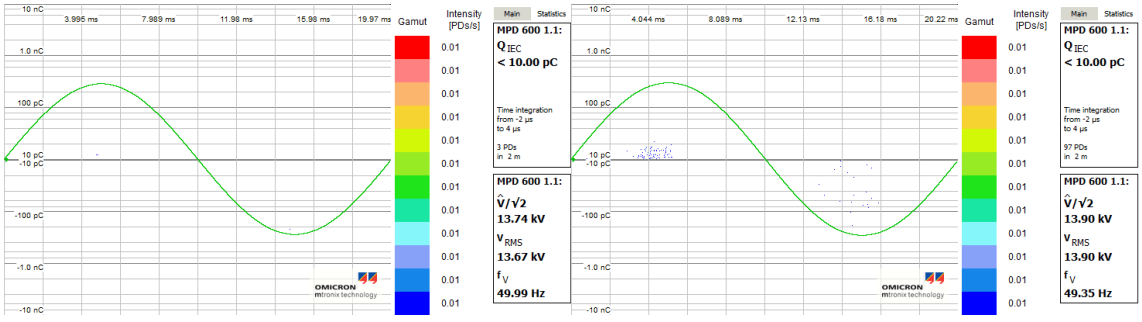

(c) Used Transformer Oil (d) Midel 7131

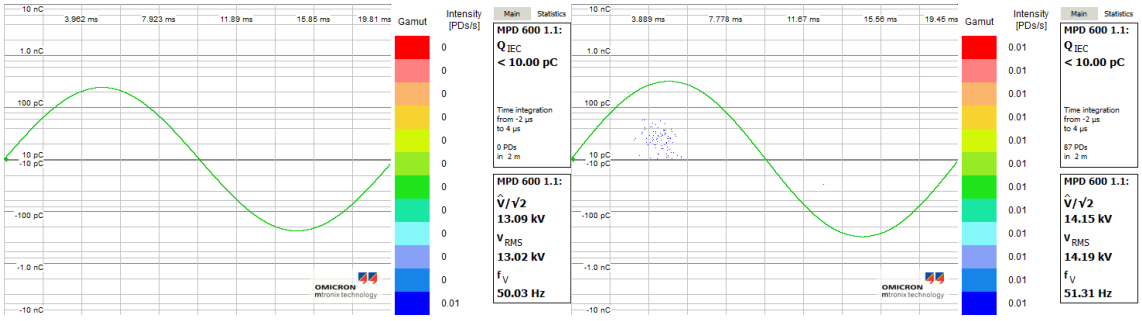

(e) Shell Diala DX (f) Galden 135

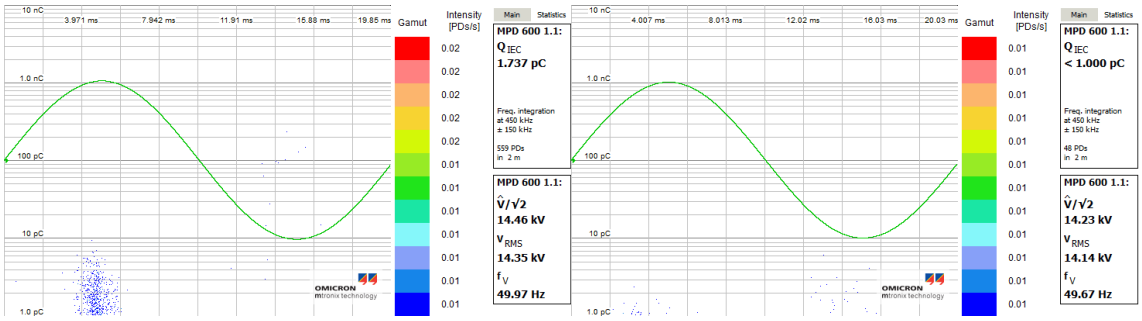

(g) Biotemp (h) Nytro 10XN

Figure 4.20: Negative wire at positive polarity. PD patterns in different liquids, d = 20 mm, $r_p \approx 7$ μm and $E_{tip} \approx 700$ kV/mm. V_{peak} = 18 - 20 kV. Total time is 2 min

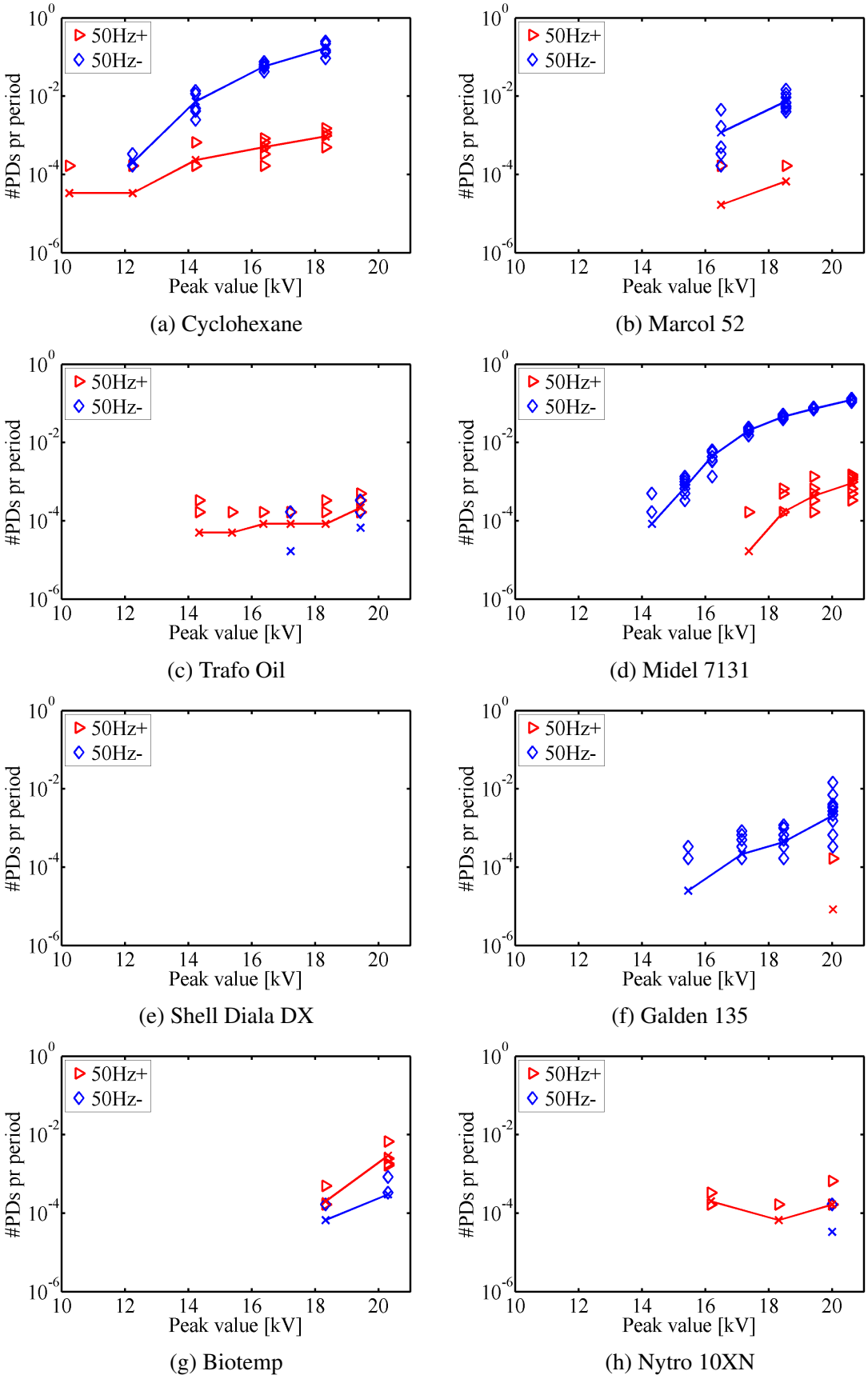

(a) Cyclohexane (b) Marcol 52

(c) Trafo Oil (d) Midel 7131

(e) Shell Diala DX (f) Galden 135

(g) Biotemp (h) Nytro 10XN

Figure 4.21: PD rates measured in different liquids, $d = 20$ mm, $r_p \approx 7$ μm and $E_{tip} \approx 700$ kV/mm. Total time is 2 min

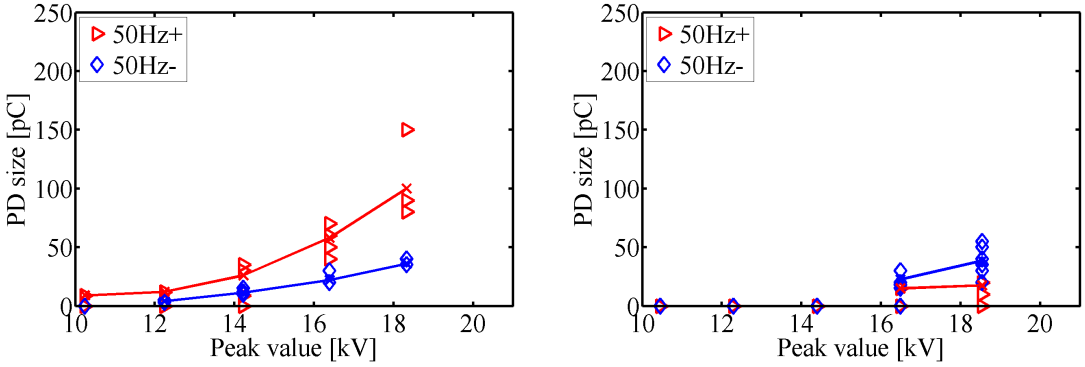

(a) Cyclohexane

(b) Marcol 52

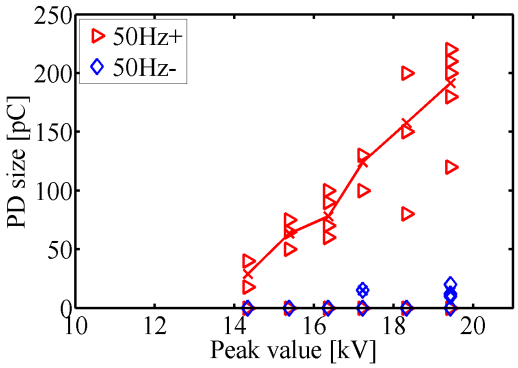

(c) Trafo Oil

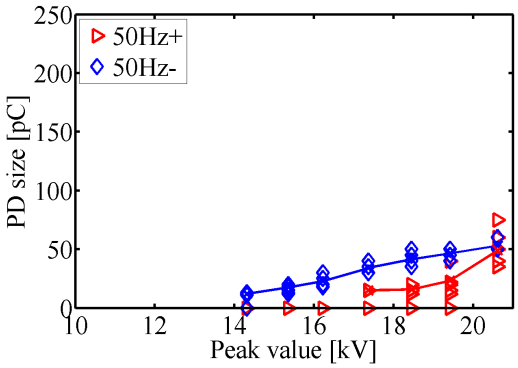

(d) Midel 7131

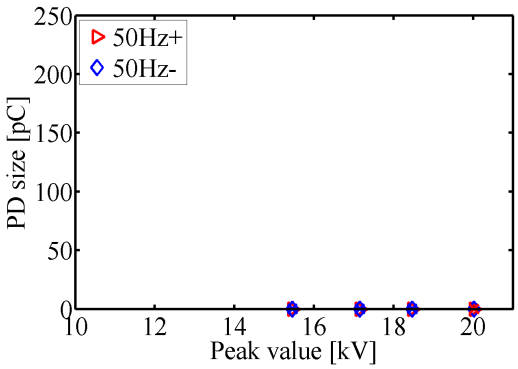

(e) Shell Diala DX

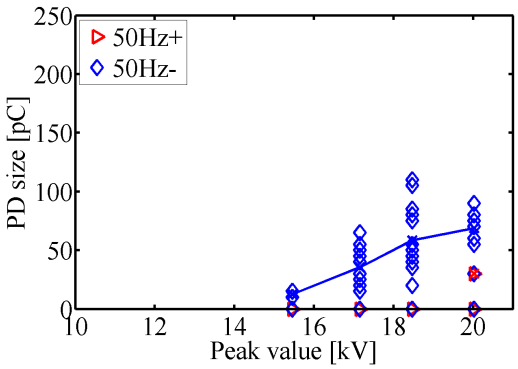

(f) Galden 135

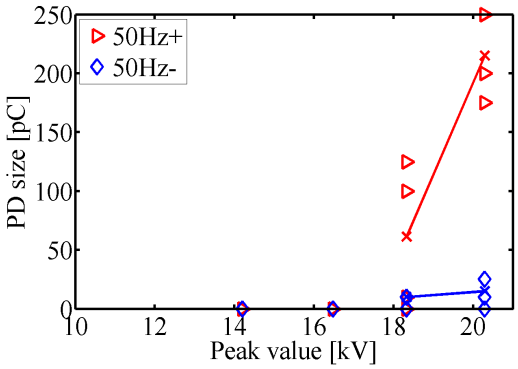

(g) Biotemp

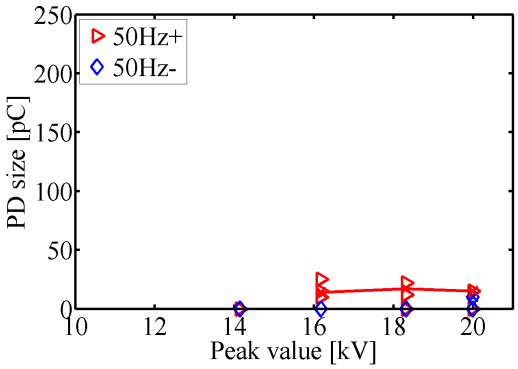

(h) Nytro 10XN

Figure 4.22: Maximum PD magnitude in different liquids, d = 20 mm, $r_p \approx 7$ μm and $E_{tip} \approx 700$ kV/mm. Total time is pr sample is 2 min

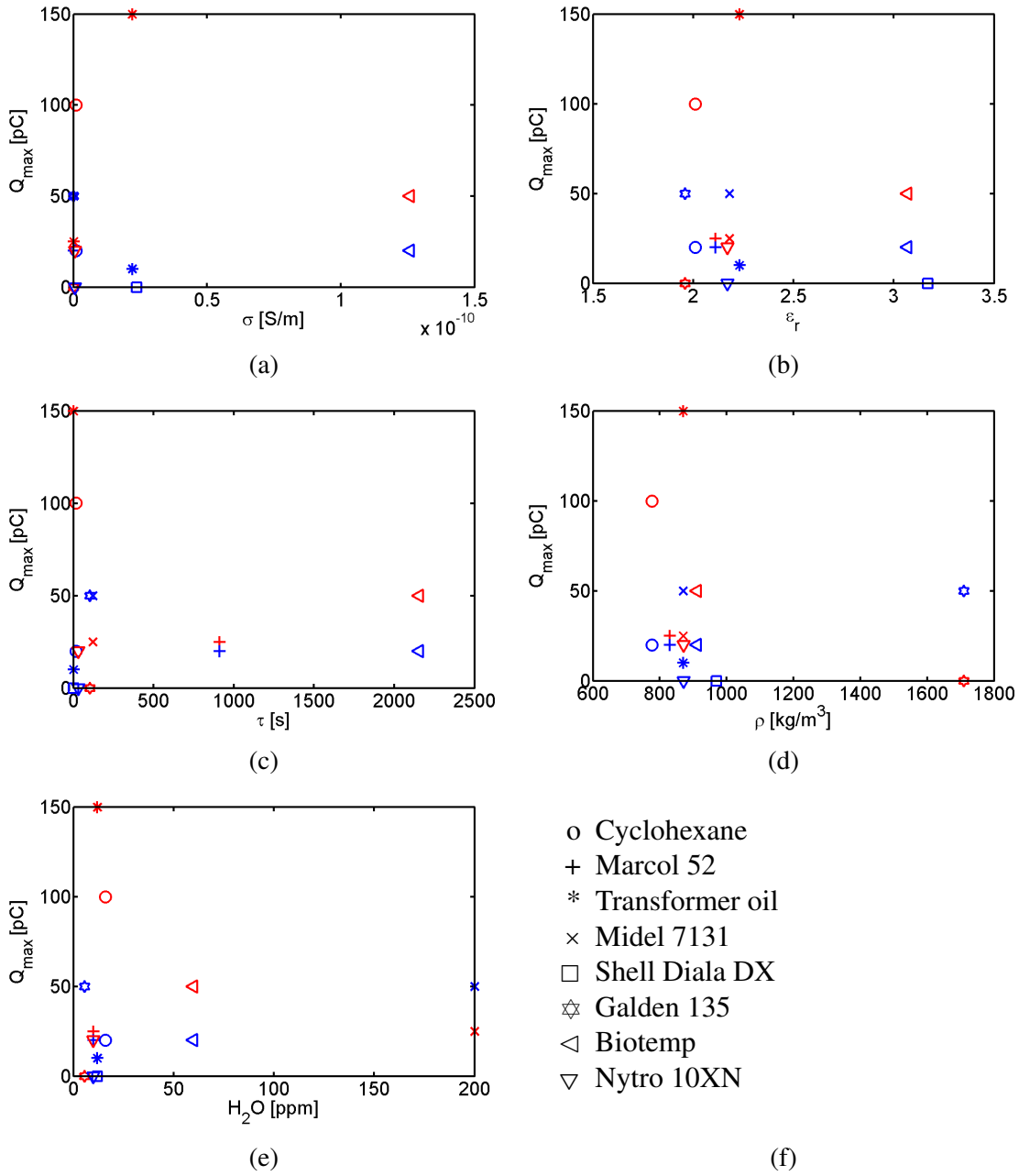

Figure 4.23: Dependence of PD magnitude measured in the liquids verseus measured properties; Table 4.1. Red marking are positive PDs and blue marking are negative PDs. Voltage level approximately 18 kV. No apparent relation between the different parameters and the discharge level.

4.2.6 X-rayed test cell

The current was not affected by the X-ray, but the PD phase pattern had a huge burst when exposed to X-rays, Figure 4.24 and Figure 4.25.

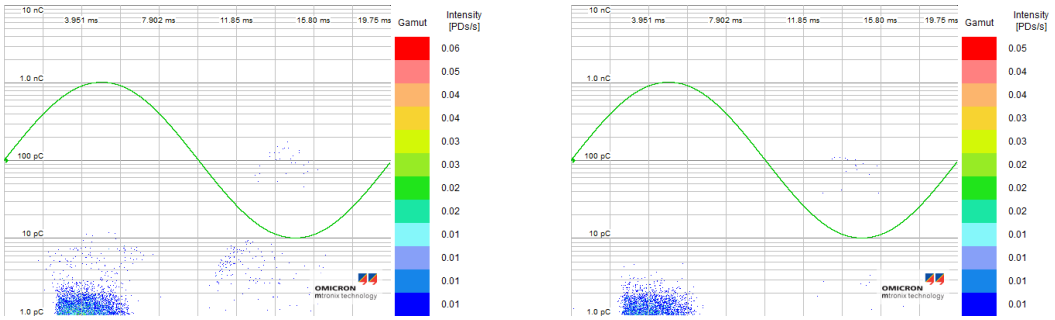

(a) 2 minutes PD pattern for 50 Hz with 6 seconds X-ray exposure

(b) 2 minutes PD pattern for 50 Hz without X-ray exposure

Figure 4.24: X-rayed test cell. Corresponding PD-pattern and a reference without X-ray in Nytro 10XN. Voltage level, 20 kV, r_p = 6 μm. Note the difference in PDs at both polarities at below 10 pC.

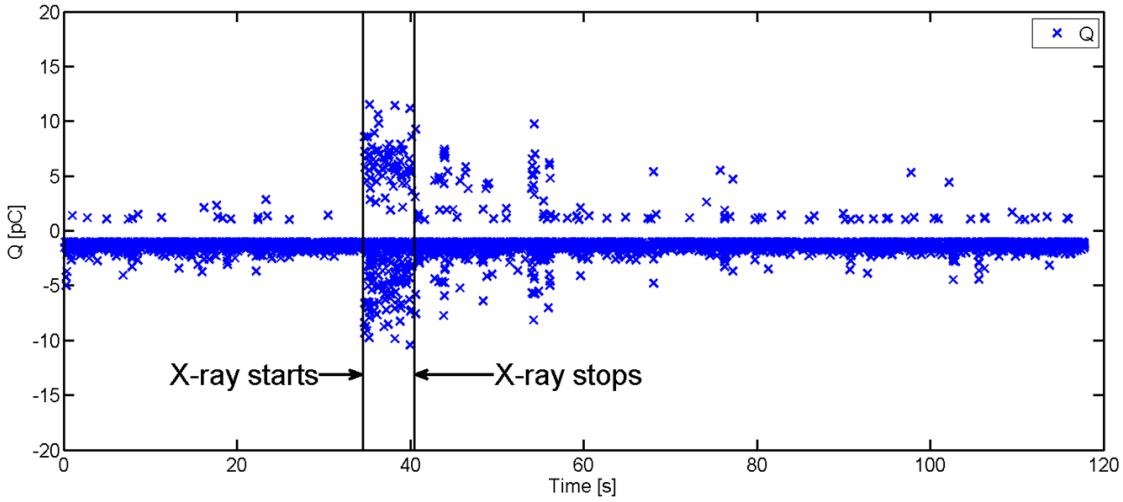

Figure 4.25: PDs, blue crosses, during a two minutes X-ray experiment. The test cell was exposed for X-rays in 6 seconds. An AC voltage of 20 kV_{peak} and 50 Hz was applied during the whole two minutes period.

4.3 Images captured with optics

Streamers were also observed at the polarity change in a square wave when changing the tip field from negative to positive. These streamers are shown in Figure 4.26 in a picture of an area of 0.95 mm × 0.775 mm.

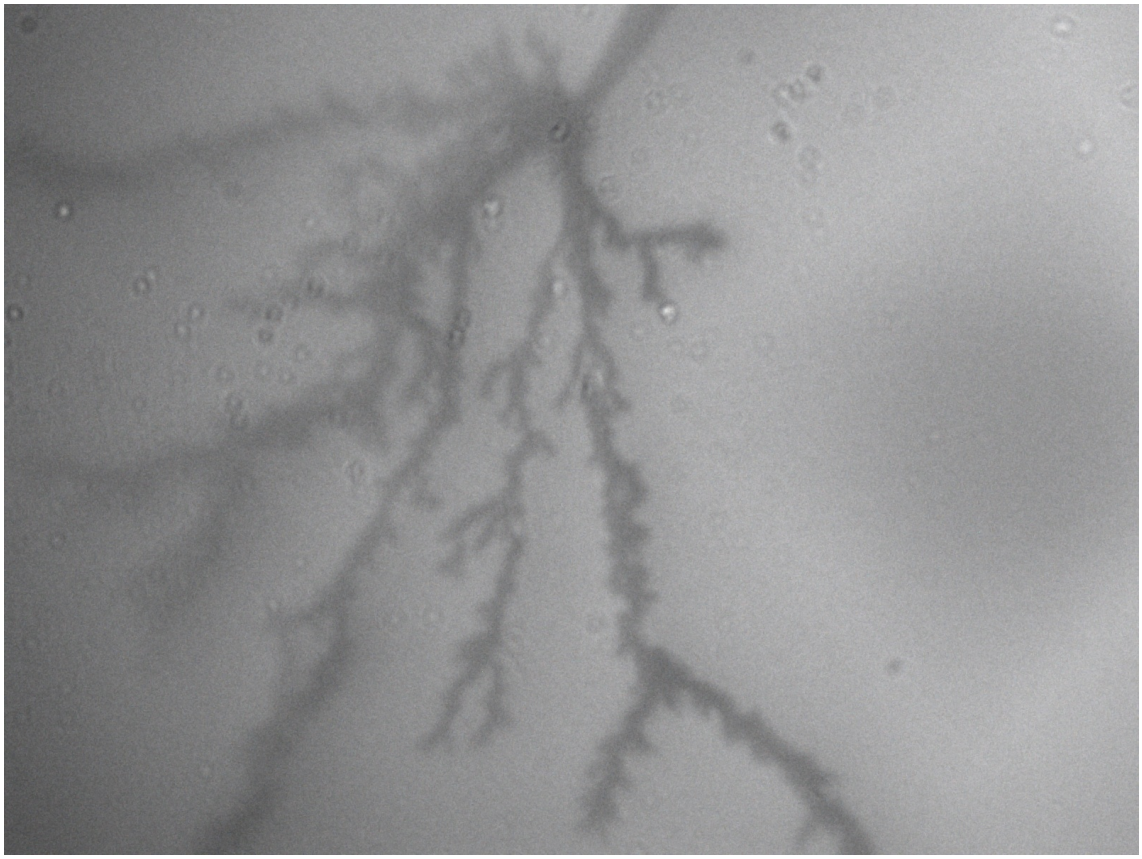

Figure 4.26: Streamer in Midel 7131 when changing polarity from negative to positive, 40kV difference

Chapter 5

Discussion

These experiments have been performed in order to get a better understanding of space charges in insulating liquids and their influence on partial discharges. Partial discharges are said to degrade and age insulating liquid and are therefore important to understand in order to get reliable operational power electronics in subsea environments. When understanding the underlying physics of the phenomena it can be possible to test the suitability of liquids with a proper method.

Firstly, some important choices are discussed and then the conductive current from space charges are discussed. Finally partial discharges are discussed and important mechanisms mentioned.

5.1 Important choices

A full study of all the different involved parameters affecting space charges and PDs would have been unnecessary, time consuming and ineffective due to already known literature which explains this well. Therefore, several qualified choices were made based on earlier experiments described in the literature.

When studying PDs, there are several possible geometries to choose between. The point plane geometry was chosen in order to obtain a strong electrical field locally at a relatively low voltages. The localized strong field region provides the possibility of *knowing* where the events happen and thereby use optics to make photographies of streamers. The divergence of the electrical field also leads to creation of streamers without reaching breakdown, which usually is the case in a plane-plane configuration.

It is important to choose the right frequency region. The capacitive current increase linearly with frequency and therefore for sufficiently large frequencies (>>10 Hz), the conductive current is non-detectable in the noise of the system. Therefore, frequencies below 10 Hz were mostly chosen. One way to deal with the high frequency noise and AC signal is to use a differential amplifier and a perfectly balanced bridge measurement, as Ingebrigtsen did in his PhD [37]. In doing so, a long time is needed to adjust the bridge perfectly. Filtering of the signal is possible, but the signal generator provide a non-perfect sine and then all the frequencies are needed in order to reproduce the signal correctly. In

addition, square waves need as many frequencies as possible. This leaves the option of a low frequency region and some noise.

Variations in the point-plane distance is not significant to the PD experiment. The electrical field vary linearly with distance, equation (2.6) and the sensitivity equation, equation (2.7) states a small change in the electrical field for changes in the gap distance. This is in accordance with Lesaint and Top [6] who experienced that different distances did not affect the partial discharges significantly, in contrast to the tip radii which is most important. However, higher voltages results in larger PDs, which corresponds to a longer streamer length. Therefore, a certain distance is chosen in order to be able to study high voltages without breakdown.

The commercial PD-measure system Omicron has a variety of possibilities and settings. Omicron measures currents and uses digital processing to derive the charge. The threshold value for PDs has been set to 10 pC and integration in the time domain. Integration in the frequency domain is also possible, but the polarity of the PDs is then not correctly registered in Omicron, which is a problem known by the manufacturer. However, when using frequency integration, the threshold value might be below 1 pC. Despite this, time domain integration was chosen in order to measure all pulses in a PD correctly. PDs in liquids are often a sum of several minor discharges building branches in a tree-structure, like the images taken by shadow graphics, see Figure 4.26. When integrating in the frequency domain, it is not certain whether a train of short pulses is measured as one or more events. For low level PDs, the event time is short and frequency integration is assumed to work well. In this experiment, larger PDs were recorded and time integration were necessary.

The experiment is most sensitive to changes in the tip radius. Equation (2.7) states that small changes in the tip radius results in significant changes in the electric field. This was confirmed during the experiment. Another fact is that the tip radius is not constant in time when an electric field is applied: The tip radius was seen to increase with time, and thereby a time dependent electrical field distribution occur, see Figure 5.1.

Assuming there is a constant rate of volume reduction of the tungsten needle, which is etched for a given voltage, there is possible to calculate the time dependence of the tip radius. Approximating the etching area to a half sphere:

$$\begin{aligned} \frac{d(Volume)}{dt} = A &= 2\pi r_p^2 \frac{dr_p}{dt} \\ At &= \frac{2}{3}\pi r_p^3 \\ r_p(t) &= \sqrt[3]{\frac{3A}{2\pi}t} \\ r_p(t) &= C\sqrt[3]{t} \end{aligned}$$

The constant C is, when performing a data fitting, 5.7694 at 18 kV. This gives a constant volume reduction rate of the tungsten needle of

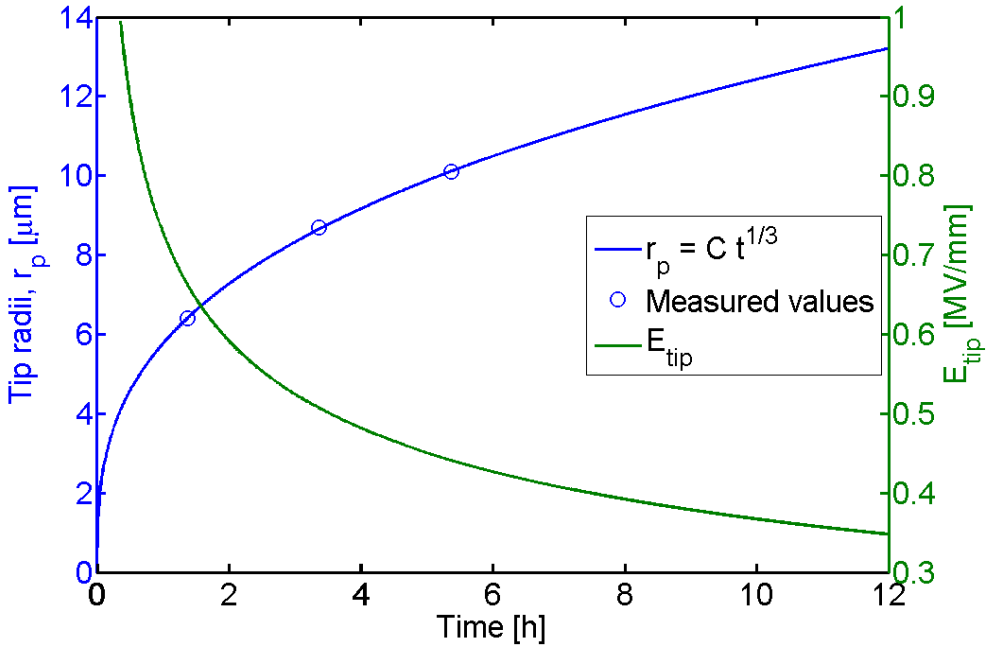

Figure 5.1: Changes in tip radius with time and corresponding electrical field, measured in Midel 7131, V = 18 kV_{pk}.

$$C = \sqrt[3]{\frac{3A}{2\pi}} = 5.7694\frac{\mu m}{\sqrt[3]{h}}$$
$$A \approx 400\frac{(\mu m)^3}{h}$$

From the experience with increasing tip radii during measurement, tip radii of about 5μm -7μm were used in order to get quasi-stable conditions with as small radius as possible. Figure 5.1 shows the problem of increasing tip radius with time.

Different liquids were chosen in order to have a width in the results and to see whether there are differences between liquids or not.

5.2 Space charges and conductive current

An electrical field generates charges in a liquid through dissociative ionization and electrode mechanisms like field emission and tunneling. These effects are larger for stronger electrical fields. According to the Shockley-Ramo theorem, equation (2.43), only charges near the tip contribute significantly to the measured current due to a localized strong electrical field.

Figure 5.2 illustrates the idea of charge generation and how they affect the electrical field. Assuming no initial charges, region **1** illustrates that the field follow the applied voltage to a certain point, region **2**. At this voltage level, there have been generated space charges.

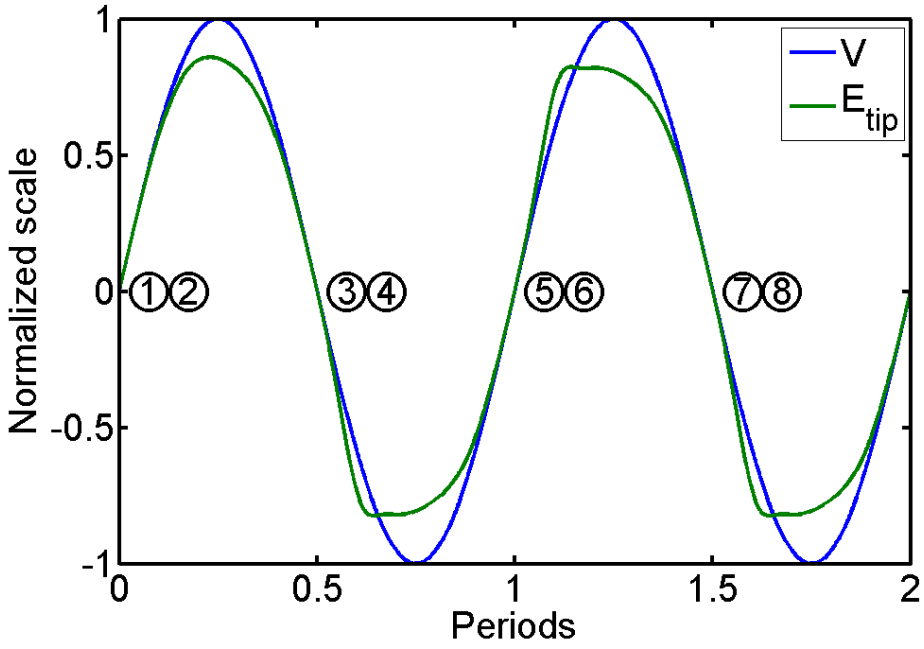

Figure 5.2: Schematics of field change because of space charges. Region **1**: No space charges, regions **2**,**4**,**6**,**8**: Homocharge, regions **3**,**5**,**7**: Heterocharge from previous half period. This is the result from a polarity symmetric charge generation.

Heterocharges are transported to the tip where they neutralize in contact with the electrode and newly created homocharges are transported away from the tip. It is then a net homocharge in the bulk and a reduction in the electrical field might be observed. Dissociative ionization creates ion pairs, but heterocharges move fast to the tip and neutralize and homocharges move slowly away and change the electrical field due to the divergent field. Field emission and field ionization will make the field asymmetric in its polarity. These processes inject homocharges. After the polarity changes, the homocharges become heterocharges and enhance the field, region **3**. Heterocharges in this region tend to move towards the electrode, but the newly created homocharges closer to the tip are transported away, creating a liquid flow which transports the heterocharge away as well. This leads to region **4**, and so on. Figure 2.1 describes this alternating charge distribution in the gap.

Field emission and field ionization require strong electrical field strengths. In cyclohexane, see Table 2.1, the required field strengths are above the strengths obtained by the geometrical electrical field for most radii used. However, asymmetric currents are measured in cyclohexane that strongly indicates field emission to occur. This is explained by field enhancement from dissociated ions near the tip, the electrical field might be strong enough if heterocharges are present close to the tip. Field emission only consider the field strength at the tip and not elsewhere. The ions will last a certain time and give a current due to a certain relaxation time in the liquid.

5.2.1 Tip radii dependence

The electrical field is sensitive to the tip radius. A small, probable change of 5 μm + 1 μm results in 22% decrease in the geometrical electric field, according to equation (2.2). A smaller radius will increase the electrical field in a smaller area around the tip, and decrease insignificant in the rest of the area, described in Figure 2.3. The active volume, where the processes are said to happen, is increased for increased tip radius, but the maximum electrical field is decreased. This results in decreased dissociative ionization and electrode effects and thereby a lower space charge current is measured in Galden 135, Figure 4.2, and Marcol 52, Figure 4.3 for increasing tip radius.

From Figure 4.3 it seems that there is no significant difference between the maximum current for r_p = 1 μm and r_p = 5.8 μm. This might indicate that there are two outer factors contributing to the space charge current; both the active volume and the electrical field magnitude. The dissociative ionization increase for increasing electrical field, and the active volume decreases for increasing tip radii. The similarity in Figure 4.3 for r_p = 1 μm and r_p = 5.8 μm indicates that these two factors together have a maxima. Another explanation is that space charges produced at r_p = 1 μm enhance the electrical field in such a way that it de facto acts as the same as r_p = 5.8 μm. This is, however, not the case for Galden, where the current is decreasing for increasing tip radii. One reason might be the difference in the middle radii r_p = 8.6 μm and r_p = 5.8 μm, and thereby a significant difference in the electrical field.

One pecularity was observed in Galden for 0.1 Hz. The negative conductive current polarity was smaller than the positive polarity, see Figure 4.2. This might originate from a stronger field enhancement in Galden than the other liquids, or stronger field ionization than field emission.

The conductive current increases slower with respect to the alternating voltage for the largest tip radius, r_p = 15μm, than for lower radii. This might originate from weak electrical field for the same applied voltage. Figure 5.3 illustrates approximately how the space charge induced current is affected by the tip radii r_p.

5.2.2 Frequency dependence

Heterocharges from the previous half period enhance the field at the tip. This field enhancement stress the liquid and more ions are created due to dissociative ionization and electrode effects. A higher frequency gives less time for the ions to drift, and all ions remain close to the tip.

Figures 4.2 and 4.3 show how the current changes with frequency. At low frequencies, the conductive current is shifted to the falling edge of the voltage. This might indicate that heterocharges from the previous half period do not enhance the field because they drift too far away from the tip.

For higher frequencies, a larger number of space charges seems to be created due to stronger field from heterocharges from the previous half period. Heterocharges are close to the tip in the strong field volume, and according to the Shockley-Ramo theorem, these charges should contribute significantly to the current. Heterocharges drift towards the

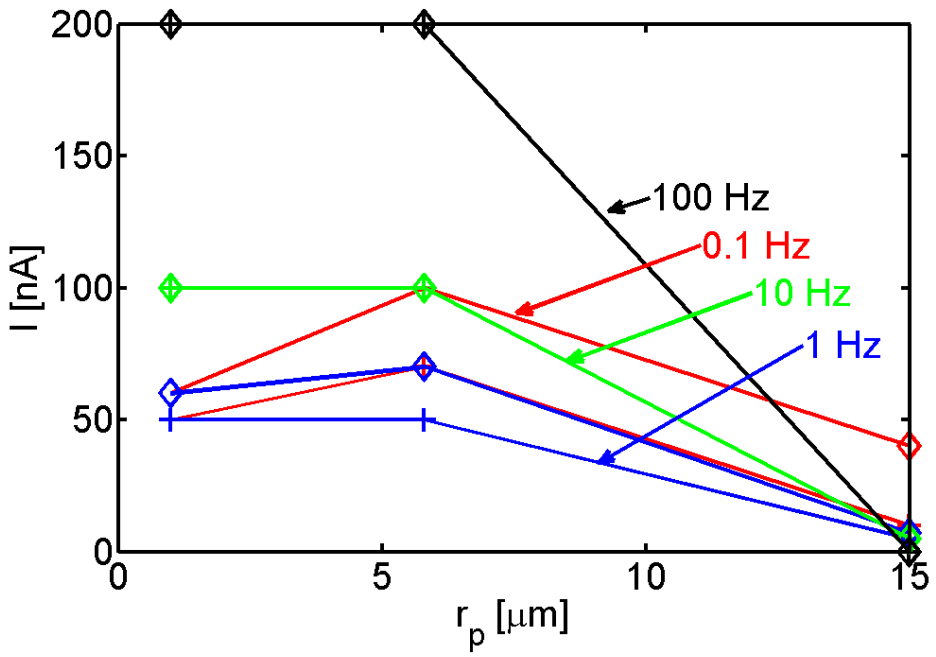

Figure 5.3: Schematics of change in the conductive current in Marcol 52 for changing tip radii r_p. '+' indicates a peak for positive half period of the current and '$\diamond$' a peak for negative half period. The difference in polarity for certain frequencies might be explained by field emission present at these frequencies due to strong enough field.

electrode and enhance the field. Homocharges are created closer to the tip and thus a stronger force on the homocharge leaving a strong flow *from* the high field region and a total field reduction on the falling edge and a small current due to charges far away in a reduced electrical field.

The peaks of the conductive current increase slightly with increasing frequency, as seen in the investigated frequencies, 0.1 Hz,1 Hz,10 Hz, 100 Hz in Figure 4.4 at small tip radii. The larger tip radii have an opposite behaviour and a decrease in peak value for increasing frequencies is observed. This might indicate that the charges present in the large active volume around the large radius tip lower the electrical field below the critical value for the ion production for increasing frequency. It seems like the ions pile up in the active volume for high frequencies and thereby cause a field reduction. At smaller radii, the active volume is smaller and the ions are transported away and the active volume remains with strong field.

The current peaks for Cyclohexane in Figure 4.5 show how the conductive current vary for different frequencies. The current grows stronger when the frequency is increased. At low frequencies, the charges are transported into the bulk of the liquid and 'stored'. When increasing the frequency, these charges might drift towards the electrode due to electrohydrodynamics. The current is weakened when reducing the frequency. This might be explained by charge transport to a weak field area where they are 'stored'.

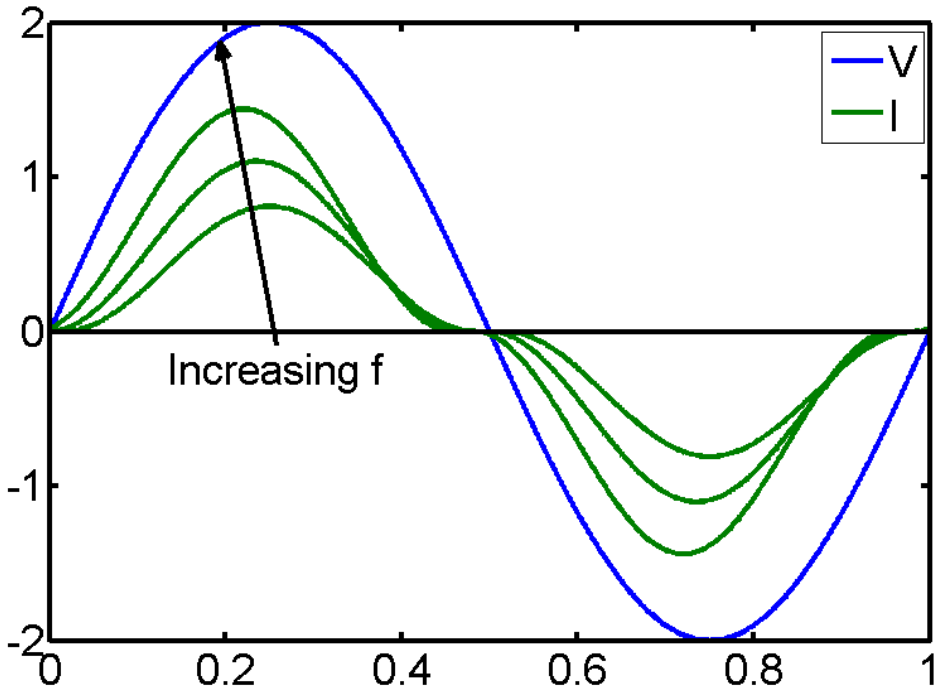

Figure 5.4: Schematics of change in space charge current for changing frequency. This is an effect of shorter transport distance of heterocharges due to strong field at the tip

5.2.3 Voltage dependence

The electrical field is linear in the voltage, see equation (2.2). For low voltages, see Figure 4.6a, the conductive current follows the voltage on the rising edge. This might be explained by a small amount of ionized molecules and thereby no significant field change and the increase is therefore happening at a constant rate. This results in a quadratic increase in the current, Figure 4.6c, 4.6f and 4.6i. For higher voltages, Figure 4.6d and 4.6g, the only difference is in the magnitude of the signal and not in the shape. It seems like the current is quadratic in the voltage in some region for all voltage levels. New mechanisms are happening at higher voltages. Field emission seems to start affecting the negative polarity at around 10 kV.

5.2.4 Different wave form dependency

For different voltage shapes, see Figure 4.7, it is shown that for unipolar AC, the current is either on or off, but for bipolar AC, the current needs some time to enter into stable conditions. This might indicate that heterocharges are present and affect the current because their relaxation time is longer than the period. It seems like the molecular polarization mechanism is important due to large charged liquid molecules. For homocharges, there are a certain number of charges that 'rest' when the voltage is zero. The relaxation time prevents all of the ions to recombine to neutral molecules.

5.2.5 Liquid dependence

The overall conductive current *shape* is the same for all the liquids tested. The differences arise when comparing the amplitude and performing detailed analysis on the rising and the falling edge, Figure 4.9, and asymmetry in the polarity.

All liquids except Shell Diala DX and Galden HT 135 have a small flattening area for rising voltages at the rising edge at positive polarity; Figures 4.8a, 4.8b, 4.8c and 4.8d. This effect might be clearer in Figures 4.9a, 4.9b, 4.9c and 4.9d where the same data are plotted as current versus voltage instead of both voltage and current versus time. The only one that has this effect on the negative polarity is the transformer oil that has been in service for a long time, see Figure 4.8c. This looks like Figure 2.6 which is obtained in a parallel plate configuration. Because the field is highly divergent in the chosen geometry, this figure is not the answer, but it gives some ideas on how it works locally. When space charges are produced, they enhance the field and different effects might occur. If it is assumed that for a specific value of V, there is not produced significantly more ions, the current will be flat, as shown in the different Figures in 4.8.

Field emission follow Fowler-Nordheim (e^- into the liquid) and field ionization (e^- tunneled into the metal). These are the two mechanisms that might explain the differences in the current with respect to polarity. Electrons are more easily transferred from the insulating material than the other way, see Figure 2.9. However, there is an abundance of electrons in the conductor at the negative half period, leaving a larger total probability for field emission than for field ionization. This difference might explain the higher negative current than the positive current. This mechanism seems to be liquid dependent, because the positive and the negative current peaks and shapes have the same size for some of the liquids, and others do not have the same peaks and shapes. The work functions of the different liquids therefore have to be different.

When plotting the current versus the square of the voltage, straight lines are obtained, see Figure 4.9. This indicates that the current increases like the square of the voltage. The mechanisms with this property is the corona current described in equations (2.37) and field emission equation (2.38) in chapter 2.2.5 and space charge limited current in equation (2.39). It is discovered that the current amplitude rise more slowly than it is falling. This might be explained by the relaxation time when the amplitudes are almost the same, see Figure 4.9a (τ = 17) and 4.9b (τ = 911). For the other liquids, the difference has to be connected to the electrohydrodynamics and the creation of charges. Galden, Figure 4.9f, has an almost perfect quadratic relationship between the current and the voltage.

Nytro 10XN and Shell Diala have almost the same current shapes, this is logical, due to quite similar chemical composition and properties. The same might be said about Biotemp and Midel 7131 which is also quite similar in chemical composition.

Different liquids have different composition and therefore different properties. Polar and nonpolar liquids will tend to act differently with field emission and field ionization. Only nonpolar liquids have been studied.

5.2.6 Comparison between the measured current in the point electrode with the results from simulations

The simulation has been performed under the assumption that charges only interact with the geometric field. This is a crude approximation, but will provide some qualitative results. In addition, it is assumed that only charges in a small volume around the tip are contributing to the current, which is likely to be the case anyway. The number of charges are constant during the simulation, no new charges are created or destroyed. This was done to simplify the simulation as much as possible. On the other hand, this might be the case in liquids with long relaxation time where the charges are present for a relatively long time.

A simulation of space charges in a gap has been performed, the results are shown in Figure 4.10. The Shockley-Ramo theorem has been used to calculate the contribution to the current from each charge, randomly distributed in pairs in the bulk. Due to limited computer power, the simulated number of ions were 1/1000 of the actual number. The current was then multiplied by the same factor, under the assumption that the charges were stochastically distributed.

However, it is assumed that the charges do not affect each other in order to get a model that is easier to simulate. This is not the case in reality. In reality, the charges enhance the field and reduces the total current. This means that the simulated results will only give an upper bound for the current given by space charge movement.

Dissociative ionization will mainly happen in the active volume and therefore the simplification of placing ion pairs randomly all over the liquid is not correct. However, charges outside the active volume will not, according to Shockley Ramo theorem, affect the total current significantly. It is therefore not relevant to the results, whether or not these charges are present.

Figure 4.10b describes an almost perfect quadratic relationship between the current and the voltage. This means that charges in a geometric field in the rotational hyperboloid approximation contribute in a quadratic way to the total current as a function of voltage. If an even production of both positive and negative charges happen, then the corresponding current should be quadratic in the voltage.

For Cyclohexane, the simulated current is about 50 nA in both polarities. The measured current is approximately 50 nA for negative polarity and 20 nA for positive polarity. This difference indicates that there exist different charge production processes for negative and positive polarities. Although, Figures in 4.8 indicates that there are different influences of positive and negative polarity in different liquids. The simulation, however, will give a symmetric current due to a constant number of known ions present and not considering the dissociative ionization and recombination.

5.2.7 Time dependence and relaxation

The current-voltage curve in Figure 4.9 show the fact that the space charges need some time to be created. This means that for falling edge at negative polarity and low frequency the current lags behind the voltage. (But different for higher frequency and smaller tip

radii, see Figure 4.3) This is generally not the case for positive polarity where it seems to be more difficult to produce and transport ions. The field at the tip is also enhanced by heterocharges and reduced by homocharges. With homocharges, the field is enhanced a longer distance from the tip, while the field at the tip is reduced. This means that the current should be stronger for homocharges than heterocharges. The significant difference between positive and negative polarity clearly indicates that negative charges are more easily produced than positive charges. This means that there are some mechanisms which affect negative charge production and not the positive charge production.

If just dissociative ionization occurred, the current would almost be symmetric for both polarities. Diala DX and Galden 135 in Figure 4.9e and 4.9f clearly show this symmetry and it is therefore assumed that the current is space charge limited and ions are mainly produced by dissociative ionization. However, for the other liquids, the current is highly asymmetric and therefore it exist a mechanism affecting only the negative charges.

Relaxation time and polarization were described in chapter 2.2.3 and the knowledge of Table 2.1 for different relaxation times and Figure 4.8 clearly indicate that there is a relation between the relaxation time τ and the amplitude of the current. (Although not in all liquids). The unknown transformer oil has a smaller current amplitude Figure 4.8c and relaxation time (0.90 s) than the new Diala DX Figure 4.8e which has a longer relaxation time (122 s). The relaxation time is not responsible alone; Cyclohexane and Marcol 52 have different relaxation times by a factor 10, but the conductive current is almost identical. Just a slight difference in creation and recombination of ions. This is easier to see in Figure 4.9a and 4.9b where the Cyclohexane current rises before the current in Marcol 52.

Midel 7131 has the largest current, permittivity and water content. This might indicate that water content increase the conductivity and ion creation.

5.2.8 Statistical part

The current could also have some statistical variation, which has been measured in Cyclohexane, but not in the other liquids. Figure 4.11 shows this peculiarity. The current might be weak for a long time before it suddenly rises to a high value and then drops exponentially down to its former value. These statistical fluctuations might be triggered by particles or micro bubbles, (Suggested by P. Atten and A. Denat in a discussion) or large discharges. This might be the case, because some microscopic particles are observed, the origin is unknown but possibly paper pieces from the cleaning process.

Degradation of liquids happen locally. Therefore, local conditions are most important. This makes it important to have some idea of the prehistory of the liquid. PDs degrade the liquid by for instance carbonization that occur locally. van Brunt, [24], mentioned that PDs are affected by the whole prehistory of the liquid. This means that correlations might be discovered and due to random activity, one will never get exactly the same results.

5.2.9 Electrohydrodynamics

Electrohydrodynamics makes the liquid flow, and if it flows fast enough, the flow becomes turbulent and impossible to predict. This also creates unpredictable concentrations of space charges, which affect the electrical field and the creation of PDs.

Charged particles in a liquid in an electrical field will start a liquid jet, [22]. The viscosity of the liquid will make a flow because the particles stick together. Liquid jets at high speed will enter a turbulence region which leads to unpredictable currents. The charges might then be transported elsewhere in the gap and come back later without being recombined first due to a certain relaxation time.

5.2.10 Semi conclusion on space charges

The space charge current is mainly dependent on the creation of ions due to dissociative ionization. Dissociative ionization is a symmetric process and will give a symmetric current, which is confirmed in simulations. However, deviations from this symmetric current is experienced, this means that there are more processes involved in creating charges in the bulk. The tungsten electrode is stressed by a strong field at the tip, and electrons are injected into the liquid with field emission, or withdrawn by tunneling electrons into the metal from the liquid, creating ions. The field emission is more likely to happen, and therefore the negative current should be stronger than the positive current.

When increasing the frequency, the space charges do not travel far away from where they were created. This implies a larger concentration of ions in the active volume of the liquid and a field enhancement due to heterocharges from the previous half period is likely to occur. Therefore the conductive current is shifted to the rising edge of the voltage. The current amplitude is smaller at the falling edge, possibly due to field reduction from the homocharges already present in the bulk. The liquids have a relaxation time that let the ions be present for a longer time in such a way that they are not only dependent on the voltage level, but also their prehistory to a certain extent.

The measured current I is the induced current from the movement of space charges the gap. According to the Shockley-Ramo theorem, only the charges in the region near the tip contribute to the total current. Space charges change the total electrical field. However, this enhancement is difficult to calculate and only qualitative aspects might be deduced. It is considered as another thesis to calculate and simulate the field contribution from space charges.

5.3 Partial discharges

Partial discharges are local breakdowns taking place in materials affected by strong electrical field stress. They are often the summation of a number of smaller events that lasts for several micro seconds, like creation of a micro bubble, and breakdown inside the gas bubble. This is why the time integration in Omicron is set to [-2μs, 4μs] to get one event and not several. Pulse pile-up interference might occur.

PDs may degrade the liquid and have a statistical nature. Is it possible to predict anything when knowing a PD sequence?

5.3.1 Tip radii dependence

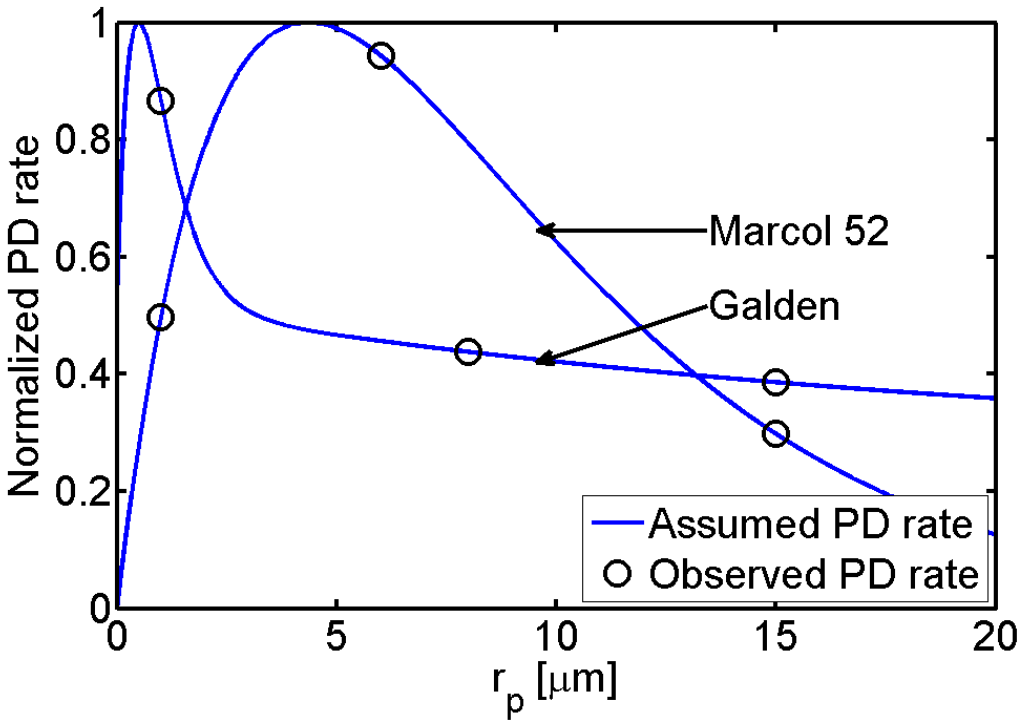

Figure 5.5: Schematics of the change in PD rate for changing tip radii r_p. Deduced from Figure 4.12. The curves are uncertain, but might illustrate the change in PD rate.

As earlier discussed about tip radii and active volume, a reduction of the electrical field will decrease the active volume. This might be the explanation for the difference between Figure 4.12b and 4.12d. One might expect that smaller radii lead to more PDs than larger radii. This might indeed be the case! Under the assumption of a constant maximum value for rate times PD charge, the calculations will yield a high activity relatively small PDs and a slightly smaller intensity allows larger PDs to occur. This might be the case in Marcol 52, see Figure 4.12b, where there might be many PDs below the noise level which are not recorded. The negative discharges are assumed more intense than the positive and are smaller in amplitude.

There are liquid dependences, the Galden 135 and Marol 52 have different PD patterns with approximately the same tip radii, see Figure 4.12. This might originate from different chemical structures and other chemical or physical properties.

Figure 5.5, based on results in Figure 4.12, illustrates schematically how the PD intensity above a certain threshold value is changing with changing tip radii r_p. This figure is not accurate, but made to illustrate that decreasing the radii do not monotonically increase the PD activity. When decreasing the tip radii, the electrical field at the tip will increase rapidly, according to Figure 2.3.

5.3.2 Frequency dependence

With high frequencies, it is possible for heterocharges to stay to next half period in the active volume due to relatively small mobility. This enhance the field on the rising edge and thereby increase the inception probability. Low frequencies do not enhance the field in the same way, and homocharges will dominate and the field is therefore not strong enough for PD inception.

Figure 4.14 shows a direct connection between the PD rate and the frequency of the AC voltage. For low frequencies, see Figure 4.14b, there are no PDs larger than 1 pC over a period of two minutes. When increasing the frequency, Figure 4.14c and 4.14d, the PD rate increases linearly. The amplitude distribution seems to be almost the same for the latter two cases, but with a different PD rate.

The conductive current increases just a little for increasing frequency. Due to limited speed, the charges will not travel a long distance at high frequencies, but stack in a small area. This leads to a local field enhancement and the high concentration of ions leads to unstable local conditions that eventually leads to local breakdown. This might explain the increase in the partial discharge activity.

5.3.3 Different waveforms

Different waveforms, as in Figure 4.15, will create different space charges and thereby the contribution to the electrical field. For DC, and low frequency square wave, the space charges drift away from the tip and starts a liquid jet. This leads to unstable conditions and an unpredictable distribution of space charges and hence electrical field distribution. Different waveforms have different electric field distributions and thereby the inception voltages are obtained at different phase angles in the period. Square waves have reached the inception voltage and thereby have PDs in the whole period, Figures 4.15a, 4.15e and 4.15f. For triangular and sine wave, the inception field is reached at different places in the phase, Figure 4.15b, 4.15c and 4.15d.

5.3.4 Partial discharge correlations

Figure 4.17 and 4.16 show how the PDs occur relative to each other. Especially with Cyclohexane, it is noticed that large positive PDs are always preceded by a negative PDs in the previous half period and followed by PDs in the next half period, due to heterocharges. This strongly indicates that large positive PDs are correlated to the memory of the system. This is in accordance with van Brunt [24] who stated that PDs have memory effects.

A recording of Midel 7131 were performed over two hours. This resulted in a huge number of PDs. The statistics is visualized in Figure 4.18 where it is clear that it is a geometric distribution. The large variation in half periods for a given low normalized sample is due to few recorded samples. Either one discharge or none, when the diagram should have e.g. 0.1 samples. The results in this figure are almost a proof that PDs follow a geometric distribution for the time between events. This is the discrete variant of the exponential distribution that is connected to Poisson distributions. A Poisson distribution is a good

model for the occurrence of radioactive decay, Cannizzaro et al. (1978) [42]. This means that the statistics of PDs might relate to the similar processes that cause radioactive decay.

On the other hand, Cyclohexane has a larger activity level than Midel. This results in a large number of events in short time and the corresponding curve, Figure 4.19, is almost fitted to a geometric distribution except for a small number of half periods. This indicates that the PDs are *in some way correlated to each other*.

5.3.5 Different liquids

Different liquids have different physical and chemical properties, and thereby the inception voltage and partial discharge pattern look different. It is seen, in Figure 4.20, that especially Cyclohexane have a huge number of PDs. The well-used unknown Transformer oil, Figure 4.20c, has just a few large PDs and no PDs above 10 pC.

The over all shape of the PD patterns are always the same: A lot of small negative PDs and a few large positive PDs.

5.3.6 Inception voltage

Figure 4.21 show how the number of PDs per period varies for different liquids and voltages. The shape of the curves are almost the same for all liquids and the rate increases with voltage. The activity of positive PDs are lower than for the negative, but relatively they increase by the same factor.

Normally, the positive PDs are larger than the negative, see Figure 4.22, but not always. The maximum size also varies a lot with time. Galden, see Figure 4.22f, has maximum charge during 2 min from 20 pC to 120 pC in several samples. This is a large variation, that must be considered when testing liquids.

The inception voltage is difficult to define. There will always be a probability for a PD to occur. Nevertheless, the size of the PDs will be small for low voltages. Large tip radii r_p do also produce small sized PDs..

PD activity decreases with increasing formation of space charges. Figure 4.2 and 4.3 show weaker conductive current for increasing frequency and decreasing conductive current for larger r_p over a certain value.

5.3.7 X-ray and abundance of electrons

When the test cell was exposed of X-rays, a lot of small discharges around 1-10 pC occurred in Nytro 10XN in both polarities, see Figure 4.24 and Figure 4.25. This has as far as my supervisor knows, not been demonstrated before. This might originate from large quantities of electrons being available and therefore a more frequent PD rate than otherwise. A higher PD rate also relates to small PD size. Figure 5.6 tries to explain why small and not large PDs are happening.

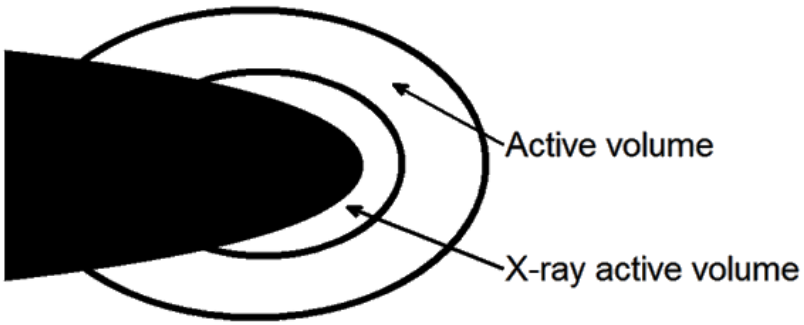

Figure 5.6: Schematics of the area of PD events

PDs have been shown to be a stochastical phenomenon dependent on available electrons. The X-ray experiment has shown that the stochastical factor was not present during X-raying and PDs are concluded to be dependent on available electrons.

5.3.8 General considerations

PDs are dependent on strong electrical field for initiation. The strong field evaporates the liquid and PD happen inside the micro-bubbles formed, Kattan et al. [23]. PD might also occur if the liquid becomes ionized under high field and thereby form a conducting volume. It is clear that PD is a strong electrical field phenomenon.

In general, it is observed that PDs appear on the rising edge in both polarities where the electrical field is enhanced. The number of negative PDs are larger than the number of positive PDs, but the positive PDs are larger than the negative PDs. This might originate from the fact that negative PDs are easily produced, compared to the positive PDs. Because electrons are formed more easily, the negative PDs are more probable to happen. The difference in size might be explained by different propagation mechanisms for positive and negative PDs. This has not been investigated in this thesis.

From the previous section, it is clear that Midel 7131 has the largest current and thereby the largest presence of space charges. Midel 7131 also has a larger amount of positive partial discharges than the other liquids, see Figure 4.20.

Cyclohexane has the largest rate in both polarities. If the space charge current should be directly correlated to the occurrence of partial discharges, Marcol 52 should have the same high activity, which the results show.

All liquids, except Galden 135, have a correlation between large conductive current and PD rate. A large current does also give a higher PD rate.

Statistical fluctuations results in unpredictable behavior and active and non-active periods are observed, more in some liquids than in other. This implies that test methods should consider a proper time aspect of the test.

Large positive PDs are found to be correlated to negative PDs in the previous half period, see Figure 4.17, and the negative are also influenced by a large positive in the previous half period. Negative PDs have generally a geometric distribution.

Figure 4.23 shows that there is no obvious relation between conductivity, permittivity, water content or density and the partial discharges. It all depends on the chemical structure of the liquid. This statement need further research to prove. However, Ingebrigtsen et al. [31] showed that different additives in Cyclohexane affected the streamers differently. This might strongly indicate that the chemical structure are important, especially the liquid's ability of ionize and of providing or capture electrons.

5.4 Advantages and disadvantages with IEC 61294

IEC 61294 is a method of finding the inception voltage of PDs in liquid insulation by raising the voltage at a constant rate of 1 kV/s. The inception voltage of mineral oils and synthetic esters seems to fit this method quite well, as their PDs appear after a geometric distribution and thereby statistics might defend the ten tests per liquid procedure. On the other hand, Galden, a fluorite liquid, has another PD profile, where PDs are appearing in unpredictable groups and thereby it is unknown whether tests reveal the right inception voltage.

Another aspect of the IEC 61294 test is the certainty of the test to reveal the right inception voltage, due to statistical fluctuations in the PD activity. Liquids are experienced not to have the same statistical behavior. Therefore one should consider if the test method should work for all liquids, or just a limited number of liquids. One main aspect for test methods is to discover whether a new liquid is trustworthy or not comparable to known well-used liquids. The new liquids might have different statistical behaviour, unknown before testing. Therefore it might be beneficial to have one test method covering all liquids.

Given the PD inception value is trustworthy, do we actually *know* that this test make sense? PDs are known to degrade the liquid, but are there any proofs for single PDs to affect the suitability of liquids? During tests in this experiment, the well-used, old transformer oil, was demonstrated to have a few PDs above 100 pC, Figures 4.20c, 4.21c and 4.22c. This proves that the rate is not correlated to the size of the PDs. Cyclohexane for instance, has both a large rate and large maximum PDs, Figures 4.20a, 4.21a and 4.22a, while Midel 7131 just has a large rate, but not large maximum PDs.

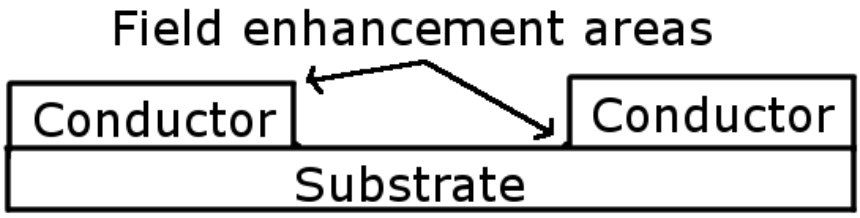

Figure 5.7: Typical power electronic configuration with field enhancement areas.

IEC 61294 is a method based on a very divergent field in a point-sphere geometry. When building power apparatus one tries to avoid to create these field enhancement areas. For

power electronics it cannot be fully avoided. A lot of different designs occur with sharp edges between substrates, see Figure 5.7.

The test method do not differentiate between single PD occurrence above the threshold and a lot of PDs right below the threshold value. The latter might be more dangerous than the first over time. Figure 5.8 illustrates this point. The red PDs will pass the test due to being below the threshold value for rejection. The blue PDs are just above the threshold and will be rejected.

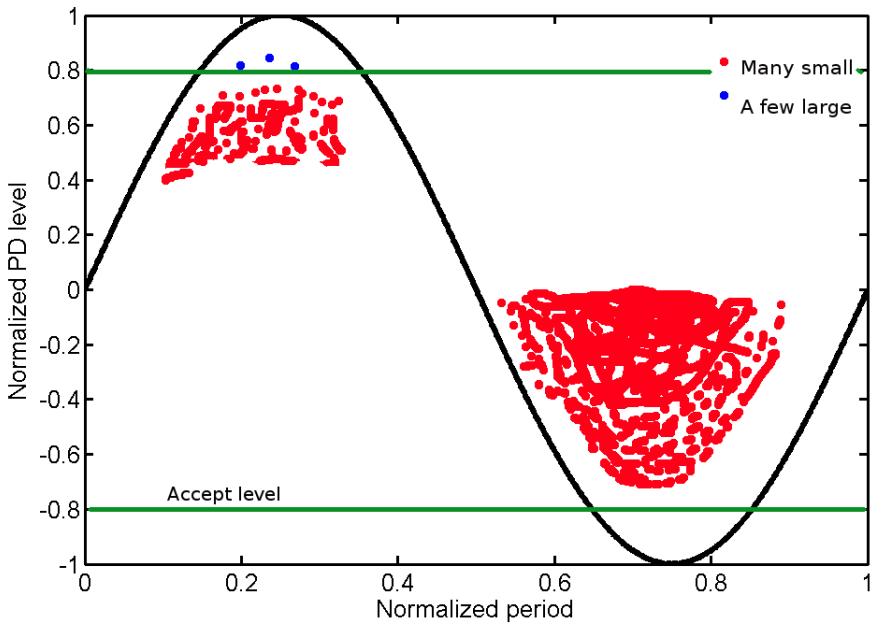

Figure 5.8: Possible scenario for IEC 61294, where there are a few large PDs in one liquid and a lot smaller PDs in another liquid. The first liquid will fail the test, the other pass.

Despite all the disadvantages mentioned here, the test method will prove that the liquid is suitable if no PDs happen at all. The problems arise when there is doubt if the liquid is suitable or not. A liquid that just pass the test will be uncertain. Other test methods are then needed. When comparing different test methods, not considered here, one might get slightly different results. The role of viscosity, temperature and thereby the speed of the charges are important.

5.5 Power electronics

Power electronics operate with rapidly rising signals and relatively high voltages. Sleeping mode voltage is often on, leaving space charges in the insulation when it is quickly grounded when starting working.

The geometry of power electronics is different from the geometry tested here. However, general physical understanding might be concluded from simpler geometries and transmitted to cases that are more complex. It has been concluded that space charges strongly affect the electrical field and partly shield or enhance the volume (homo/heterocharges)

that creates the strong field and thereby the PDs. This knowledge provides an important background when discussing power electronics and chips. It is then possible to locate weak spots and deduce some space charge creation that might reduce the electrical field and prevent partial discharges from occurring. However, if the frequency is too high, this shielding effect is shown to not have any effect, Figure 4.14.

When testing power electronics under operational conditions, one must consider the impedances of the cables carefully in order to avoid unwanted reflexes when applying high frequencies. This implies that measurements becomes more complicated to perform.

Chapter 6

Concluding remarks

Partial discharges (PDs) have a stochastic nature, but also possess memory effects from earlier PDs or electrical stress. Measurements over a certain period of time are therefore needed in order to obtain reliable data. PD inception requires a strong electrical field above a threshold value to happen. Field enhancement factors are therefore of great importance in order to understand PDs.

Space charges change the electrical field distribution and increase or reduce the PD rate and size, dependent on the polarity of the charges and the electrode. Dissociative ionization is identified as the most important process of ion production. Asymmetric processes which also contribute to charge generation are field emission (negative electrode) and field ionization (positive electrode). Asymmetries in the currents are therefore described as a result of different magnitudes of field emission and field ionization.

Heterocharges close to the tip enhance the electrical field. This enhancement was observed to increase the PD rate. The charges drift a longer distance at lower frequencies and thereby heterocharges from the previous half period are less important than at higher frequencies, where the charges stay close to the tip. There is a tendency of PDs to happen at the rising edge of the sine voltage. This fits well with the heterocharges from previous half period present at the rising edge and homocharges present at the falling edge. The charge distribution is therefore of importance for PDs. Long liquid relaxation times and electrohydrodynamics make an unpredictable situation for the electrical field distribution.

IEC 61294 requires that no PDs larger than 100 pC may occur to qualify the liquid as well working. Due to statistical fluctuations, it might happen that some large PDs occur at a rate of 1/h. Some liquids might have a large rate for PDs just below 100 pC and none above. We do not know which of these cases are dangerous, but the IEC method might qualify the liquid with lots of PDs and not the one with rarely occurring PDs. Other liquids have their PDs in groups and during testing, one might be ‘lucky’ to hit the silent or active period and thus wrongly judge the liquid as well working.

This thesis has provided experimental results on conductive currents and PD rates in different liquids. It is found that different liquids have different PD patterns and different space charge concentrations that might distinguish them. However, there is not found any clear connection between important parameters like permittivity, density, conductivity or water content and the space charges and PDs. This indicates that the chemical structure is more important than these physical factors. An abundance of electrons present (X-rays) start a lot of small sized PDs. This indicates that electrons might start small PDs by

electron avalanches.

Chapter 7

Suggestions for further work

It would be beneficial to do PD tests on more realistic geometries relevant for power electronics. Square edges and chips would be interesting to investigate, both by measuring the current and PD behaviour. More realistic geometries should be the next scope.

A long time experiment - possibly over several years - should be performed in order to test how the PDs change over time, or an accelerated test. It would be interesting to find correlations between PDs in short time and PDs or degradation in long time service. Tests should be performed on transformer oil that has been used for several years. Several samples with some years of service between could be interesting.

Power electronics have a high dV/dt and faster pulse switches should be investigated further with better instrumentation.

An in depth study and characterization of the statistics of partial discharges might be of interest. This involves the creation of partial discharge phase probability distributions for different liquids. A statistical characterization of PD behaviour in liquids might prove liquid test models reliable.

7.1 Limitations

High frequencies have been difficult to study due to noise. The noise was some percent of the maximum signal amplitude. The capacitive current increases faster vs frequency than the conductive current. Therefore the interesting conductive current signal are hidden in the noise band of the system for high frequencies.

A difference amplifier might be used for steep rise voltages, but due to experiences with tidy adjustments from earlier work, this was not done in this thesis. The benefits were not considered to be worth the added effort when taking in account the time spent. In later studies, one might want the accuracy obtained from a differential amplifier. If this was taken into use it would be possible to obtain more exact results for higher frequencies where the capacitive current is large.

The high voltage amplifier, Trek, has a limitation of maximum 20 kV_{peak}. But, it also has the ability of amplification of frequencies from 0.05 Hz to 20 kHz. The possibility

of low frequency voltages was considered valuable, due to noise, and therefore higher voltages was not obtained. Higher voltages would have revealed new injection processes, but then space charges would not have been possible to investigate in the way it has been performed in this thesis.

A high voltage transformer should be tested in order to get voltages above 20 kV_{peak}. The disadvantage of the transformer is the optimized operation around 50 Hz and it is not possible to both get low frequency and higher voltage than 20 kV_{peak}. If possible, several physical processes happen at higher frequencies, e.g. tunnelling.

Chapter 8

Acknowledgement

I am honoured and grateful for all help given to me by my enthusiastic supervisor Lars Lundgaard and greatly thankful to his colleages Dag Linhjell and Gunnar Berg at SINTEF Energy AS for their enthusiastic support. They have been invaluable to my work.

I also want to thank my supervisor at the Department of physics, NTNU, Steinar Raaen, who made it possible for me to do this work.

Bibliography

[1] IEC61294. Insulating liquids - determination of the partial discharge inception voltage (pdiv) - test procedure, 1993.

[2] L.E. Lundgaard and S.L. Kyrkjeeide. Evaluation of dielectric liquids by measurement of their partial discharge characteristics. In *Conference on Electrical Insulation and Dielectric Phenomena (CEIDP)*, pages 901 –909, oct 1994.

[3] A. Denat. Conduction and breakdown initiation in dielectric liquids. In *IEEE International Conference on Dielectric Liquids, (Trondheim Norway)*, pages 1 –11, june 2011.

[4] V.T.A. Tho, J.L. Auge, and O. Lesaint. Partial discharges and light emission from ceramic substrates embedded in liquids and gels. In *IEEE International Conference on Dielectric Liquids (Trondheim, Norway)*, pages 1 –4, june 2011.

[5] L. Donzel and J. Schuderer. Nonlinear resistive electric field control for power electronic modules. *IEEE Transactions on Dielectrics and Electrical Insulation*, 19(3):955 –959, june 2012.

[6] O. Lesaint and T.V. Top. Streamer inception in mineral oil under ac voltage. In *IEEE International Conference on Dielectric Liquids, (Trondheim, Norway)*, pages 1 –5, june 2011.

[7] A. Denat, B. Gosse, and J. P. Gosse. High field dc and ac conductivity of electrolyte solutions in hydrocarbons. *Journal of Electrostatics*, 11(3):179–194, 1982.

[8] P. Moon and D.E. Spencer. *Field Theory Handbook*. Springer-Verlag, New York, 2nd edition, 1971.

[9] Olof Hjortstam, Joachim Schiessling, Yuriy V. Serdyuk, and Stanislaw M. Gubanski. Measurements of ion mobility in transformer oil: Evaluation in terms of ion drift. In *Proceedings of 2012 IEEE Conference on Electrical Insulation and Dielectric Phenomena 2, Montreal Canada*, pages 357–360, October 2012.

[10] P. Atten, B. Malraison, and M. Zahn. Electrohydrodynamic plumes in point-plane geometry. *IEEE Transactions on Dielectrics and Electrical Insulation*, 4(6):710–718, Dec.

[11] A.A. Zaky and R. Hawley. *Conduction and Breakdown in Mineral Oil*. Peter Peregrinus, 1973.

[12] A. Denat, J. P. Gosse, and B. Gosse. Electrical conduction of purified cyclohexane in a divergent electric field. *IEEE transactions on electrical insulation*, 23(4):545–554, 1988.

[13] G. Berg. *Physics of electrical breakdown of transformer oil*. PhD thesis, NTNU, December 1995.

[14] P. Atten, J.N. Foulch, and H. Benqassmi. High field conduction of liquids in contact with polymeric material with reference to electrorheological fluids. In K.O. Havelka and F.E Filisko, editors, *Progress in Elecrorheologhy*, pages 231–243. Plenum press, New York and London, 1995.

[15] L. Onsager. Deviations from ohm's law in weak electrolytes. *The Journal of chemical physics*, 2(9):599–615, 1934.

[16] J.S. Townsend. *The Theory of Ionization of Gases by collisions*. Constable, London, 1910.

[17] T.J. Lewis. The electrode-liquid interface under high fields. In *Proceedings of 2002 IEEE 14th International Conference on Dielectric Liquids*, pages 91 – 94, 2002.

[18] R.S. Sigmond. *Elektron og Ionefysikk Kompendium*. 1988.

[19] S. Ramo. Currents induced by electron motion. *Proceedings of the IRE*, 27(9):584 – 585, sept. 1939.

[20] W. Shockley. Currents to conductors induced by a moving point charge. *Journal of Applied Physics*, 9(10):635–636, 1938.

[21] R. Coelho and J. Debeau. Properties of the tip-plane configuration. *Journal of Physics D: Applied Physics*, 4(9):1266–1280, 1971.

[22] P. Atten and M. Haidara. Electrical conduction and ehe motion of dielectric llquids in a knife-plane electrode assembly. *IEEE Transactions on Electrical Insulation*, EI-20(2):187–198, April.

[23] R. Kattan, A. Denat, and O. Lesaint. Generation, growth, and collapse of vapor bubbles in hydrocarbon liquids under a high divergent electric field. *Journal of Applied Physics*, 66(9):4062–4066, 1989.

[24] R.J. Van Brunt. Stochastic properties of partial-discharge phenomena. *IEEE Transactions on Electrical Insulation*, 26(5):902–948, Oct.

[25] R. J. Van Brunt and S. V. Kulkarni. Stochastic properties of trichel-pulse corona: A non-markovian random point process. *Phys. Rev. A*, 42:4908–4932, Oct 1990.

[26] R. H. Fowler and L. Nordheim. Electron emission in intense electric fields. *Proceedings of the Royal Society of London. Series A*, 119(781):173–181, 1928.

[27] M. von Laue. Comment on k.zuber's measurement of the spark discharge delay time. *Ann.Phys.Leipzig*, 76:261–265, 1925.

[28] R.J. Van Brunt, E. W. Cernyar, P. Von Glahn, and T. Las. Variations in the stochastic behavior of partial-discharge pulses with point-to-dielectric gap spacing. In *Conference Record of the 1992 IEEE International Symposium on Electrical Insulation*, pages 349–353, Jun.

[29] John Lilley. *Nuclear Physics Prinsiples and Applications*. Wiley, 2001.

[30] K. Siodla, W. Ziomek, and E. Kuffel. The volume and area effect in transformer oil. In *Electrical Insulation, 2002. Conference Record of the 2002 IEEE International Symposium on*, pages 359–362, Apr.

[31] S. Ingebrigtsen, L. E. Lundgaard, and P. . Astrand. Effects of additives on prebreakdown phenomena in liquid cyclohexane: Ii. streamer propagation. *Journal of Physics D: Applied Physics*, 40(18):5624–5634, 2007.

[32] S. Ingebrigtsen, L. E. Lundgaard, and P. . Åstrand. Effects of additives on prebreakdown phenomena in liquid cyclohexane: I. streamer initiation. *Journal of Physics D: Applied Physics*, 40(17):5161–5169, 2007.

[33] H. M. Jones and Kunhardt E. E. Development of pulsed dielectric breakdown in liquids. *J. Phys D: Appl. Phys*, 28(1):178–188, 1995.

[34] P Gournay and O Lesaint. A study of the inception of positive streamers in cyclohexane and pentane. *Journal of Physics D: Applied Physics*, 26:1966–1974, 1993.

[35] M. Kim and R.E. Hebner. Initiation from a point anode in a dielectric liquid. *IEEE Transactions on Dielectrics and Electrical Insulation*, 13(6):1254–1260, December.

[36] M. Haidara and A. Denat. Electron multiplication in liquid cyclohexane and propane. *IEEE Transactions on Electrical Insulation*, 26(4):592–597, Aug.

[37] Stian Ingebrigtsen. *The Influence of Chemical Composition on Streamer Initiation and Propagation in Dielectric Liquids*. PhD thesis, NTNU, 2008.

[38] Z.D. Wang, Q. Liu, X. Wang, P. Jarman, and G. Wilson. Discussion on possible additions to iec 60897 and iec 61294 for insulating liquid tests. *Electric Power Applications, IET*, 5(6):486 –493, july 2011.

[39] B.A. Grigorev. Experimentelle untersuchung der wärmekapazität von cyclohexan. *Izv.Vyssh.Uchebn.Zaved.Neft Gas*, pages 61–65, 1975.

[40] V.V. Pugach. Wärmeleitfähigkeit von cyclohexan und cyclohexen bei hohen drücken. *Izv.Vyssh.Uchebn.Zaved.Neft Gas*, pages 48–51, 1980.

[41] M.E. Minas Da Piedade. Ebulliometric apparatus for the measurement of enthalpies of vaporization. *Thermochim.Acta 249*, pages 113–120, 1995.

[42] F. Cannizzaro, G. Greco, S. Rizzo, and E. Sinagra. Results of the measurements carried out in order to verify the validity of the poisson-exponential distribution in radioactive decay events. *International Journal of Applied Radiation and Isotopes*, 29(11):649–652, 1978.

Appendix A

Prolate spheroid coordinates

The geometry of a point-plane gap make the use of prolate spheroid coordinates beneficial when approximating the wire to a rotational hyperboloid. Prolate spheroid coordinates are shown in Figure A.1.

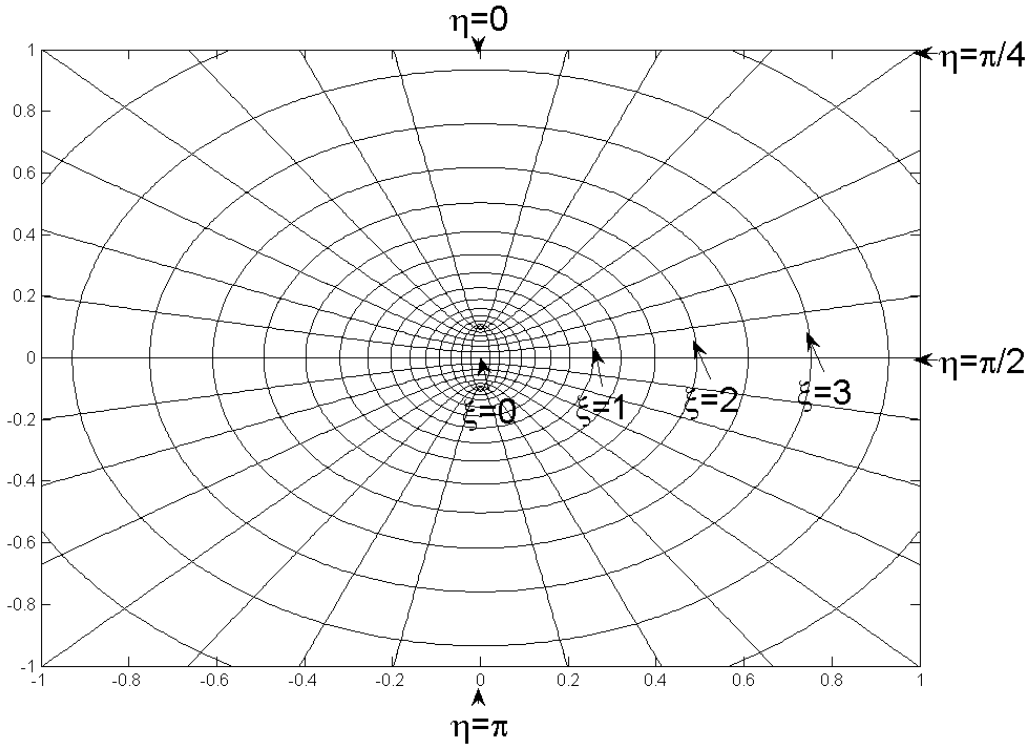

Figure A.1: Prolate spheroid coordinates, rotational coordinate ϕ around the $\eta = 0, \eta = \pi$-axis

The connection between Cartesian and Prolate spheroid coordinates are given by $(x, y, z) \rightarrow (\xi, \eta, \phi)$ where $\xi \in [0, \infty), \eta \in [0, \pi)$ and $\phi \in [0, 2\pi)$

$$
\begin{aligned}
x &= a\sinh\xi\sin\eta\cos\phi \\
y &= a\sinh\xi\sin\eta\sin\phi \\
z &= a\cosh\xi\cos\eta
\end{aligned}
$$

$$
\nabla\mathbf{E} = \frac{1}{a(\sinh^2\xi+\sin^2\eta)}\frac{1}{\sin\eta}\frac{\partial}{\partial\eta}\left(\sqrt{\sinh^2\xi+\sin^2\eta}\sin\eta E_\eta\right)
$$

and the Laplacian of a scalar field is

$$
\begin{aligned}
\nabla^2\Phi = &\frac{1}{a^2(\sin^2\eta+\sinh^2\xi)}\left[\frac{\partial^2\Phi}{\partial\eta^2}+\frac{\partial^2\Phi}{\partial\xi^2}+\cot\eta\frac{\partial\Phi}{\partial\eta}+\coth\xi\frac{\partial\Phi}{\partial\xi}\right] \\
&+\frac{1}{a^2\sinh^2\xi\sin^2\eta}\frac{\partial^2\Phi}{\partial\phi^2}
\end{aligned}
$$

The gradient of a potential is

$$
\nabla\Phi = \frac{1}{a\sqrt{\sinh^2\xi+\sin^2\eta}}\frac{\partial\Phi}{\partial\xi}\hat{\xi}+\frac{1}{a\sqrt{\sinh^2\xi+\sin^2\eta}}\frac{\partial\Phi}{\partial\eta}\hat{\eta}+\frac{1}{a\sinh\xi\sin\eta}\frac{\partial\Phi}{\partial\phi}\hat{\phi}
$$

The Laplace equation is separable in prolate spheroid coordinates. In addition, several symmetries occur. Rotational symmetry along z-axis and the η-lines represent equipotential lines:

$$
V = f(\eta)
$$

$$
\begin{aligned}
\nabla^2 V = \frac{1}{a^2(\sinh^2\xi+\sin^2\eta)}\left[\frac{\partial^2 V}{\partial\eta^2}+\cot\eta\frac{\partial V}{\partial\eta}\right] &= 0 \\
\frac{\partial^2 V}{\partial\eta^2}+\cot\eta\frac{\partial V}{\partial\eta} &= 0
\end{aligned}
$$

which has the solution

$$
V(\eta) = B\ln\tan\eta/2 \tag{A.1}
$$

where B is a constant depending on the boundary conditions:

$$
\begin{aligned}
B &= \frac{V}{\ln(\tan((\pi/2-\sqrt{(1-d/a)\cdot 2})/2+\pi/4))} \\
a &= d+r_p/2
\end{aligned}
$$

The electric field is then

$$
\begin{aligned}
\mathbf{E} = \nabla V &= \frac{1}{a\sqrt{\sinh^2\xi+\sin^2\eta}}\frac{\partial V}{\partial\eta}\hat{\eta} \\
&= \frac{1}{a\sqrt{\sinh^2\xi+\sin^2\eta}}\frac{C}{\sin\eta}\hat{\eta}
\end{aligned}
$$

Appendix B

Matlab script 1

The following function is used in the script in this appendix. The function reads one conductive current vector and a voltage vector. Then the zero crossings in the voltage are found and the script finds the maximum current peak value, variance and mean value of the current peaks per period in both positive and negative polarity.

```
1  %Do statistics on a given data sample for each half period
2  function [pmax,pmean,pvar,nmax,nmean,nvar,mp] = statGage(nonlin↩
       ,Vt) %Whole periods
3
4       lenT = length(Vt);
5       Vt2 = Vt - (max(Vt) + min(Vt))/2;
6       t1 = smooth(smooth(smooth(Vt2(1:lenT-1))));
7       t2 = smooth(smooth(smooth(Vt2(2:lenT))));
8       tt = t1.*t2;
9       x = find(tt < 0);
10
11      last = length(x); % # Zero-crossings
12
13      if((last+1)/2 ~= floor((last+1)/2))
14          last = last - 1;
15      end
16
17      m = linspace(0,0,(last-1));
18      mp = linspace(0,0,(last-1));
19      for i = 1:last-1
20          [m(i),tmp] = max(abs(smooth(smooth(nonlin(x(i):x(i+1))))↩
                ));
21          mp(i) = x(i) + tmp;
22      end
23
24      if Vt(x(1)+10) > 0
25          start = 0; %0 or 1
26      else
27          start = 1;
```

```
28      end
29
30      nmax = max(m(mod(start+1,2)+1:2:last-1));
31      pmax = max(m(mod(start,2)+1:2:last-1));
32      nvar = var(m(mod(start+1,2)+1:2:last-1));
33      pvar = var(m(mod(start,2)+1:2:last-1));
34      nmean = mean(m(mod(start+1,2)+1:2:last-1));
35      pmean = mean(m(mod(start,2)+1:2:last-1));
36
37  end
```

The current analysis script starts with choosing several parameters for the different liquids. Then the data from the oscilloscope are loaded. Several recordings are possible to do in one run. For each sample, the script removes the capacitive current by derive the voltage and subtract the capacitance times the derivative of the voltage from the current. Then the conductive current remains, this signal is low pass filtered by a Fourier transform and all frequencies above $100 f_0$ are set to 0, where f_0 is the frequency of the voltage. The script also finds important parameters as the frequency and magnitudes of the signals. Then it plots the results in different ways.

```
1   close all;
2
3   %%%%%%%%%%%%%%%%%%%%%%%%%%%%%%%%%%%%%%%%%%%%%%%%%%%%%%%%%%%%%%%%%%%%%%%%
4   %%%%%%%%%% Chose one oil: %%%%%%%%%%%%%%%%%%%%%%%%%%%%%%%%%%%%%%%%%%%%%%
5   %%%%%%%%%%%%%%%%%%%%%%%%%%%%%%%%%%%%%%%%%%%%%%%%%%%%%%%%%%%%%%%%%%%%%%%%
6
7   %oil = 'Cyclohexane';
8   %oil = 'Marcol';
9   %oil = 'TrafoOil';
10  %oil = 'Midel7131';
11  %oil = 'Nytro10XN';
12  %oil = 'DialaDX';
13  %oil = 'Galden135';
14  %oil = 'Biotemp';
15  oil = 'Nytro';
16
17  savePictures = 1;
18  plotting = 1;
19  gaugeSignal = 0;
20  fontSize = 30;
21  linewidth = 5;
22
23  nri = [0:9];
24
25  stp = 3; %numbers for the right periods
26  str = 1;
27  %%%%%%%%%%%%%%%%%%%%%%%%%%%%%%%%%%%%%%%%%%%%%%%%%%%%%%%%%%%%%%%%%%%%%%%%
28  %%%%%%%%%% Loading the sensitivity: %%%%%%%%%%%%%%%%%%%%%%%%%%%%%%%%%%%%
29  %%%%%%%%%%%%%%%%%%%%%%%%%%%%%%%%%%%%%%%%%%%%%%%%%%%%%%%%%%%%%%%%%%%%%%%%
30
```

```
31 path = sprintf('C:\\Users\\Torstein\\Documents\\Master\\Results↩
       \\GageScope\\%s\\Sensitivity%s.txt',oil,oil);
32 sensload = load(path);
33
34 %%%%%%%%%%%%%%%%%%%%%%%%%%%%%%%%%%%%%%%%%%%%%%%%%%%%%%%%%%%%%%%%
35 %%%%%%%%%% Important constants: %%%%%%%%%%%%%%%%%%%%%%%%%%%%%%%%
36 %%%%%%%%%%%%%%%%%%%%%%%%%%%%%%%%%%%%%%%%%%%%%%%%%%%%%%%%%%%%%%%%
37
38 scrsz = get(0,'ScreenSize'); %Get the screen size to set the ↩
       figure appropriate
39
40 %The relative permittivity of the different liquids
41 switch oil
42     case 'Cyclohexane'
43         epsr = 2.034;
44         d = 20;%mm
45     case 'Marcol'
46         epsr = 2.11;
47         d = 20;%mm
48     case 'Midel7131'
49         epsr = 3.2;
50         d = 20;%mm
51     case 'Nytro10XN'
52         epsr = 2.2;
53         d = 20;%mm
54     case 'Nytro'
55         epsr = 2.2;
56         d = 17;%mm
57     case 'DialaDX'
58         epsr = 2.2;
59         d = 20;%mm
60     case 'TrafoOil'
61         epsr = 2.2;
62         d = 20;%mm
63     case 'Galden135'
64         epsr = 1.92;
65         d = 20;%mm
66     case 'Galden200'
67         epsr = 1.94;
68         d = 20;%mm
69     case 'Biotemp'
70         epsr = 3.065;
71         d = 17;
72
73 end
74
75 % Adjusting the capacitance
76 C = epsr*1.005e-13;
77
78 %%%%%%%%%%%%%%%%%%%%%%%%%%%%%%%%%%%%%%%%%%%%%%%%%%%%%%%%%%%%%%%%
79 %%%%%%%%%% Processing the chosen samples: %%%%%%%%%%%%%%%%%%%%%%%
```

```
80 %%%%%%%%%%%%%%%%%%%%%%%%%%%%%%%%%%%%%%%%%%%%%%%%%%%%%%%%%%%%%%%%%%%%%%%%
81
82 vec = zeros(length(nri),6); %Vector for statistics
83 vecs = linspace(1,length(nri),length(nri)); %Vector for ↩
       statistics
84
85 totpeak = []; %To save the current peaks
86 positions = linspace(0,0,length(nri));
87 previous = 1;
88
89 for i = 1:length(nri)
90     nr = nri(i);
91     sens = sensload(nr+1,2); %Load the sensitivity, read from ↩
          the oscilloscope
92     [t,Vs,I,Vt,Trig] = loadGage(oil,nr); %Load the data sample
93
94     %The derivative of the Trek voltage
95     dt = (t(21)-t(1))/20;
96     d1 = diff(smooth(Vt));
97     der = 2000*smooth(smooth([d1(1);d1]))/dt; %The derivative ↩
          of V
98
99     lenT = length(Vt);
100    Vt2 = Vt - (max(Vt) + min(Vt))/2;
101    t1 = smooth(smooth(smooth(Vt2(1:lenT-1))));
102    t2 = smooth(smooth(smooth(Vt2(2:lenT))));
103    tt = t1.*t2;
104    indx = find(tt < 0); %Find the zero-crossings
105    last = length(indx);
106    if((last+1)/2 ~= floor((last+1)/2))
107        last = last - 1;
108    end
109    tott = t(indx(last))-t(indx(1));
110    f = (last-1)*0.5/(tott); %Find the frequency
111    %C = 0;
112    nonlin = smooth(I*sens-der*C)*1e9; %The conductive current ↩
          nA
113
114    %%%%
115    fs = 1/(t(2)-t(1)); %Sampling frequency
116    NL = fftshift(fft(nonlin))/length(nonlin);
117    frequencies = linspace(-fs/2,fs/2,length(NL)); %FFT of ↩
          signal
118    NL(abs(frequencies) > 100*f) = 0; %Remove f >100f0
119
120    nl = ifft(NL)*length(NL);
121    nl(2:2:length(nl)) = -nl(2:2:length(nl));
122    nonlin = real(nl); %Low pass filtered signal
123    %%%%
124
125    %Adjustment factor, DC
```

```
126     nl = smooth(smooth(smooth(nonlin)));
127     tmpV = [Vt(indx(1))-nl(indx(1)),Vt(indx(2))-nl(indx(2)),Vt(↩
           indx(3))-nl(indx(3))];
128     gauge = mean(tmpV);
129     if (gaugeSignal == 1)
130         nonlin = nonlin + gauge;
131     end
132
133     [pmax,pmean,pvar,nmax,nmean,nvar,maxvaluepos] = statGage(↩
           nonlin,Vt);
134
135     vec(i,1) = pmax;
136     vec(i,2) = nmax;
137     vec(i,3) = pmean;
138     vec(i,4) = nmean;
139     vec(i,5) = pvar;
140     vec(i,6) = nvar;
141
142
143     newlength = length(totpeak) + length(maxvaluepos);
144     tmp = linspace(0,0,newlength);
145     tmp(1:length(totpeak)) = totpeak;
146     tmp(length(totpeak)+1:newlength) = nonlin(maxvaluepos);
147     totpeak = tmp;
148
149     %Find the positions of the different samples
150     positions(i) = previous + length(maxvaluepos);
151     previous = positions(i);
152
153     factor = tott/length(maxvaluepos);
154
155     [pos,neg,tot] = GageIntegrate(t,nonlin,Vt);
156
157     voltageLevel = 2*max(abs(Vs));%-min(Vs);
158     capacitiveCurrent = C*(max(der(indx(str):indx(stp)))-min(↩
           der(indx(str):indx(stp))))*1e9/2;
159     plotlabelV = sprintf('V_{peak}: %4.2f kV',voltageLevel);
160     plottitle = sprintf('Frequency: %4.2f Hz, I_C = %4.2fnA',f,↩
           capacitiveCurrent);
161     plotlabelI = sprintf('Conduction current');
162
163     plottitle2 = sprintf('%s, %s',plottitle,plotlabelV);
164
165     %Plot the different signals
166     if ( plotting == 1)
167         h = figure('Position',[20 20 1.5*scrsz(4)*2/3 scrsz(4)↩
               *2/3],'PaperSize',[1.5*16 32],'PaperPositionMode', '↩
               auto');
168         plot(t,Vt/max(abs(Vt))*max(nonlin),t,nonlin,t,0*t,'k','↩
               LineWidth',linewidth);
169         set(gca,'FontSize',fontSize,'LineWidth',linewidth)
```

```
170         ylabel('Current [nA]')
171         xlabel('Time [s]')
172         title(plottitle)
173         legend(plotlabelV,plotlabelI,'Location','NorthEast')
174         if (savePictures == 1)
175             filename = sprintf('C:\\Users\\Torstein\\Documents↩
                    \\Master\\Results\\MATLAB\\%s\\%sNonlin%d.png',↩
                    oil,oil,nr);
176             saveas(h,filename)
177         end
178         %%%%%
179         h = figure('Position',[20 20 1.5*scrsz(4)*2/3 scrsz(4)↩
                *2/3],'PaperSize',[1.5*16 32],'PaperPositionMode', '↩
                auto');
180         plot(t(indx(str):indx(stp)),Vt(indx(str):indx(stp))/max↩
                (abs(Vt))*max(abs(nonlin(indx(str):indx(stp)))),t(↩
                indx(str):indx(stp)),nonlin(indx(str):indx(stp)),t(↩
                indx(str):indx(stp)),0*t(indx(str):indx(stp)),'k','↩
                LineWidth',linewidth);
181         set(gca,'FontSize',fontSize,'LineWidth',linewidth)
182         ylabel('Current [nA]')
183         xlabel('Time [s]')
184         xlim([t(indx(str)),t(indx(stp))]);
185         mx = max(Vt(indx(str):indx(stp))/max(abs(Vt))*max(abs(↩
                nonlin(indx(str):indx(stp)))));
186         ylim([-mx,mx])
187         title(plottitle)
188         legend(plotlabelV,'Location','SouthEast')
189         %%%%%
190         if (savePictures == 1)
191             filename = sprintf('C:\\Users\\Torstein\\Documents↩
                    \\Master\\Results\\MATLAB\\%s\\%sNonlinOnePeriod↩
                    %d.png',oil,oil,nr);
192             saveas(h,filename)
193         end
194
195         aaa = 1;
196         h = figure('Position',[20 20 aaa*1.5*scrsz(4)*2/3 aaa*↩
                scrsz(4)*2/3],'PaperSize',[aaa*1.5*16 aaa*16],'↩
                PaperPositionMode', 'auto');
197         plot(t(indx(str):indx(stp)),0*t(indx(str):indx(stp)),'k↩
                ','LineWidth',linewidth)
198         hold on
199         [AX,H1,H2] = plotyy(t(indx(str):indx(stp)),2*Vt(indx(↩
                str):indx(stp)),t(indx(str):indx(stp)),nonlin(indx(↩
                str):indx(stp)));
200         set(get(AX(2),'Ylabel'),'String','Non-capacitive ↩
                current [nA]','FontSize',fontSize,'LineWidth',↩
                linewidth)
201         set(get(AX(1),'Ylabel'),'String','Voltage [kV]','↩
                FontSize',fontSize,'LineWidth',linewidth)
```

```
202
203         set(H1,'LineStyle','-','LineWidth',linewidth);
204         set(H2,'LineStyle','-','LineWidth',linewidth);
205
206         mxy1 = max(abs(2*Vt(indx(str):indx(stp))));
207         mxy2 = max(abs(nonlin(indx(str):indx(stp))));
208
209         set(AX(1),'ylim',[-mxy1,mxy1]);
210         set(AX(2),'ylim',[-mxy2,mxy2]);
211
212         set(AX,'FontSize',fontSize,'LineWidth',linewidth)
213         set(AX,'position',[0.175 0.175 .65 .65])
214
215         set(AX,'xlim',[t(indx(str)),t(indx(stp))]);
216         hold off
217         title(plottitle)
218         xlabel('Time [s]')
219
220         if (savePictures == 1)
221             filename = sprintf('C:\\Users\\Torstein\\Documents↩
                    \\Master\\Results\\MATLAB\\%s\\%↩
                    sNonlinOneIIPeriod%d.png',oil,oil,nr);
222             saveas(h,filename)
223         end
224
225         %%%%%
226         h = figure('Position',[20 20 1.5*scrsz(4)*2/3 scrsz(4)↩
                *2/3],'PaperSize',[1.5*16 16],'PaperPositionMode', '↩
                auto');
227         plot(t(maxvaluepos),nonlin(maxvaluepos),'ok','LineWidth↩
                ',linewidth);
228         set(gca,'FontSize',fontSize,'LineWidth',linewidth)
229         ylabel('Currentpeak [nA]')
230         xlabel('Time [s]')
231         title(plottitle2)
232         legend('I-I_C','Location','NorthEast')
233
234         if (savePictures == 1)
235             filename = sprintf('C:\\Users\\Torstein\\Documents↩
                    \\Master\\Results\\MATLAB\\%s\\%sNonlinPK%d.png'↩
                    ,oil,oil,nr);
236             saveas(h,filename)
237         end
238
239         h = figure('Position',[20 20 1.5*scrsz(4)*2/3 scrsz(4)↩
                *2/3],'PaperSize',[1.5*16 16],'PaperPositionMode', '↩
                auto');
240         plot((2*Vt(indx(str):indx(stp))),(nonlin(indx(str):indx↩
                (stp))),'.k','LineWidth',linewidth);
241         set(gca,'FontSize',fontSize,'LineWidth',linewidth)
242         ylabel('Noncapacitive current [nA]')
```

```
243         xlabel('Voltage [kV]')
244         title(plottitle)
245
246         if (savePictures == 1)
247             filename = sprintf('C:\\Users\\Torstein\\Documents\\Master\\Results\\MATLAB\\%s\\%sNonlinIsfaV%d.png',oil,oil,nr);
248             saveas(h,filename)
249         end
250
251          h = figure('Position',[20 20 1.5*scrsz(4)*2/3 scrsz(4)*2/3],'PaperSize',[1.5*16 16],'PaperPositionMode', 'auto');
252         plot(sign(Vt(indx(str):indx(stp))).*(2*Vt(indx(str):indx(stp))).^2,(nonlin(indx(str):indx(stp))),'.k','LineWidth',linewidth);
253         set(gca,'FontSize',fontSize,'LineWidth',linewidth)
254         ylabel('Noncapacitive current [nA]')
255         xlabel('Voltage^2 [kV]^2')
256         title(plottitle)
257         xlim([-voltageLevel.^2,voltageLevel.^2])
258
259         if (savePictures == 1)
260             filename = sprintf('C:\\Users\\Torstein\\Documents\\Master\\Results\\MATLAB\\%s\\%sNonlinIsfaVpow2v%d.png',oil,oil,nr);
261             saveas(h,filename)
262         end
263
264     end
265
266 end
267
268 h = figure('Position',[20 20 1.5*scrsz(4)*2/3 scrsz(4)*2/3],'PaperSize',[1.5*16 16],'PaperPositionMode', 'auto');
269 plot(vecs,vec(:,1),'bo',vecs,vec(:,2),'ro',vecs,vec(:,3),'-bx',vecs,vec(:,4),'-rx','LineWidth',linewidth,'MarkerSize',10)
270 set(gca,'FontSize',fontSize,'LineWidth',linewidth)
271 ylim([0,150])
272 ylabel('Nonlin I [nA]')
273 xlabel('Sample')
274 title(plottitle2)
275 legend('max(positive)','max(negative)','mean(positive)','mean(negative)')%,'var(positive)','var(negative)')
276
277 if (savePictures == 1)
278     filename = sprintf('C:\\Users\\Torstein\\Documents\\Master\\Results\\MATLAB\\%s\\%sNonlinStat%dto%d.png',oil,oil,nri(1),nri(length(nri)));
279     saveas(h,filename)
280 end
```

```
281
282 %%%%
283 len = length(totpeak);
284 pos = linspace(1,len,len);
285 for i = positions
286     for j = i:len
287         pos(j) = pos(j) + 50;
288     end
289 end
290 pos = pos*factor;
291
292 plottitle3 = sprintf('Non-capacitive current peak in half ↩
       period \n %s, %s',plottitle,plotlabelV);
293
294 h = figure('Position',[20 20 1.5*scrsz(4)*2/3 scrsz(4)*2/3],'↩
       PaperSize',[1.5*16 16],'PaperPositionMode', 'auto');
295 plot(pos,totpeak,'o','LineWidth',linewidth);-
296 set(gca,'FontSize',fontSize,'LineWidth',linewidth)
297 ylabel('Nonlin I [nA]')
298 xlabel('Approx time [s]')
299 title(plottitle3)
300
301 if (savePictures == 1)
302     filename = sprintf('C:\\Users\\Torstein\\Documents\\Master↩
          \\Results\\MATLAB\\%s\\%sNonlinStatPK%dto%d.png',oil,oil↩
          ,nri(1),nri(length(nri)));
303     saveas(h,filename)
304 end
305
306 lengthh = length(totpeak);
307 h = figure('Position',[20 20 1.5*scrsz(4)*2/3 scrsz(4)*2/3],'↩
       PaperSize',[1.5*16 16],'PaperPositionMode', 'auto');
308 plot((totpeak(1:lengthh-1))./((totpeak(2:lengthh))),'xk','↩
       LineWidth',linewidth);
309 set(gca,'FontSize',fontSize,'LineWidth',linewidth)
310 ylabel('I(i)/I(i+1)')
311 xlabel('Period no')
312 title(plottitle2)
```

Appendix C

Matlab script 2

The script for PD statistics loads data exported from Omicron to Matlab. Vectors containing the time, voltage, charge and phase position of all PD events are then stored in Matlab. The script finds the frequency of the voltage, then finds all zero crossings in the voltage. Then it counts the PDs and finds the number of half periods to next PD and the previous PD. This is then plotted. In addition, the number of half periods with a certain number of half periods to the next PD are grouped together and fitted to a geometric distribution. Both sorted by magnitude of the PD and number of PDs per half period.

```
1  %Omicron recorded
2  close all;
3
4  %%%%%%%%%%%%%%%%%%%%%%%%%%%%%%%%%%%%%%%%%%%%%%%%%%%%%%%%%%%%%%%%%%%%%%%%%%%%
5  %%% Chose parameters: %%%%%%%%%%%%%%%%%%%%%%%%%%%%%%%%%%%%%%%%%%%%%%%%%%%%%%%
6  %%%%%%%%%%%%%%%%%%%%%%%%%%%%%%%%%%%%%%%%%%%%%%%%%%%%%%%%%%%%%%%%%%%%%%%%%%%%
7
8  savePictures = 1;
9  %oil = 'Cyclohexane';
10 %oil = 'DialaDX';
11 %oil = 'Midel7131';
12 oil = 'Galden135';
13 nr = 0001;
14
15 %%%%%%%%%%%%%%%%%%%%%%%%%%%%%%%%%%%%%%%%%%%%%%%%%%%%%%%%%%%%%%%%%%%%%%%%%%%%
16 %%% Load from file generated by Omicron mtronix %%%%%%%%%%%%%%%%%%%%%%%%%%%%
17 %%%%%%%%%%%%%%%%%%%%%%%%%%%%%%%%%%%%%%%%%%%%%%%%%%%%%%%%%%%%%%%%%%%%%%%%%%%%
18
19 folder = sprintf('C:\\Users\\Torstein\\Documents\\Master\\↩
      Results\\Omicron\\%s\\StreamMatlab\\%4.0f',oil,nr);
20 folder = regexprep(folder,' ','0');
21 ph = importPHData(folder,'unit1.1');
22 [t,q] = importQData(folder,'unit1.1');
23 q = -q;
24 [tv,v] = importVData(folder,'unit1.1');
25 v = -v;
```

```
26
27 scrsz = get(0,'ScreenSize'); %Get the screen size to set the ↩
       figure appropriate
28
29 %%%%%%%%%%%%%%%%%%%%%%%%%%%%%%%%%%%%%%%%%%%%%%%%%%%%%%%%%%%%%%%%
30 %%% Find the frequency and zero crossings %%%%%%%%%%%%%%%
31 %%%%%%%%%%%%%%%%%%%%%%%%%%%%%%%%%%%%%%%%%%%%%%%%%%%%%%%%%%%%%%%%
32
33 %%%Frequency
34 lenT = length(v);
35
36 t1 = v(1:lenT-1);
37 t2 = v(2:lenT);
38
39 tt = t1.*t2; %The shifting of t1 and t2 provide a negative ↩
       number in the crossings
40 indx = find(tt < 0); %Zero crossings
41 last = length(indx);
42 if((last+1)/2 ~= floor((last+1)/2)) %To get an whole periods
43     last = last - 1;
44 end
45
46 %The frequency from time
47 frequency = (last-1)*0.5/(tv(indx(last))-tv(indx(1)));
48
49 indx1 = find(t == tv(indx(1)));
50 indx2 = find(t == tv(indx(last)));
51
52 %Zero crossings at times
53 timeZero = tv(indx);
54
55 %Find # PDs and Qpk pr half period:
56 numberOfHalfperiods = length(indx) - 1;
57
58 %Get the phase with correct length:
59 phase = linspace(0,2*pi,indx(3)-indx(1)+1);
60
61 %For the analysis, know which phase is the positive tip.
62 if v(indx(1) + 1) > 0
63     pos = 1; %Odd numbers negative tip (positive here)
64 else
65     pos = 0; %Odd numbers positive tip
66 end
67
68 %%%%%%%%%%%%%%%%%%%%%%%%%%%%%%%%%%%%%%%%%%%%%%%%%%%%%%%%%%%%%%%%
69 %%% Allocating memory for the statistics %%%%%%%%%%%%%%%
70 %%%%%%%%%%%%%%%%%%%%%%%%%%%%%%%%%%%%%%%%%%%%%%%%%%%%%%%%%%%%%%%%
71
72 halfperiodsNumberPD = linspace(0,0,numberOfHalfperiods); %To ↩
       count # PDS
```

```
73 halfperiodsMaxQPD = linspace(0,0,numberOfHalfperiods); %To find max Q
74
75 %Find |Qmax| in each half period
76 k = 1; %Start in first half period
77 lengde = length(q);
78 for i = 1:lengde
79     k = find((t(i) > timeZero & t(i) < tv(indx(last))),1,'last');
80
81     halfperiodsNumberPD(k) = halfperiodsNumberPD(k) + 1;
82     if abs(q(i)) > abs(halfperiodsMaxQPD(k))
83         halfperiodsMaxQPD(k) = q(i);
84     end
85 end
86
87 %Find the half periods with PDs:
88 verd11 = find(halfperiodsNumberPD);
89 lengde2 = length(verd11); %# half periods
90 periodDistance = linspace(0,0,lengde2-1); %Half periods to next pd
91
92 for i = 1:lengde2-1
93    periodDistance(i) = verd11(i+1)-verd11(i);
94 end
95 %Transfer Qmax to an array containing zero 0 PDs.
96 PDs = linspace(0,0,lengde2);
97 for i = 1:lengde2
98    PDs(i) = halfperiodsMaxQPD(verd11(i));
99 end
100
101 %%%
102
103 neg = find(PDs < 0);
104
105 %%%%%%%%%%%%%%%%%%%%%%%%%%%%%%%%%%%%%%%%%%%%%%%%%%%%%%%%%%%%%%%%%%%%%%%%%%%%
106 %%% Plot and save the results  %%%%%%%%%%%%%%%%%%%%%%%%%%%%%%%%%%%%%%%%%%%%
107 %%%%%%%%%%%%%%%%%%%%%%%%%%%%%%%%%%%%%%%%%%%%%%%%%%%%%%%%%%%%%%%%%%%%%%%%%%%%
108
109 kV = max(v)/1000;
110 title1 = sprintf('Total time elapsed %4.2f s. Voltage amplitude %4.2f kV',t(length(t)),kV);
111
112 h = figure('Position',[20 20 1.5*scrsz(4)*2/3 scrsz(4)*2/3],'PaperSize',[1.5*16 16],'PaperPositionMode', 'auto');
113 plot(periodDistance,'.','LineWidth',1.5,'MarkerSize',10)
114 set(gca,'FontSize',16,'LineWidth',2)
115 xlabel('Period no. with PD')
116 ylabel('# Half periods to next PD')
117
118 if (savePictures == 1)
```

```
119     filename = sprintf('C:\\Users\\Torstein\\Documents\\Master↩
            \\Results\\MATLAB\\%s\\%s%dPDstreamHPtoNextPD.png',oil,↩
            oil,nr);
120     saveas(h,filename)
121 end
122
123 %%%%
124
125 phaselabel = sprintf('Phase, frequency = %6.2fHz',frequency);
126
127 h = figure('Position',[20 20 1.5*scrsz(4)*2/3 scrsz(4)*2/3],'↩
        PaperSize',[1.5*16 16],'PaperPositionMode', 'auto');
128 plot(ph*360,q*1e12,'.k',phase*180/pi,-v(indx(1):indx(3))*sign(v↩
        (indx(1)+10))/max(v)*max(abs(q)*1e12),'LineWidth',.1,'↩
        MarkerSize',5);
129 set(gca,'FontSize',16,'LineWidth',2)
130 xlabel(phaselabel)
131 ylabel('Q [pC]')
132 xlim([0,360])
133
134 if (savePictures == 1)
135     filename = sprintf('C:\\Users\\Torstein\\Documents\\Master↩
            \\Results\\MATLAB\\%s\\%s%dPDstreamPhasePlot.png',oil,↩
            oil,nr);
136     saveas(h,filename)
137 end
138
139 %%%%
140
141 [a nmbr] = max(abs(q));
142 h = figure('Position',[20 20 1.5*scrsz(4)*2/3 scrsz(4)*2/3],'↩
        PaperSize',[1.5*16 16],'PaperPositionMode', 'auto');
143 plot(tv,v/1000,t,q*1e12,'-x','LineWidth',2,'MarkerSize',10);
144 set(gca,'FontSize',16,'LineWidth',2)
145 xlabel('Time [s]')
146 ylabel('Q [pC], V[kV]')
147 legend('V','Q')
148 %xlim([0,max(tv)]) %Set xlim in order to be able to see the ↩
        results
149
150 if (savePictures == 1)
151     filename = sprintf('C:\\Users\\Torstein\\Documents\\Master↩
            \\Results\\MATLAB\\%s\\%s%dPDstreamPDsequence.png',oil,↩
            oil,nr);
152     saveas(h,filename)
153 end
154
155 %%%%
156
157 place = find(halfperiodsNumberPD);
158 places = place(2:length(place)-1);
```

```
159
160 h = figure('Position',[20 20 1.5*scrsz(4)*2/3 scrsz(4)*2/3],'↩
    PaperSize',[1.5*16 16],'PaperPositionMode', 'auto');
161 plot(halfperiodsMaxQPD(places)*1e12,periodDistance(2:length(↩
    place)-1),'o',halfperiodsMaxQPD(places)*1e12,periodDistance↩
    (1:length(place)-2),'x','LineWidth',2,'MarkerSize',10);
162 set(gca,'FontSize',16,'LineWidth',2)
163 title(title1)
164 legend('Half periods to next PD','Half period since last PD','↩
    Location','NorthEast')
165 xlabel('Q_{Max} [pC]')
166 ylabel('# half periods')
167
168 if (savePictures == 1)
169     filename = sprintf('C:\\Users\\Torstein\\Documents\\Master↩
        \\Results\\MATLAB\\%s\\%s%dPDstreamSizevsNextPD.png',oil↩
        ,oil,nr);
170     saveas(h,filename)
171 end
172
173 %%%%
174
175 h = figure('Position',[20 20 1.5*scrsz(4)*2/3 scrsz(4)*2/3],'↩
    PaperSize',[1.5*16 16],'PaperPositionMode', 'auto');
176 plot(halfperiodsNumberPD(place),[periodDistance,0],'o',↩
    halfperiodsNumberPD(place),[0,periodDistance],'x','LineWidth↩
    ',2,'MarkerSize',10);
177 set(gca,'FontSize',16,'LineWidth',2)
178 title(title1)
179 legend('Half periods to next PD','Half period since last PD')
180 xlabel('# PDs pr half period (When PD)')
181 ylabel('# Half periods to/since next/last PD')
182
183 if (savePictures == 1)
184     filename = sprintf('C:\\Users\\Torstein\\Documents\\Master↩
        \\Results\\MATLAB\\%s\\%s%dPDstreamNumbervsNextPD.png',↩
        oil,oil,nr);
185     saveas(h,filename)
186 end
187
188 %%%%
189
190 pdo = [periodDistance,0];
191 opd = [0,periodDistance];
192 hpnr = halfperiodsNumberPD(place);
193
194 len01 = max(hpnr);
195 len02 = max(opd);
196 histogram = zeros(len01,len02+1);
197
198 for i = 1:length(place)
```

```
199     histogram(hpnr(i),opd(i)+1) = histogram(hpnr(i),opd(i)+1) + ↩
            1;
200 end
201
202 legend1 = [];
203 for j = 1:len01
204     legend10 = sprintf('%2.0f PD pr period',j);
205     leg10 = '                 ';
206     leglen = length(legend10);
207     leg10(17-leglen:16) = legend10;
208
209     legend1 = [legend1;leg10];
210 end
211
212 %%%Adjustable %%%%%%%%%%%%%
213 maxPDno = 4;
214 pds = (1:maxPDno);
215 legends = (1:maxPDno+1);
216 lambda = 0.02; %Factor in geometric distribution
217 %%%%%%%%%%%%%%%%%%%%%%%%%%%%%%%
218
219 x = linspace(0,len02-1,len02);
220
221 p = sum(histogram(1,1:2:len02))/(sum(histogram(1,1:2:len02).*x↩
        (1:2:len02)));
222 Pr = (1-p).^x*p;
223
224 for i = 1:len01
225     histogram(i,:) = 0.5*0.5*histogram(i,:)/sum(histogram(i,:));
226 end
227
228 testleg1 = sprintf('(1-%1.3f)^k%1.3f',p,p);
229 testleg= '                 ';
230 leglen1 = length(testleg1);
231 testleg(17-leglen1:16) = testleg1;
232 legend1(maxPDno+1,:) = testleg;
233
234 %%%%
235 h = figure('Position',[20 20 1.5*scrsz(4)*2/3 scrsz(4)*2/3],'↩
        PaperSize',[1.5*16 16],'PaperPositionMode', 'auto');
236 plot(x(1:2:len02),histogram(pds,1:2:len02),'o',x,Pr,'k','↩
        LineWidth',3,'MarkerSize',10)
237 set(gca,'FontSize',16,'LineWidth',2)
238 xlabel('Half periods to next PD')
239 ylabel('Normalized samples')
240 legend(legend1(legends,:))
241
242 if (savePictures == 1)
243     filename = sprintf('C:\\Users\\Torstein\\Documents\\Master↩
            \\Results\\MATLAB\\%s\\%s%dPDstreamToNextPD.png',oil,oil↩
            ,nr);
```

```
244     saveas(h,filename)
245 end
246
247 %%%
248
249 h = figure('Position',[20 20 1.5*scrsz(4)*2/3 scrsz(4)*2/3],'↩
       PaperSize',[1.5*16 16],'PaperPositionMode', 'auto');
250 semilogy(x(1:2:len02),histogram(pds,1:2:len02),'o',x,Pr,'k','↩
       LineWidth',3,'MarkerSize',10)
251 set(gca,'FontSize',16,'LineWidth',2)
252 legend(legend1(legends,:))
253 xlabel('Half periods to next PD')
254 ylabel('Normalized samples')
255
256 if (savePictures == 1)
257     filename = sprintf('C:\\Users\\Torstein\\Documents\\Master↩
           \\Results\\MATLAB\\%s\\%s%dPDstreamToNextPD2.png',oil,↩
           oil,nr);
258     saveas(h,filename)
259 end
260
261 %%%
262
263 hpmq = halfperiodsMaxQPD(places)*1e12;
264 hppd = periodDistance(2:length(place)-1);
265 minhpmq = min(hpmq);
266 maxhpmq = max(hpmq);
267 minhist = floor(minhpmq/10)*10;
268 maxhist = floor(maxhpmq/10)*10;
269
270 Factor = 10; %Adjustable %eg10
271 len = ceil(((maxhist-minhist))/ Factor)+1+1;
272 len2 = ceil(max(hppd));
273 histogram2 = zeros(len,len2);
274
275 test = linspace(0,0,length(hppd));
276
277 for i = 1:length(hppd)
278    histogram2(min(floor(((hpmq(i)-minhist))/Factor)+1,len),min(↩
          ceil((hppd(i))),len2)) = histogram2(min(floor(((hpmq(i)-↩
          minhpmq))/Factor)+1,len),min(ceil((hppd(i))),len2)) + 1;
279    test(i) = floor(((hpmq(i)-minhpmq))/Factor)+1;
280 end
281
282 legend2 = [];
283 for j = 1:len
284     legend20 = sprintf('%4.1fpC',minhist + Factor*(j-1));
285     leg20 = '          ';
286     leglen = length(legend20);
287     leg20(10-leglen:9) = legend20;
288     legend21 = sprintf('%4.1fpC',minhist + Factor*(j));
```

```
289     leg21= '          ';
290     leglen = length(legend21);
291     leg21(10-leglen:9) = legend21;
292     leg = sprintf('%s to %s',leg20,leg21);
293     legend2 = [legend2;leg];
294 end
295 legend2 = [legend2;leg];
296
297 if(0)
298 xes = minhist+Factor/2:Factor:maxhist+Factor/2;
299
300 h = figure('Position',[20 20 1.5*scrsz(4)*2/3 scrsz(4)*2/3],'↩
    PaperSize',[1.5*16 16],'PaperPositionMode', 'auto');
301 bar(xes,(histogram2(1:len-1,2:2:len2)));
302 xlabel('Q [pC]')
303 ylabel('Histogram, PD next period')
304 xlim([-60,60])
305 if (savePictures == 1)
306     filename = sprintf('C:\\Users\\Torstein\\Documents\\Master↩
        \\Results\\MATLAB\\%s\\%s%dPDstreamHistogram.png',oil,↩
        oil,nr);
307     saveas(h,filename)
308 end
309 end
310
311 %%%Adjustable%%%
312 maxT = len;
313 Start = min(floor(((-50.1-minhist))/Factor)+1,len);
314 Stopp = min(floor(((-10.1-minhist))/Factor)+1,len);
315 Start2 = min(floor(((10.1-minhist))/Factor)+1,len);
316 Stopp2 = min(floor(((20.1-minhist))/Factor)+1,len);
317 qs = [Start:Stopp,Start2:Stopp2];
318 legends2 = [Start:Stopp,Start2:Stopp2,len+1];
319 %%%%%%%%%%%%%%%%%%
320
321 plass = min(floor(((-12.1-minhist))/Factor)+1,len);
322 periods = 1:len2;
323 p2 = sum(histogram2(plass,2:2:len2))/(sum(histogram2(plass,2:2:↩
    len2).*periods(2:2:len2)));
324 Pr2 = (1-p2).^periods*p2;
325
326 for i = 1:len
327    histogram2(i,:) = 0.5*0.25*histogram2(i,:)/sum(histogram2(i↩
       ,:));
328 end
329 testleg1 = sprintf('(1-%1.3f)^k%1.3f',p2,p2);
330 testleg= '                        ';
331 leglen1 = length(testleg1);
332 testleg(23-leglen1:22) = testleg1;
333
334 legend2(maxT+1,:) = testleg;
```

```
335
336 h = figure('Position',[20 20 1.5*scrsz(4)*2/3 scrsz(4)*2/3],'↩
       PaperSize',[1.5*16 16],'PaperPositionMode', 'auto');
337 plot(periods(2:2:len2),transpose(histogram2(qs,2:2:len2)),'o',↩
       periods,Pr2,'k','LineWidth',3,'MarkerSize',10)
338 set(gca,'FontSize',16,'LineWidth',2)
339 xlabel('Half periods to next PD')
340 ylabel('Normalized samples')
341 legend(legend2(legends2,:))
342
343 if (savePictures == 1)
344     filename = sprintf('C:\\Users\\Torstein\\Documents\\Master↩
           \\Results\\MATLAB\\%s\\%s%dPDstreamToNextPDQ.png',oil,↩
           oil,nr);
345     saveas(h,filename)
346 end
347
348 h = figure('Position',[20 20 1.5*scrsz(4)*2/3 scrsz(4)*2/3],'↩
       PaperSize',[1.5*16 16],'PaperPositionMode', 'auto');
349 semilogy(periods(2:2:len2),transpose(histogram2(qs,2:2:len2)),'↩
       o',periods,Pr2,'k','LineWidth',3,'MarkerSize',10)
350 set(gca,'FontSize',16,'LineWidth',2)
351 xlabel('Half periods to next PD')
352 ylabel('Normalized samples')
353 legend(legend2(legends2,:))
354
355 if (savePictures == 1)
356     filename = sprintf('C:\\Users\\Torstein\\Documents\\Master↩
           \\Results\\MATLAB\\%s\\%s%dPDstreamToNextPDQ2.png',oil,↩
           oil,nr);
357     saveas(h,filename)
358 end
```